2010-07-13

A Toolkit for the Construction and Understanding of 3-Manifolds

Lee R. Lambert
Brigham Young University - Provo

A Tool Kit for The Construction and Understanding of 3-manifolds

LeeR Lambert

A dissertation submitted to the faculty of
Brigham Young University
in partial fulfillment of the requirements for the degree of

Doctor of Philosophy

James W. Cannon, Chair
David G. Wright
Jessica Purcell
Denise Halverson
H. Dennis Tolley

Department of Mathematics

Brigham Young University

August 2010

Abstract

A Tool Kit for The Construction and Understanding of 3-manifolds

LeeR Lambert

Department of Mathematics

Doctor of Philosophy

Since our world is experienced locally in three-dimensional space, students of mathematics struggle to visualize and understand objects which do not fit into three-dimensional space. 3-manifolds are locally three-dimensional, but do not fit into 3-dimensional space and can be very complicated.

Twist and bitwist are simple constructions that provide an easy path to both creating and understanding closed, orientable 3-manifolds. By starting with simple face pairings on a 3-ball, a myriad of 3-manifolds can be easily constructed. In fact, all closed, connected, orientable 3-manifolds can be developed in this manner. We call this work a tool kit to emphasize the ease with which 3-manifolds can be developed and understood applying the tools of twist and bitwist construction.

We also show how two other methods for developing 3-manifolds–Dehn surgery and Heegaard splitting–are related to the twist and bitwist construction, and how one can transfer from one method to the others. One interesting result is that a simple bitwist construction on a 3-ball produces a group of manifolds called generalized Sieradski manifolds which are shown to be a cyclic branched cover of $\mathbb{S}^3$ over the 2-braid, with the number twists determined by the hemisphere subdivisions. A slight change from bitwist to twist causes the knot to become a generalized figure-eight knot.

Keywords: twist construction, bitwist construction, 3-manifolds, Dehn surgery, Heegaard splitting, Heegaard diagram.

Acknowledgments

First, I would like to thank Jim Cannon, my supervisor, for his many suggestions and constant support during this research. He has spent many hours patiently helping me to understand 3-manifolds and the basic issues and questions involved. I am grateful to the other members of my committee, as well, for their time and efforts. I would also like to thank my wife Karen and our children for their support during my studies and research. Our mathematics department secretary Lonette Stoddard as well as our technical support Jim Logan have also been very helpful during my studies and preparation of this document.

Contents

List of Tables

List of Figures

Chapter 1. Introduction

We assume that the reader has a basic knowledge of topology: compactness, connectedness, homeomorphisms, fundamental groups and covering spaces, homology, Euclidean space, spheres, and balls.

There are three standard ways of representing a compact, connected, orientable 3-manifold: Heegaard splittings, Dehn surgery, and face pairings. Each has its advantages and disadvantages.

The study of Heegaard splittings reduces the classification of 3-manifolds to the study of surface diffeomorphisms and to the study of the fascinating Gromov-hyperbolic curve complex, both of which are lower dimensional problems. However, a Heegaard diagram of even moderate complexity is difficult to analyze, and the equivalence of diagrams leads to the difficult stabilization problem [14], [8].

Dehn surgery, on the other hand, leads to the Kirby calculus, a tool that is quite efficient, and naturally treats the equivalence question among different surgery diagrams. Dehn surgery also has beautiful connections with 4-dimensional manifolds [13], [8]. However, it its difficult to recognize the geometry of the manifold from the Dehn surgery representation.

The notion of face pairings, when reduced to the 2-dimensional case, becomes the notion of edge pairings and is universally employed in the classification of 2-manifolds. Each arbitrary edge pairing yields a 2-manifold; but an arbitrary face pairing in dimension 3 with probability 1 yields only a pseudo-3-manifold [2]. However, a successful face pairing– that is, one that yields a true 3-manifold– has several favorable characteristics: (1) easily visible symmetries; (2) a natural, fundamental domain for the action of the fundamental group on the universal covering manifold; (3) can be used in algorithmic constructions of the Cayley graph of the fundamental group [1]; and, in the process, (4) can be used in approximating

the space at infinity.

The purpose of this dissertation is to show how the modified face pairing constructions, called twisted face pairings and bitwisted face pairings, can be used in conjunction with Heegaard splittings and Dehn surgery [7] [6] to supply a powerful student tool kit for the construction and analysis of interesting 3-manifolds. These twisted pairings were designed by Cannon, Floyd, and Parry to rectify the problem that most face pairings yield only a pseudo-manifold. The twisted varieties always yield a true 3-manifold. [7].

Then the point is this: after the student has been taught that 3-manifolds come in eight basic varieties, namely those modelled on the eight Thurston geometries, students would be baffled by an assignment to find interesting examples of each. They would be likely to come up with examples for the product geometries: $\mathbb{S}^1 \times \mathbb{S}^1 \times \mathbb{S}^1$, $\mathbb{S}^2 \times \mathbb{S}^1$, and $S_g \times \mathbb{S}^1$, with $\mathbb{S}^1$ a circle, $\mathbb{S}^2$ the 2-sphere, and S_g a surface of genus $g >= 2$. And of course they would consider the sphere $\mathbb{S}^3$ and projective space P^3 for spherical geometry. But where would they begin to look for hyperbolic manifolds or for the three twisted geometries, *Sol*, *Nil*, and the universal cover of $PSL_2(R)$?

Examples for all of the difficult geometries (see Chapter 7) and many rational homology spheres (finite first homology) arise from the simplest of twisted and bitwisted face pairings (see Table 8.4). We give examples of each and demonstrate how one can move from one representation of a 3-manifold to another. Is there an easy way for the student to do this? With a little coaching, students can construct relatively simple examples for themselves of manifolds based on all eight geometries.

As interesting examples, we show how twisted and bitwisted face pairings can be used to represent all of the cyclic branched covers of $\mathbb{S}^3$ branched over the trefoil knot, the figure-eight knot, and infinitely many natural generalizations of each. The trefoil and figure-eight are already treated by Cannon, Floyd, and Parry in [3], but the generalizations of each seem to be new. For the trefoil, the generalizations are the cyclic branched covers of the 2-braid knots. For the figure-eight knot, the generalizations are the cyclic branched covers of certain

lesser-known alternating 2-bridge knots that generalize the figure-eight knot.

The branched covers of the trefoil knot already include the Poincaré dodecahedral space (a spherical space with fundamental group of order 120), a manifold with the Heisenberg group (a Nil manifold) as the fundamental group, and infinitely many $PSL_2(R)$ manifolds [3]. This sequence of manifolds has the interesting property that the first homology repeats cyclically as one traverses the sequence of covers. We prove that the same periodicity (with different periods) occurs for the cyclic branched covers of each fixed 2-braid knot.

The branched covers of the figure-eight knot include spherical manifolds, an interesting Euclidean manifold, and infinitely many hyperbolic manifolds. The fundamental groups are the even exemplars of the famous Fibonacci groups of John Conway [3]. The group presentations of the generalizations are cyclic presentations, but the first homology is definitely not periodic. Since all three standard methods of representing a 3-manifold depend on the notion of *identification space* or *quotient space*, we will review that notion in Chapter 2.

In Chapter 3 we review the notions of knots and links in preparation for Dehn surgery representations.

In Chapter 4 we will define Heegaard splittings, Dehn surgery, face pairings and their twisted versions.

In Chapter 5 we will show a method for transferring from a bitwist face pairing representation of a manifold to a Dehn surgery representation of the same manifold. We will also show how to go from a bitwist face pairing to a Heegaard splitting representations of a manifold.

In Chapter 6 we show how to use a bitwist face pairing representation to calculate the fundamental group and first homology group of a 3-manifold.

In Chapter 7 we will give an example from each of the eight Thurston geometries.

Then in Chapter 8, we study the branched covers mentioned above. This chapter contains what we believe to be newly discovered material.

In Chapter 9 we pose a number of unanswered questions for future research.

Chapter 2. Quotient or Identification Space

We will frequently have some equivalence relation ($\sim$) in some topological space X, and then any points which are related, i.e. $a \sim b$, are considered to be the same point. We call the result the quotient space $X/\sim$. The function $p : X \to X/\sim$ which takes each point to its equivalence class is called an identification or quotient map. We define the open sets in the quotient space to be the sets whose pre-images are open in X. The fundamental properties of quotient spaces are given in Munkres [10], paragraph 22, pages 136 to 145.

The standard examples of quotient spaces are the circle and torus. The circle arises from unit interval $[0, 1]$, where the end points form one quivalence class and all other points form individual classes. We think of this as sewing 0 to 1. Similarly, the torus arises from the unit square $[0, 1] \times [0, 1]$, where $[0, y] \sim [1, y]$ and $[x, 0] \sim [x, 1]$ for each $x, y \in [0, 1]$. This last example is called an edge pairing.

Here is another way of viewing the torus quotient. Let's look at Figure 2.1. We see in the top left a square, like a piece of paper. If the sheet is 8.5 inches wide and we identify every point with the point .5 inches to the left of the point, we get a .5 inch strip with edges identified creating a cylinder as shown top right in Figure 2.1. If we next, in addition to identifying to the point to the left, we also identify to the point .5 inches ahead or behind each given point, as in the bottom left of Figure 2.1, we create the torus as shown in the bottom right in figure 2.1. This same result would occur if the identification extended to the entire XY-plane with unit transformations in the X or Y directions identified.

The cylinder and torus are easily visualized. Later, we will do more complicated examples, outside traditional 3-dimensional visualization. But let's do one more simple example, which is slightly different. Start with a disc as on the left in Figure 2.2. This time, in place of

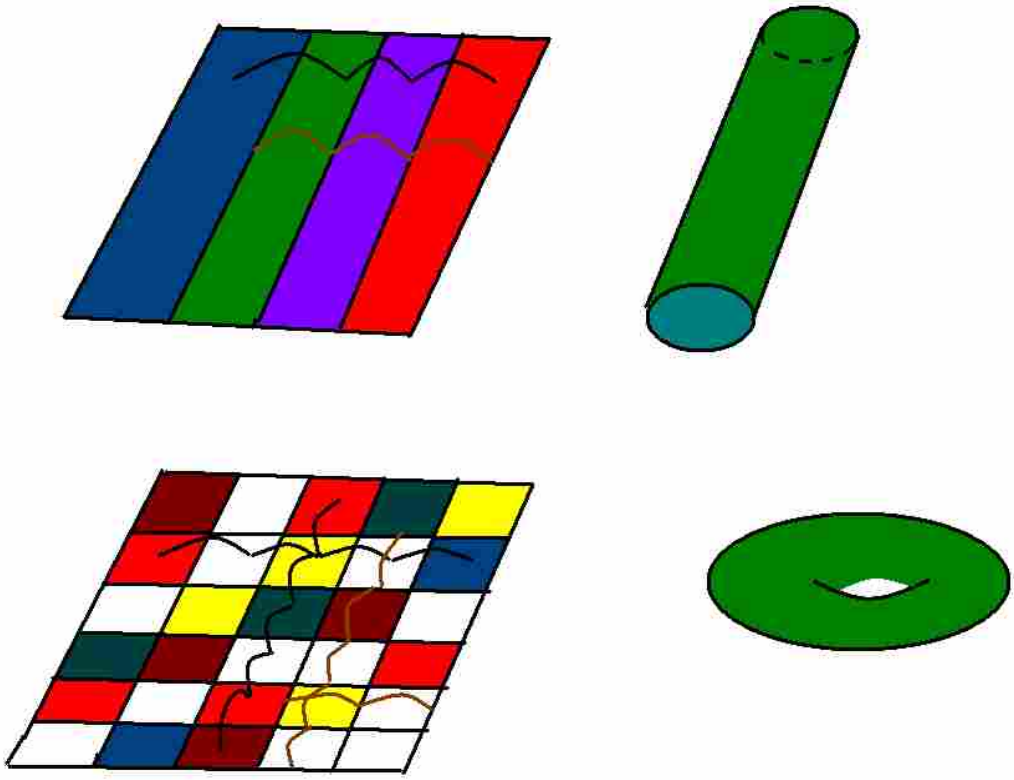

Figure 2.1: Practice with Point Identification 1

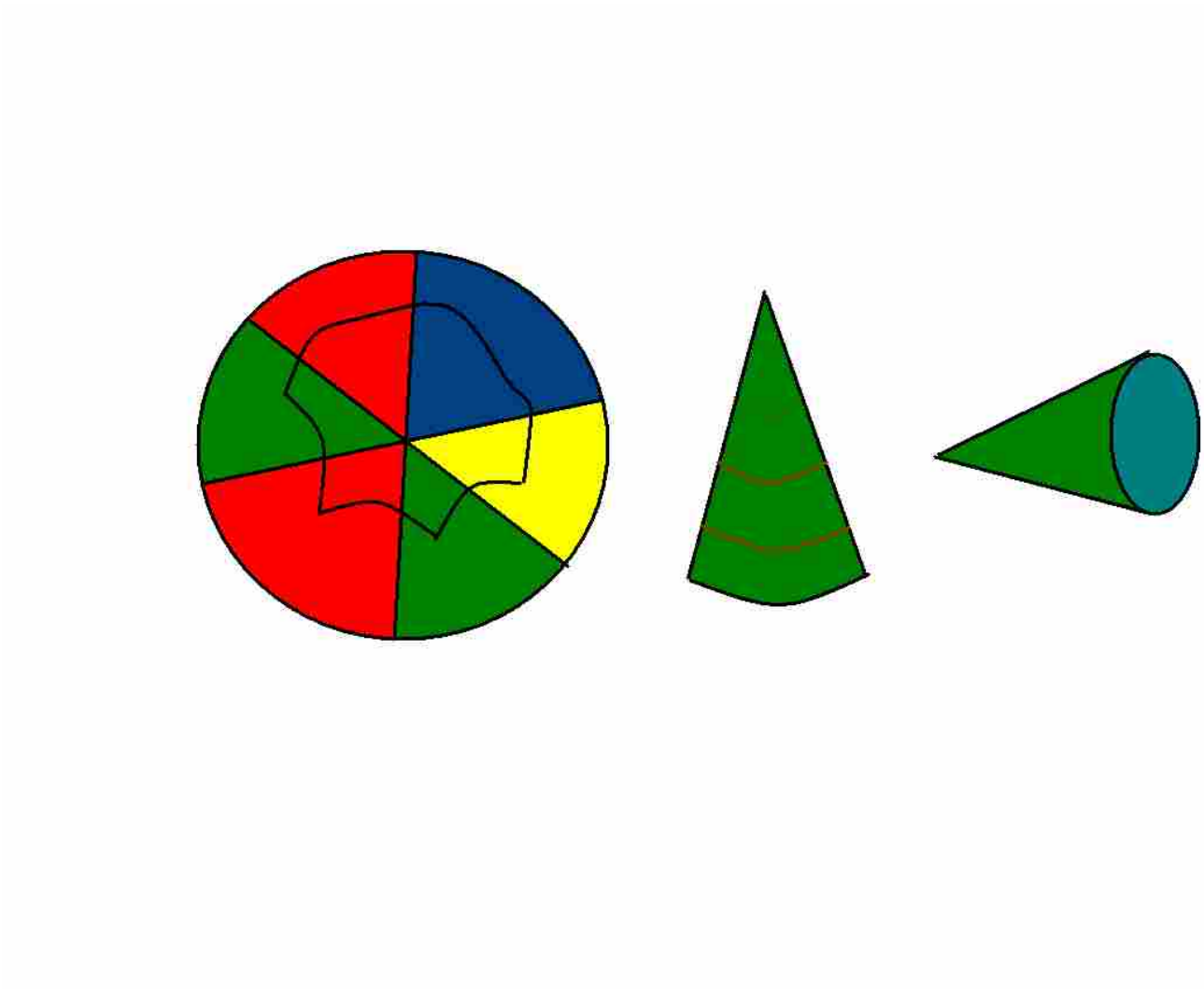

Figure 2.2: Practice with Point Identification 2

unit transformation, we do a rotation of the disc of 1/6th of a turn in a clockwise direction identifying each point with the resulting point after the rotation. We could describe the rotation as the function f and the identification $x \sim f(x)$. The result is the cone as shown next to the disc in Figure 2.2. If we extend the rotation to the entire XY-plane, we get an infinite cone.

So what is different about the simple examples in figure 2.1 and figure 2.2? In figure 2.1, each point in the final result of a cylinder or torus represents many points in the original

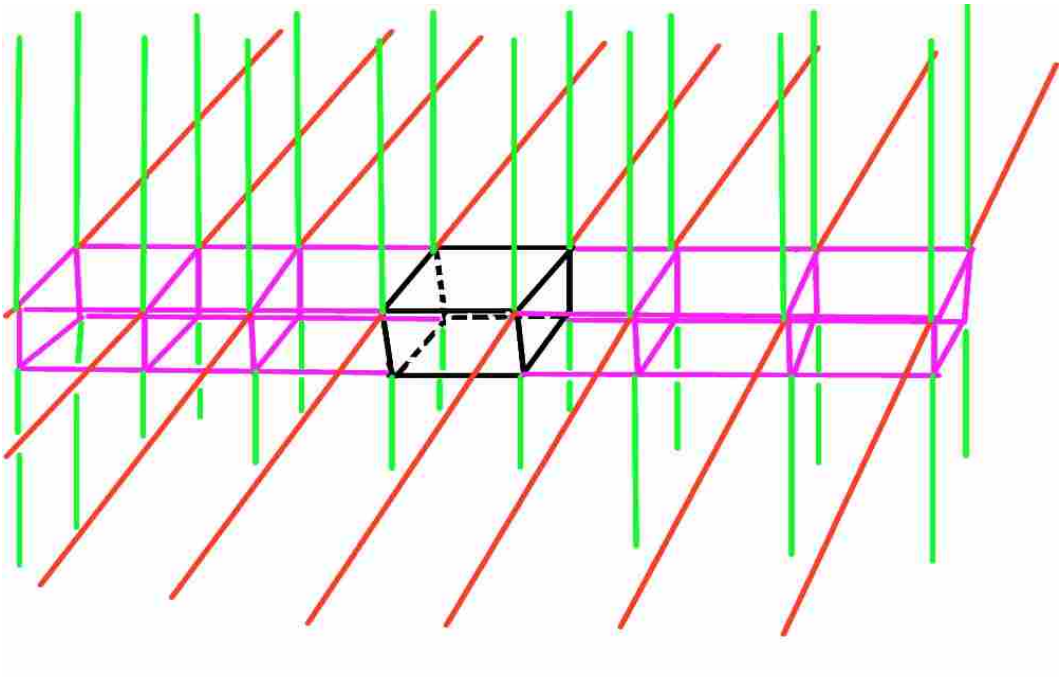

Figure 2.3: Tiling of $\mathbb{E}^3$ by Translations

figure. When described as a transformation, every point is transformed or moved. In figure 2.2, when we do the rotation, every point is moved except for the center point, which is a fixed point about which the rotation is made.

Next, let's move to three dimensions. Rather than using the plane, with unit transformations in the X or Y direction as we did the create the 2-torus, we now transform in the X, Y, and Z directions. Identifying the points which result from any unit transformation in the X, Y, or Z directions and taking the quotient space, creates a very interesting 3-manifold called the 3-torus. The 3-torus may also be created by identifying the opposite faces of a cube.

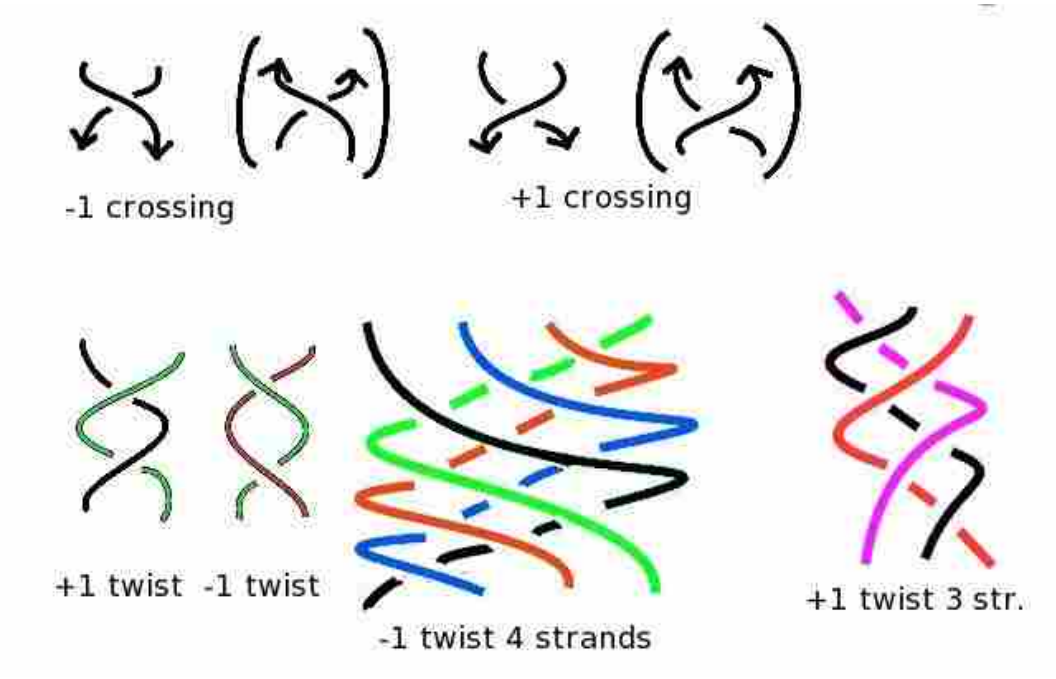

Figure 3.1: Crossings and Twists

Chapter 3. Knots and Links

We review here the notions of knots and links in preparation for Dehn surgery representations in the next chapter.

Definition 3.0.1. A *knot* is an embedding of a circle ($\mathbb{S}^1$) into $\mathbb{S}^3$. A *link* is an embedding of a finite number of circles into $\mathbb{S}^3$. The images of the individual circles are called the *components* of the link. We will assume that each component is oriented, which means that there is a preferred direction around each component indicated by an arrow.

To keep things simple, we will be dealing with smooth knots i.e., such that the embedding of $\mathbb{S}^1$ into $\mathbb{S}^3$ is smooth, avoiding so named "wild knots" which can be knotted an infinite number of times. Our pictures of Dehn surgery are links with several components, sometimes twisted about each other, and each component labeled by either a rational number or ∞

One way to analyze knots and links, is in terms of crossings and twists. At the top of Figure 3.1, we see left crossings on the left and right crossings on the right. Crossings are recognized in terms of the orientations of the segments. The crossing is assigned the number $+1$ if the top segment crosses the lower segment from left to right. The crossing is assigned the number -1 if the top segment crosses the lower segment from right to left.

Twists are independent of segment orientation. We begin with a number of segments that lie parallel to one another and twist the bundle of segments to the right or to the left some number of half or full twists. If the top segments rise to the left, the twist is called a negative twist. If they rise to the right, the twist is called a positive twist. See Figure 3.1 for examples.

Chapter 4. Representing 3-Manifolds

In this chapter we carefully define 3-manifolds, Heegaard splittings, Dehn surgery, and face pairings and their twisted versions. Unless we note otherwise, we assume a manifold to be compact, connected, and orientable. We assume that the reader is familiar with balls and spheres.

Definition 4.0.2. A *3-manifold* is a metric space M, such that each point $x \in M$ has a neighborhood $N(x)$ homeomorphic to Euclidean 3-dimensional space $\mathbb{R}^3$. A *3-manifold-with-boundary* is a metric space M such that each point $x \in M$ has a neighborhood $N(x)$ homeomorphic to closed half space $\{(x, y, z) \in \mathbb{R}^3 \mid z \geq 0\}$, or to $\mathbb{R}^3$. We define the boundary ∂M as the set of points that have no neighborhood homeomorphic to $\mathbb{R}^3$.

A *handlebody* is a 3-manifold-with-boundary formed by adding handles to a ball as in Figure 4.1. The handles are in red and the ball in green. The number of handles is called the *genus* of the handlebody. Each handle is circled by a simple closed curve that bounds a

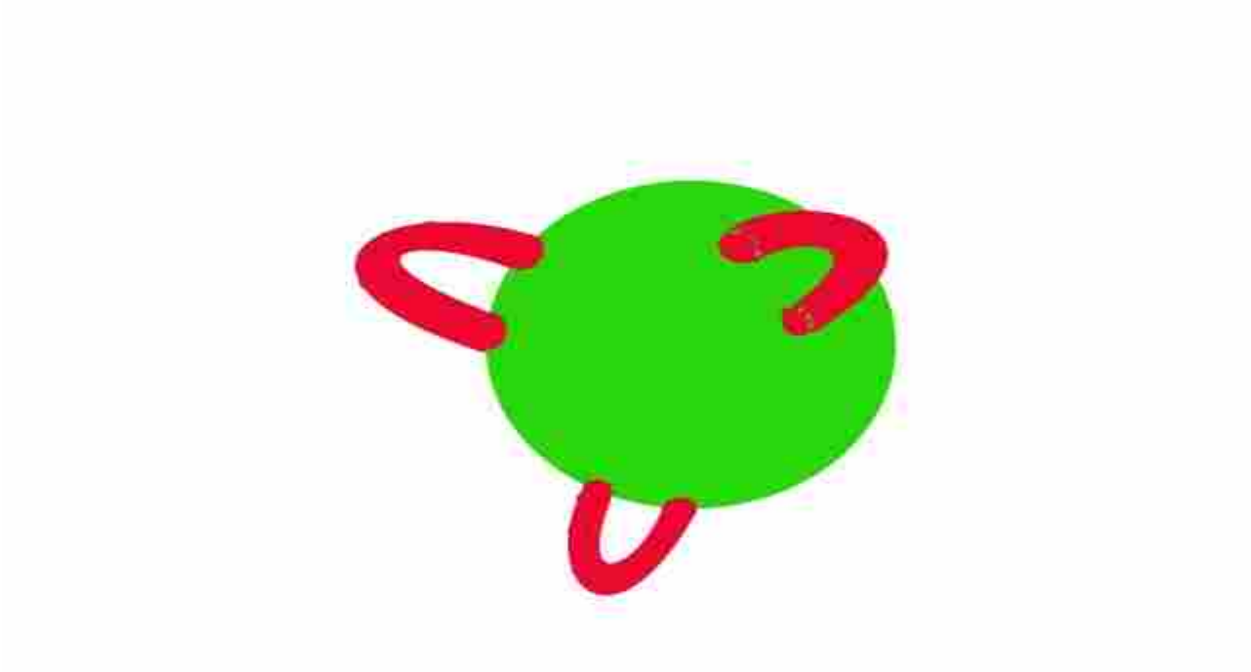

Figure 4.1: Ball with Handles

disk in the handle; such curves are called *handle curves* and the disks they bound are called *handle disks*. The handles, the handle curves, and the handle disks are highly nonunique in a handlebody. The distinguishing property of a complete family of handle disks is, that when one cuts along those disks, one obtains a topological ball.

4.1 Heegaard Splittings

Definition 4.1.1. A Heegaard splitting is a quotient space M formed from two handlebodies, H_1 and H_2 of the same genus. The equivalence relation is defined by a homeomorphism $\phi : \partial H_1 \to \partial H_2$, where two different points are equivalent if one is the image of the other under ϕ. That is, M is formed by sewing the two handlebodies together along their boundaries by a homeomorphism of their boundaries [13]. The result is always a 3-manifold.

It is an important fact that, after the identification that sews the two handlebodies

together, the resulting manifold M is completely determined, up to homeomorphism, by two sets of curves on the common boundary $\partial H_1 = \partial H_2$, namely, by a complete set of handle curves for H_1 and a complete set of handle curves for H_2. These two sets of curves comprise what is known as a *Heegaard diagram*.

4.2 Dehn Surgery

A detailed description of Dehn surgery can be found in Chapters 4 and 5 of [8] and Chapters 4, 5, and 6 of [13]. Let S denote a smooth simple closed curve in $\mathbb{S}^3$, and choose a solid torus neighborhood of S having the form $\mathbb{B}^2 \times S$, with S identified as the core $\{0\} \times S$ of the neighborhood. If we remove the interior $(\mathbb{B}^2 \setminus \partial\mathbb{B}^2) \times S$ of the neighborhood, we create a manifold M_0 with torus boundary $\partial\mathbb{B}^2 \times S$. If we then take another new solid torus $(\mathbb{B}^2 \times \mathbb{S}^1)$, which also has torus boundary, we may then identify the two boundary tori by any one of the infinitely many distinct homeomorphisms from one torus to another. The result is a (possibly new) 3-manifold M. Seldom is the new manifold homeomorphic to the original $\mathbb{S}^3$, and, consequently, the manifold M can seldom be embedded in $\mathbb{S}^3$.

To perform Dehn surgery on $\mathbb{S}^3$, we remove nice open neighborhoods $(\mathbb{B}^2 \setminus \partial\mathbb{B}^2) \times S_i$ of finitely many disjoint simple closed curves S_i to form M_0 and perform the operation of the preceding paragraph on each. The result M of this Dehn surgery depends only on the curves S_i about which the neighborhoods were formed, and the isotopy classes of the homeomorphisms that identify the torus boundaries.

Each new solid torus $(\mathbb{B}^2 \times \mathbb{S}^1)_i$ has a natural handle curve $\partial\mathbb{B}^2 \times$ point. And, in fact, M is determined by the images of these handle curves up to isotopy in ∂M_0. Each of these isotopy classes is determined by a single reduced integer fraction $r_i = p_i/q_i$ or $\infty = 1/0$. The integer p_i indicates how many times the image curve circles the image torus $\partial\mathbb{B}^2 \times S_i$ in the direction of the handle curve $\partial\mathbb{B}^2 \times \text{point}_i$ (the meridian) of the original torus $\mathbb{B}^2 \times S_i$ in $\mathbb{S}^3$. The integer q_i indicates how many times the image curve circles the image torus in the

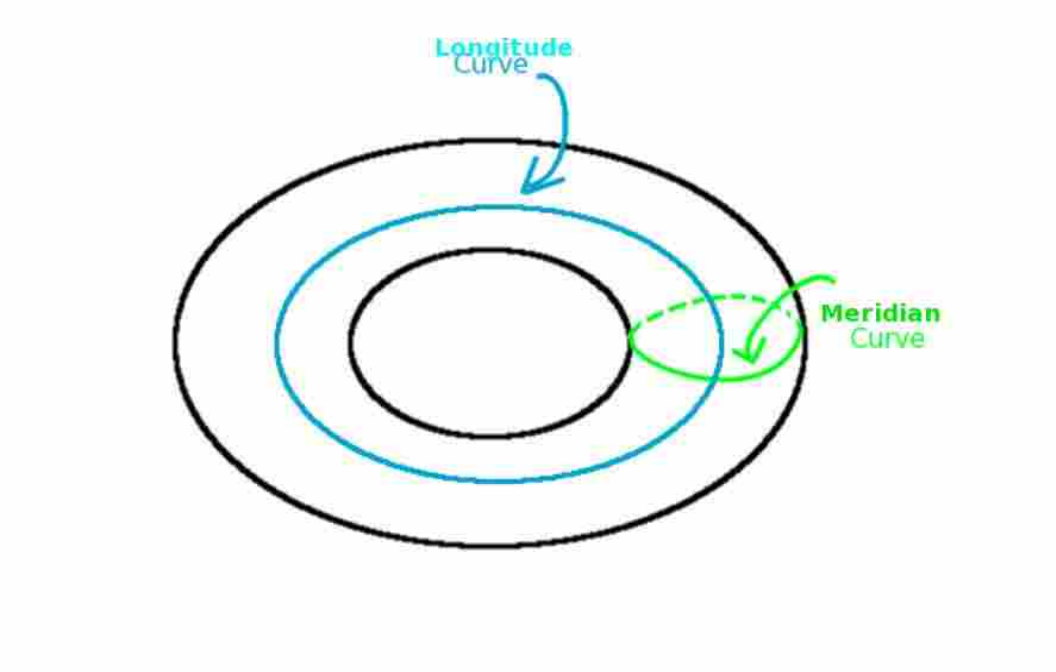

Figure 4.2: Meridian and Longitude Curves on a Torus

direction of the longitude of the original torus $\mathbb{B}^2 \times S_i$ in $\mathbb{S}^3$: the longitude is the nontrivial curve on the image torus that bounds a surface missing the interior of that torus. (The longitude is occasionally called the parallel.)

In summary, the Dehn surgery can be represented by a picture of the curves S_i with labels $r_i = p_i/q_i$.

4.3 Face Pairings, Twisted Face Pairings, and Bitwisted Face Pairings

Definition 4.3.1. A *cellulated 3-ball* or a *faceted 3-ball* is a 3-ball $\mathbb{B}^3$ together with a finite connected graph $\Gamma \subset \partial\mathbb{B}^3$ such that each complementary domain in $\partial\mathbb{B}^3$ has at least one boundary vertex and at least one boundary edge. Each complementary domain is called a *face* or *facet*. To count the number of edges on a face, walk near the boundary in the interior

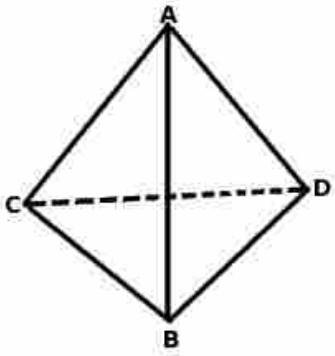

Figure 4.3: Basic Tetrahedron

of the face in the clockwise direction and count the number of edges you see. You may see and count the same edge twice from opposite sides. We will assume each edge is endowed with a linear structure, parametrized by the unit interval $[0, 1]$.

Definition 4.3.2. A *face pairing* requires a cellulated 3-ball $(\mathbb{B}^3, \Gamma)$ having an even number of faces, with the faces paired, so that both faces in a pair have the same number of edges. Then a face pairing ϵ assigns a map from each face to its partner that is an orientation-reversing homeomorphism on the interior and which pairs the boundary edges (even those counted twice) linearly. There is a natural quotient $M(\epsilon)$ created from the face pairing. Every edge e in the quotient is the image of one or more edges of the graph $\Gamma \subset \partial\mathbb{B}^2$. We call those edges of Γ that map to e equivalent. They form what is called an *edge cycle*.

In Figure 4.3 is a sample face pairing. Mappings are represented by matrices which

indicate the matching of vertices and edges.

$$1 : \begin{pmatrix} A & B & C \\ A & B & D \end{pmatrix} \qquad 2 : \begin{pmatrix} A & C & D \\ B & C & D \end{pmatrix}$$

These matrices can be used to calculate the edge cycles. The top row of a matrix lists the vertices of the face in order, clockwise or counter clockwise. The bottom row lists the vertices of the image face that are matched with the vertices directly above. Adjacent vertices label an edge, so that the matrices can be used to calculate the edge cycles, as follows.

$C_1 :\ A\ B \xrightarrow{X(1)} A\ B$ $\qquad\qquad mappings : X(1)$

$C_2 :\ B\ C \xrightarrow{X(1)} B\ D \xrightarrow{X^{-1}(2)} A\ D \xrightarrow{X^{-1}(1)} A\ C \xrightarrow{X(2)} B\ C$ $\qquad mappings : X(1)X^{-1}(2)X^{-1}(1)X(2)$

$C_3 :\ C\ D \xrightarrow{X(2)} C\ D$ $\qquad\qquad mappings : X(2)$

The symbol $X(1)$ indicates that face pairing 1 identifies edge AB with AB and BC with BD. Symbols $X^{-1}(1), X(2), X^{-1}(2)$, are used similarly. The three edge cycles calculated above are $C_1 : [AB]$, $C_2 : [BC, BD, AD, AC]$ and $C_3 : [CD]$.

This quotient space is the three sphere $\mathbb{S}^3$ [4], page 2.

For general face pairings, with probability 1 the resulting quotient $M(\epsilon)$ will not be a 3-manifold. This follows from work by Dunfield and Thurston :

2.8. Proposition [2]. *Let X be the cell complex resulting from gluing pairs of faces of n tetrahedra at random. Then the probability that X is a 3-manifold goes to 0 as $n \to \infty$.*

This difficulty is resolved by utilizing the twist and bitwist constructions [3],[4], [5], [6], [7].

Both twist and bitwist start with a face pairing and its face pairing function ϵ. We begin with the twist construction. Let the face pairing ϵ have edge cycles $C_1, \ldots, C_n$; that is, each

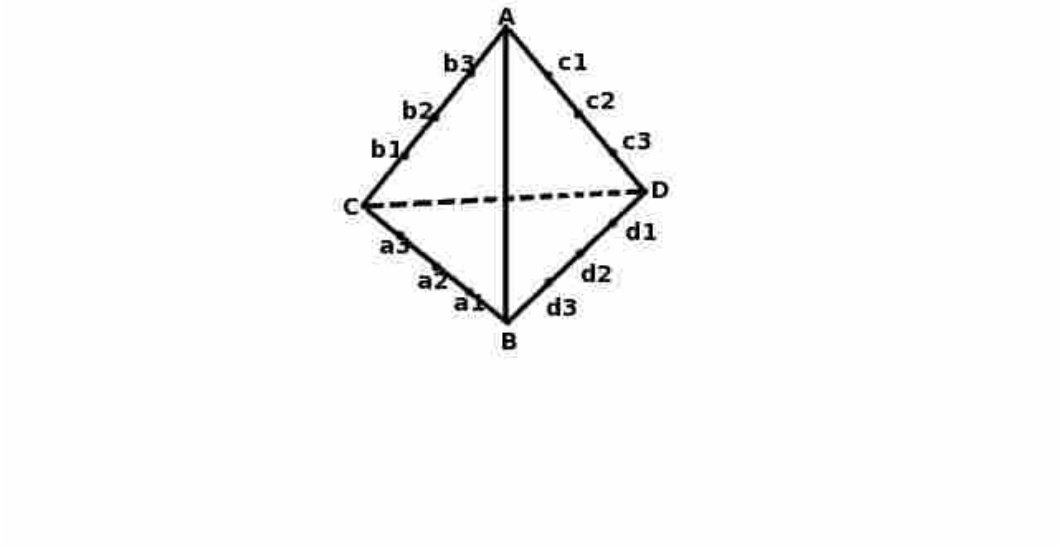

Figure 4.4: Tetrahedron Example with Subdivided Edges

C_i is a finite collection of edges of the graph Γ that are identified cyclically by the face pairing maps ϵ. Let $L(C_i)$ be the number of edges in the edge cycle C_i. Let m_i be a positive integer called a multiplier for each i. For each edge e in the edge cycle C_i, subdivide e into $m_i \cdot L(C_i)$ subedges. Do this in such a way that the face mappings respect the subdivision. Then ϵ still defines a face pairing on the subdivided graph Γ' of Γ.

Definition 4.3.3. (**Twist**)Let τ be a map defined individually on each face that takes the face to itself and advances each edge to the adjacent edge in the clockwise direction. We define a new face pairing $\epsilon \circ \tau$, called a twisted face pairing, that precedes each face mapping by the twist τ. The result $M(\epsilon \circ \tau)$ is always a 3-manifold [4].

Figure 4.4 uses the same tetrahedron example as above, but done with the twist construction

and multipliers=1. The face pairings are the following.

$$1 : \begin{pmatrix} b3 & A & B & a1 & a2 & a3 & C & b1 & b2 \\ A & B & d3 & d2 & d1 & D & c3 & c2 & c1 \end{pmatrix}$$

$$2 : \begin{pmatrix} c1 & A & b3 & b2 & b1 & C & D & c3 & c2 \\ B & a1 & a2 & a3 & C & D & d1 & d2 & d3 \end{pmatrix}$$

The new edge cycles are shown below.

$$b3\ A \xrightarrow{X(1)} A\ B \xrightarrow{X(1)} B\ d3 \xrightarrow{X^{-1}(2)} c1\ c2 \xrightarrow{X^{-1}(1)} b2\ b1 \xrightarrow{X(2)} a3\ C \xrightarrow{X(1)} D\ c3 \xrightarrow{X(2)} d1\ d2 \xrightarrow{X^{-1}(1)a2} a1 \xrightarrow{X^{-1}(2)} b3\ A$$

$$mappings : X(1)X(1)X^{-1}(2)X^{-1}(1)X(2)X(1)X(2)X^{-1}(1)X^{-1}(2)$$

$$b1\ C \xrightarrow{X(2)} C\ D \xrightarrow{X(2)} D\ d1 \xrightarrow{X^{-1}(1)} a3\ a2 \xrightarrow{X^{-1}(2)} b2\ b3 \xrightarrow{X(1)} c1\ A \xrightarrow{X(2)} B\ a1 \xrightarrow{X(1)} d3\ d2 \xrightarrow{X^{-1}(2)c2} c3 \xrightarrow{X^{-1}(1)} b1\ C$$

$$mappings : X(2)X(2)X^{-1}(1)X^{-1}(2)X(1)X(2)X(1)X^{-1}(2)X^{-1}(1)$$

It is unknown whether every compact, connected, orientable 3-manifold is a twist manifold. This possible defect is repaired by the bitwist construction.

Definition 4.3.4. (**Bitwist**) Allow the multiplier m_i to be any non-zero integer. Subdivide each edge e of edge cycle C_i into $|m_i| \cdot L(C_i)$ subedges. Rotate each edge with a positive multiplier in the clockwise direction and each edge with a negative multiplier in the counterclockwise direction, before applying ϵ; this, of course, is impossible because of the conflict between adjacent positive and negative edges. This conflict is resolved by inserting a new sticker (dangling edge) at the vertex between a negative edge followed by a positive edge in the domain of ϵ, and inserting a sticker at the vertex between a positive edge followed by a negative edge in the image domain of ϵ. The sticker in the domain splits into two edges under the pairing. The sticker in the image is the image of two edges from the domain. The

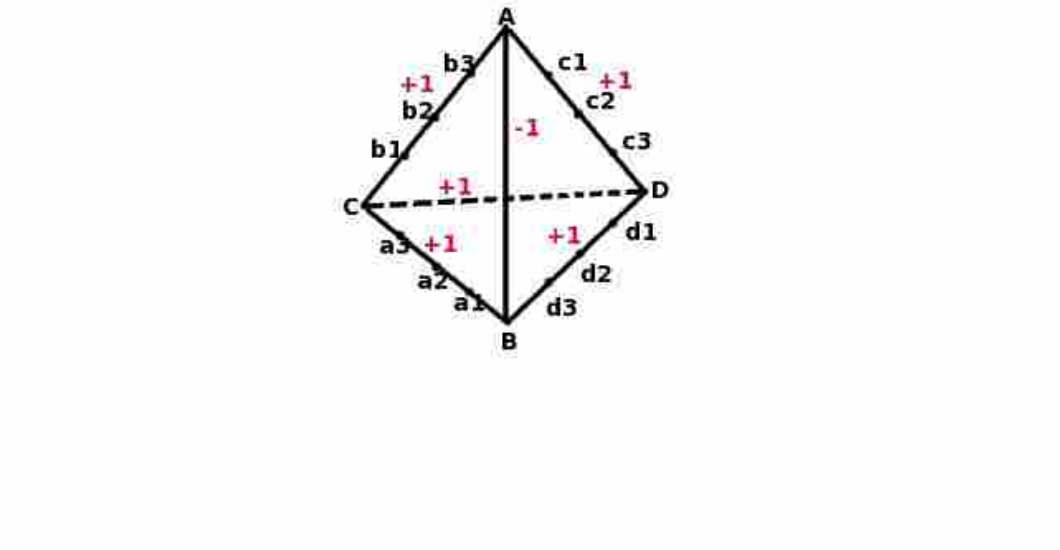

Figure 4.5: Tetrahedron Example with Bitwist Multipliers

resulting face pairing is called a *bitwist pairing*.

Figure 4.5 shows the same tetrahedron figure with subdivisions and with bitwist multipliers in red. Original edge segment AB has a -1 multiplier, all other edge segments have $+1$ multiplier. Figure 4.6 has added the necessary stickers.

The face pairings for the bitwist manifold appear below:

$$1 : \begin{pmatrix} b3 & A & B & Vb & B & a1 & a2 & a3 & C & b1 & b2 \\ A & Va & A & B & d3 & d3 & d1 & D & c3 & c2 & c1 \end{pmatrix}$$

$$2 : \begin{pmatrix} c1 & A & b3 & b2 & b1 & C & D & c3 & c2 \\ B & a1 & a2 & a3 & C & D & d1 & d2 & d3 \end{pmatrix}$$

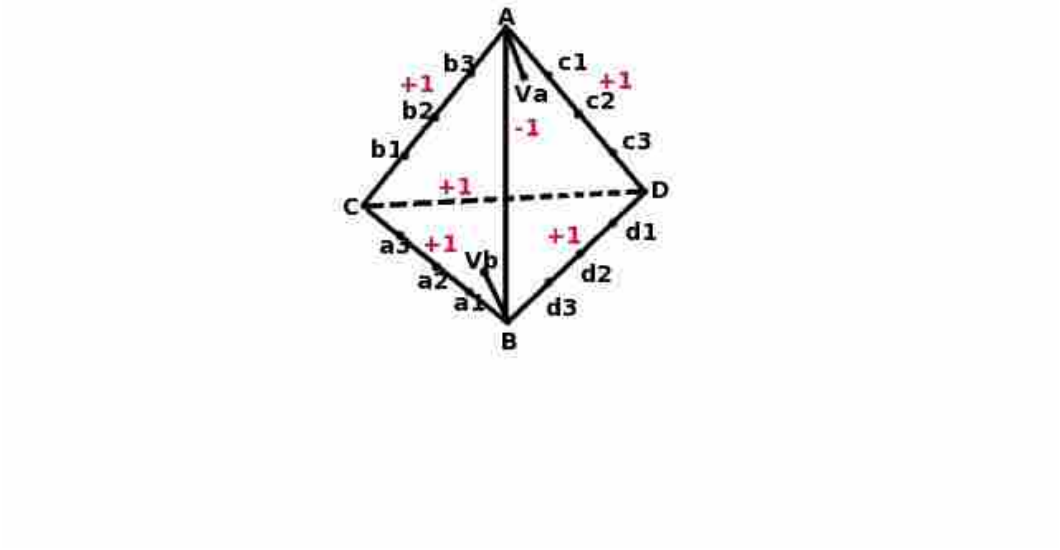

Figure 4.6: Tetrahedron with Biwist Multipliers and Stickers

Here are the new edge cycles.

$$b3\ A \xrightarrow{X(1)} A\ Va \xrightarrow{X^{-1}(1)} B\ A \xrightarrow{X^{-1}(1)} Vb\ B \xrightarrow{X(1)} B\ d3 \xrightarrow{X^{-1}(2)} c1\ c2 \xrightarrow{X^{-1}(1)} b2\ b1 \xrightarrow{X(2)} a3\ C \xrightarrow{X(1)} D\ c3 \xrightarrow{X(2)} d1\ d2 \xrightarrow{X^{-1}(1)} a2\ a1 \xrightarrow{X^{-1}(2)} b3\ A$$

$$mappings : X(1)X^{-1}(1)X^{-1}(1)X(1)X^{-1}(2)X^{-1}(1)X(2)X(1)X(2)X^{-1}(1)X^{-1}(2)$$

$$b1\ C \xrightarrow{X(2)} C\ D \xrightarrow{X(2)} D\ d1 \xrightarrow{X^{-1}(1)} a3\ a2 \xrightarrow{X^{-1}(2)} b2\ b3 \xrightarrow{X(1)} c1\ A \xrightarrow{X(2)} B\ a1 \xrightarrow{X(1)} d3\ d2 \xrightarrow{X^{-1}(2)c2} c3 \xrightarrow{X^{-1}(1)} b1\ C$$

$$mappings : X(2)X(2)X^{-1}(1)X^{-1}(2)X(1)X(2)X(1)X^{-1}(2)X^{-1}(1)$$

As we see above, there are two new edge cycles.

The result of a bitwist pairing is always a 3-manifold. Every compact connected, orientable 3-manifold is a bitwist manifold [7].

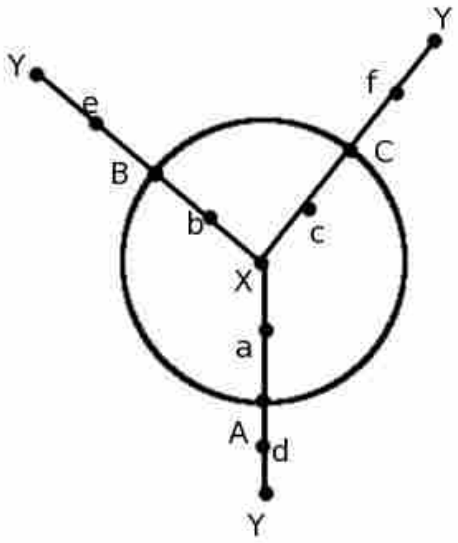

Figure 5.1: Faceted 3-Ball Q

Chapter 5. Transferring from Twisted Pairings to Heegaard Diagrams and Dehn Surgery

5.1 Twisted Pairings to Heegaard Splittings

To create the Heegaard diagram we use a method in [6]. We will construct a closed surface S and two families of curves on this closed surface to create the Heegaard diagram. To create the closed surface S, we start with Q, the faceted 3-ball with the edges subdivided as in the twist or bitwist construction. The construction of Q for an example is shown in Figure 5.1. We consider the set inside the circle as the upper hemisphere of the 2-sphere $\partial\mathbb{B}^3$. The set outside the circle, including $Y = \infty$, represents the lower hemisphere. The faces in this 3-ball in Figure 5.1 are paired by simple orthogonal projection of the three upper hemisphere faces directly down to the lower hemisphere faces.

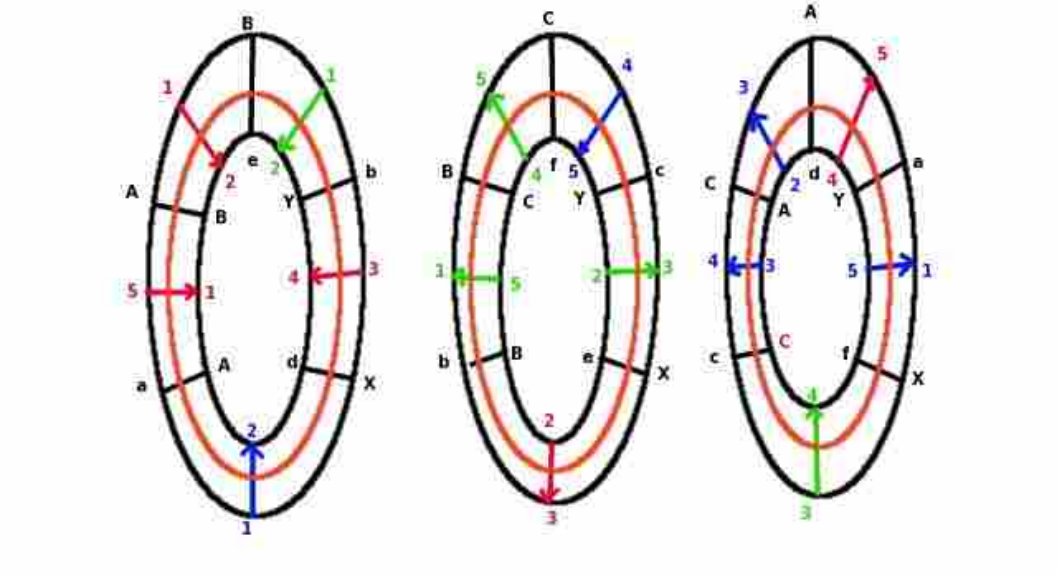

Figure 5.2: Fibonacci 3 Heegaard Diagram

We next fix a cell complex X cellularly homeomorphic to the 1-skeleton of Q. Suppose f andf^{-1} are two paired faces in Q. The twist or bitwist mapping of f to f^{-1} we call δ_f. We construct $\partial f \times [0,1]$, which we view as a 2-complex with the product cell structure. For every x in ∂f, we identify $(x,0)$ in $\partial f \times [0,1]$ with the point corresponding to x in X and we identify $(x,1)$ in $\partial f \times [0,1]$ with the point in X corresponding to $\delta_f(x)$ in ∂f^{-1}.

Doing this for every pair of faces on Q creates a cell complex Y on a closed surface. Every face of Y is a quadrilateral which we subdivide into four quadrilaterals in a straight forward way to obtain S. That is, we insert in each quadrilateral the midline from top to bottom and the midline from side to side, . We say an edge of S is vertical if it is either contained in X or is disjoint from X. We say that an edge of S is diagonal if it is not vertical. The union of vertical edges of S which are not edges of Y is a family of simple closed curves. Likewise

the union of the diagonal edges which are not edges of Y forms a family of simple closed curves. The surface of S and these two families of curves form a Heegaard diagram for our 3-manifold, which was created from the face pairings.

This construction is done in Figure 5.2. We see 3 annuli. S is created by identifying the boundary edges which have the same initial and terminal vertex. One family of curves is the three orange curves in the center of each annulus. The other family of three curves is the green, the red, and the dark blue simple closed curves transversing through all of the annuli. In the construction, X is the inside and the outside of the annuli, with the proper identifications. Y is all the black edges. Each annulus is the $\partial f \times [0,1]$ portion of S for each face f.

5.2 Twisted Pairings to Dehn Surgery Diagrams

The transition from twisted face pairings to Dehn surgery diagrams is also explained in [6]. We begin with a faceted 3-ball $(\mathbb{B}^3, \Gamma)$, face mapping ϵ, and non-zero integer multipliers m_i. These data define a twist or bitwist manifold $M(\delta)$, where δ is the collection of twist or bitwist face mappings.

In order to obtain a Dehn surgery diagram for the same manifold, we need to build a link and to label its components with appropriate rational numbers. The link will be called the *corridor complex link*. It depends only on the graph Γ and on the original face pairing ϵ and not on the multipliers or the twisted face pairing δ. The rational numbers will depend on the multipliers.

We first build a *corridor complex* as follows. We situate $\partial\mathbb{B}^3$ as the horizontal plane in Euclidean 3-space $\mathbb{R}^3$ together with the point at infinity, with the graph in the finite plane. Order the face pairs $(f_1, f_1^{-1}), \ldots, (f_n, f_n^{-1})$. Let $A_1 \subset \Gamma = \Gamma_0$ be an arc or point joining a vertex of f_1 to its image vertex in f_1^{-1}. So A_1 is an edge or vertex path connecting some vertex of f_1 to its image in f_1^{-1}. Split Γ_0 along A_1 to form a corridor joining f_1 to f_1^{-1}.

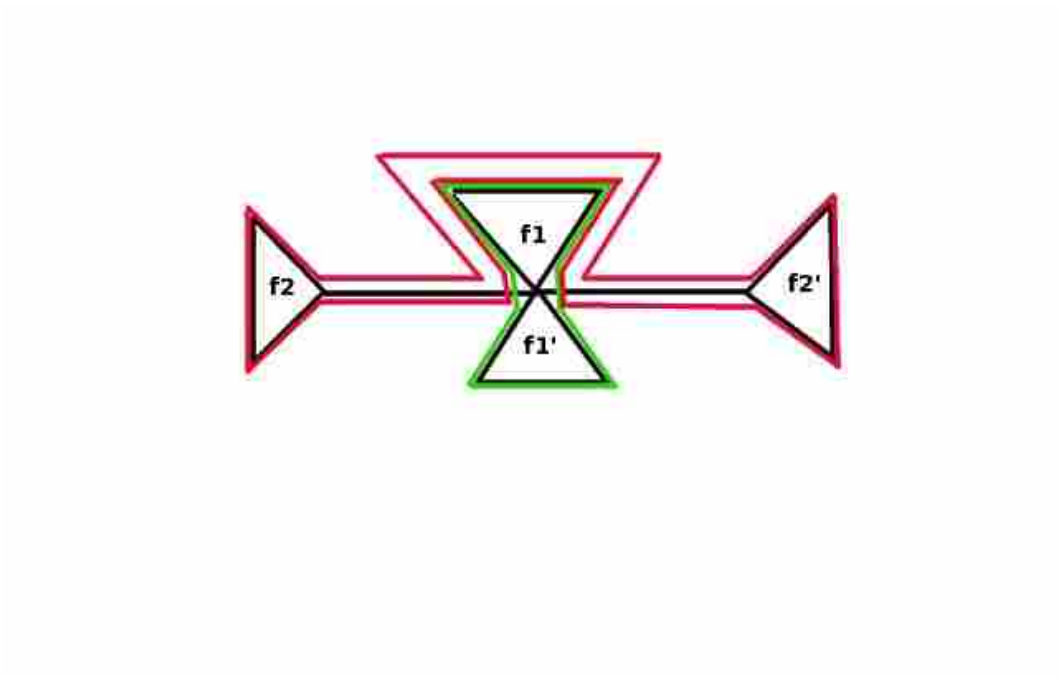

Figure 5.3: Corridor Complex Construction

See, for example, the green disk in Figure 5.3. Call the split graph Γ_1. We may think of the remaining face pairs as complementary domains of Γ_1. Let $A_2 \subset \Gamma_1$ be an arc or point joining a vertex of f_2 to its image vertex in f_2^{-1}. Split Γ_1 along A_2 to form a corridor joining f_2 to f_2^{-1}. See the red in Figure 5.3. Call this split graph Γ_2. Continue in the natural way with the remaining face pairs. The final graph Γ_n separates $\partial\mathbb{B}^3$ into n open disks. Each open disk is formed from two faces and a corridor joining them. The faces still have edges that are matched by ϵ. The first two steps in this process are shown in Figure 5.3. The first step is in green, and the second in red.

We use the corridor complex to build the *corridor complex link*. We concentrate on one disk formed from one face pair (f_i, f_i^{-1}) and its connecting corridor. The first component we construct is a vertical circle J_i that cuts through the first face f_i, orthogonal to the horizontal

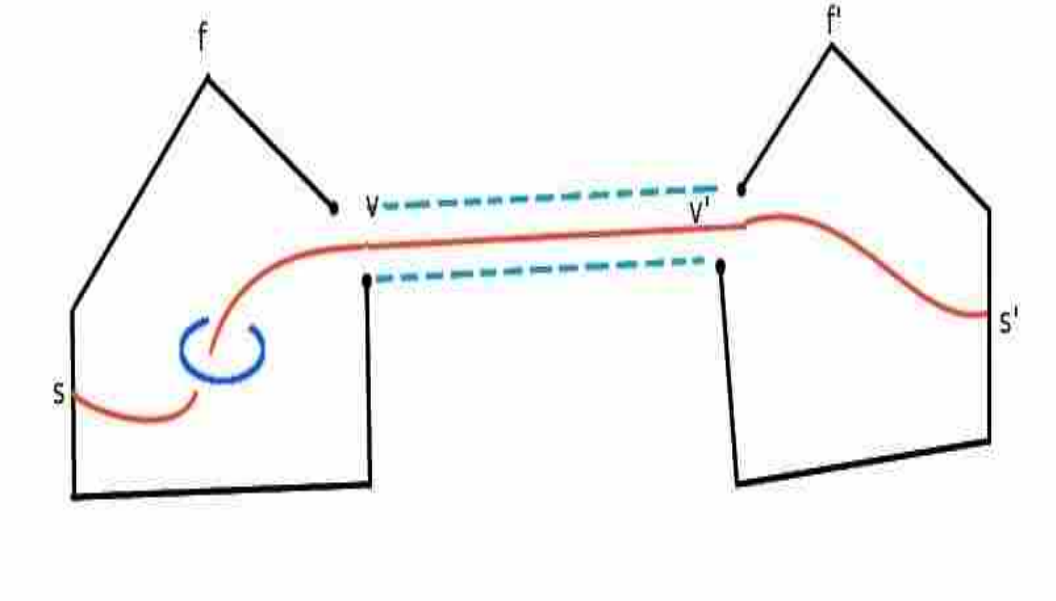

Figure 5.4: Partial Corridor Complex Link

plane, intersecting f_i at two points. This is called the *face component*. The face component is pictured in light blue in Figure 5.4. If f_i has k_i edges matched to the k_i edges of f_i^{-1} by ϵ, then we construct k_i disjoint arcs in our disk, all passing through the face component J_i in the same direction, each joining the midpoint of an edge of f_i with the midpoint of the corresponding edge of f_i^{-1}. One of these arcs is pictured in 5.4 as a red arc. If an edge has been split in forming corridors, then we extend these arcs under the corridors to meet their split partner. These arcs, as extended, meet arcs from other disks to form a family of simple closed curves called *edge components*. Each edge component corresponds exactly to an edge cycle, and joins the edges in that cycle. The corridor complex link is the union of the face components and the edge components. An example of a completed corridor complex link is in Figure 5.6.

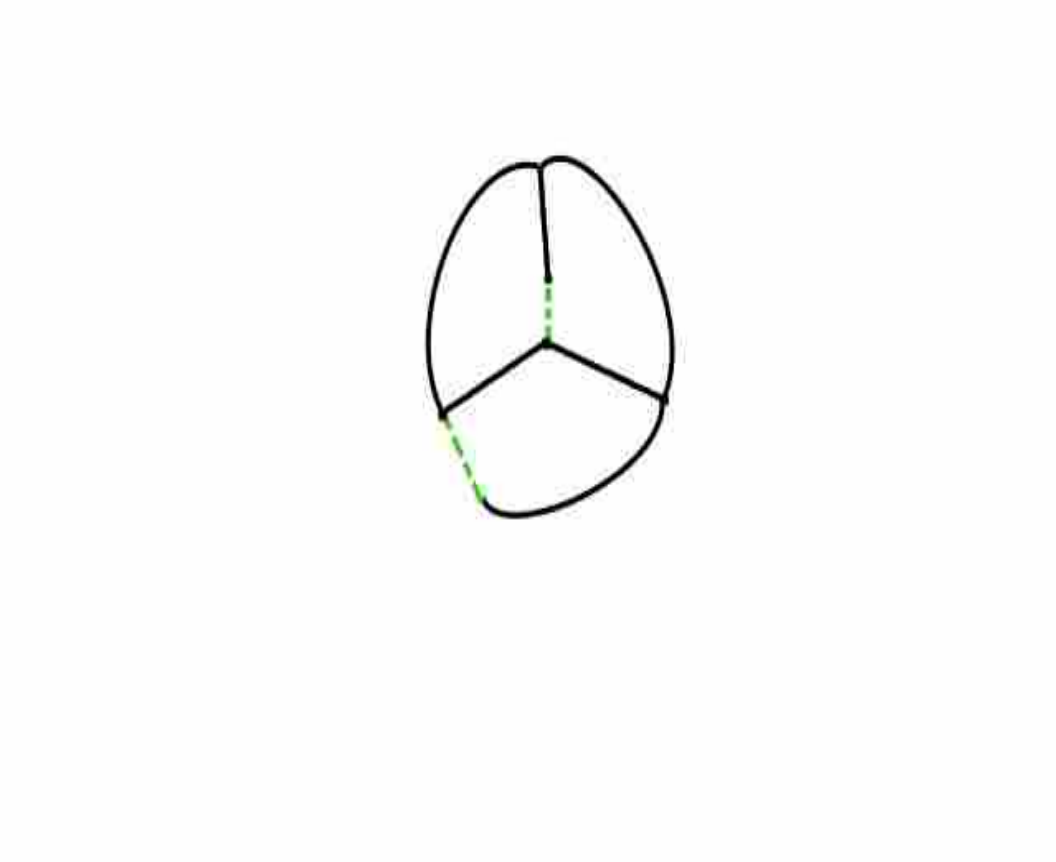

Figure 5.5: Initial Corridor Complex

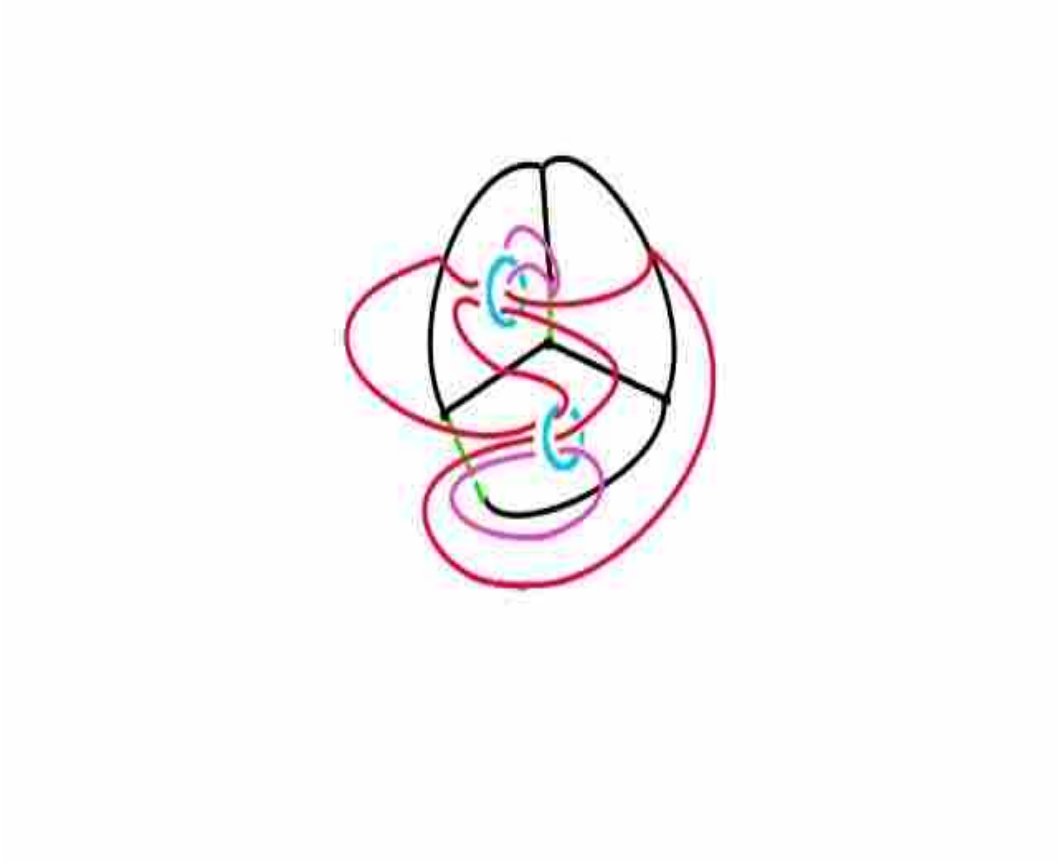

Figure 5.6: Corridor Complex Link

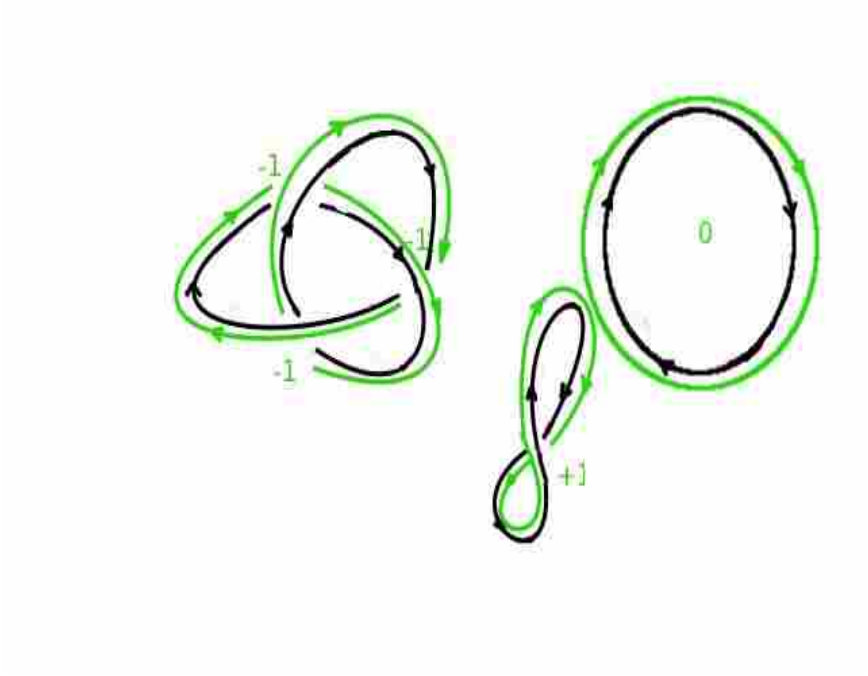

Figure 5.7: Blackboard Framing Examples

In order to complete the Dehn surgery, we need to assign rational numbers to the components. The face components are given the rational number 0. The edge component associated with edge cycle C_i is assigned the number equal to the sum of $1/m_i$ and the blackboard framing (defined below) of the edge component.

Definition 5.2.1. Let K be a smooth oriented knot in $\mathbb{S}^3$ with a normal knot projection in the xy plane. If we traverse K in the direction of the orientation, then, with the positive z direction considered to be vertical, at each point in the projection of K there is a notion of "left" and "right" which changes from point to point. Let K' be a knot formed from K by translating the point a small distance horizontally to the left of K. The knots K and K' will form the boundary of an annulus or ribbon, and the ribbon will have projection in the plane that lies flat in the plane. See Figure 5.7. Then the linking number of K with

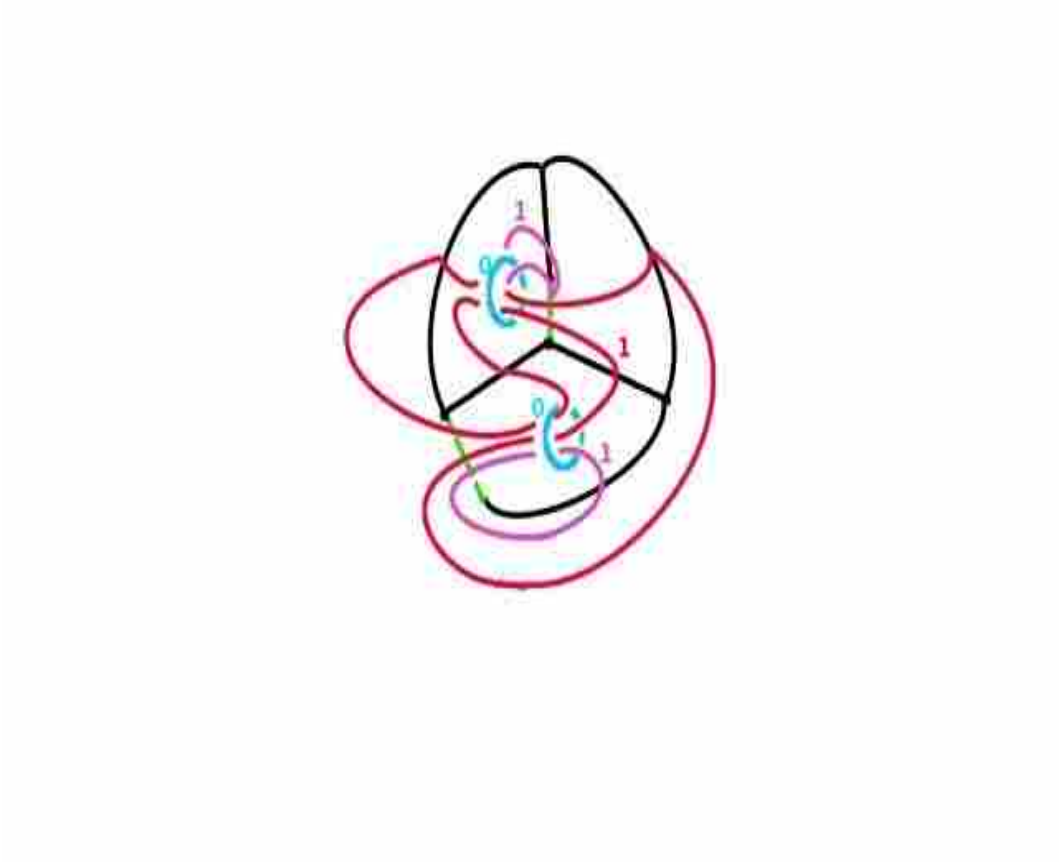

Figure 5.8: Corridor Complex Link with Surgery Coefficients

K' is called the blackboard framing of K. The linking number is calculated by adding the crossing numbers of K with K'. This number depends upon the particular knot projection of K and is not a knot invariant.

In Figure 5.7 we see on the left the blackboard framing for a particular projection of the trefoil knot which is equal to -3. The twisted unknot in the middle has a blackboard framing of +1. This knot is isotopic to the untwisted unknot on the right, which has pictured blackboard framing of 0, showing that the blackboard framing is not a knot invariant and is dependent upon the particular knot projection.

To see an example of construction of a corridor complex consider the example shown in Figure 5.5, which is a face pairing of a pyramid or 4 faceted 3-ball. The corridors between faces are degenerate corridors (split points) and are indicated by dotted green lines. Next, in Figure 5.6 we add the face and edge components to the corridor complex to complete the link. By looking at the completed link, we can see the face mappings and the edge mappings. In Figure 5.8, we add the surgery coefficients to complete the diagram.

Chapter 6. Using Face Pairings to Calculate Fundamental Group and First Homology

We start with a faceted 3-ball $(\mathbb{B}^3, \Gamma)$, face pairing maps ϵ, multipliers m_i, and twist or bitwist face pairing maps δ. There are edge cycles for ϵ and for δ.

6.1 Fundamental Group

If a face pairing maps face f_i to face f_i^{-1}, we introduce a letter $X(i) = X(f_i)$ that represents a generator for the fundamental group. The letter $X(f_i^{-1}) = X^{-1}(i)$ represents the inverse mapping from f_i^{-1} to f_i.

With each edge e in an edge cycle, and each face f_i containing that edge, we associate a word in the generators, as follows. The first letter is $X(i)$. The image of that edge is on two faces, namely f_i^{-1} and another face f_j which shares the image edge e'. The second letter will be $X(j)$. As we continue this process, we will complete the edge cycle and return to the original edge e. This completes the word $W(e, f_i)$ associated with e and the face f_i. The edge e itself is on two faces. If the second face is f_k, then the word $W(e, f_k) = W(e, f_i)^{-1}$.

This process could have been carried out with respect to ϵ with the original graph Γ, or with respect to δ and the subdivided graph Γ'. We distinguish the words by the symbols W_ϵ and W_δ. We consider the two separate cases, ϵ and δ.

Case ϵ. In this case the result $M(\epsilon)$ of the face pairing may not be a 3-manifold. However, if the vertices are deleted, we do have a noncompact 3-manifold $M_0(\epsilon)$. This 3-manifold has fundamental group with presentation

$$\pi_1(M_0) = < X(i) \mid W_\epsilon(e, f_i) > .$$

Case δ. In this case the result $M(\delta)$ is always a 3-manifold. This 3-manifold has fundamental group

$$\pi_1(M_0) = < X(i) \mid W_\delta(e, f_i) > .$$

Both of these cases are covered in [4] page 5. The calculation of these groups can be simplified first by choosing only one relator for each edge cycle.

The calculation of the relators W_δ can be further simplified by expressing them in terms of the relators W_ϵ and the multipliers m_i. We will create one relator for each face pair (f, f^{-1}). First we list the edges $e_1, \ldots, e_n$ of f in clockwise order. Define $m(e_i)$ to be the multiplier associated with the edge class containing e_i. Then the relator is

$$W_\epsilon(e_1, f)^{m(e_1)} \cdot W_\epsilon(e_2, f)^{m(e_2)} \cdots W_\epsilon(e_n, f)^{m(e_n)}.$$

6.2 First Homology

To calculate first homology, we simply abelianize the fundamental group. It is difficult to actually understand the fundamental group, but the first homology group can be completely understood. We will give examples in the work which follows.

Chapter 7. Using the Tools of Twist and Bitwist To Create Examples Of the Eight Geometries

7.1 The Three 2-Dimensional Geometries and the Eight 3-Dimensional Geometries

First of all, why are the eight 3-dimensional geometries important? These ideas are discussed by Scott in [15] as well as by Thurston in [16] and by Cannon in [1]. We saw in our example in Chapter 2 that by using translations of $\mathbb{E}^2$, and creating the quotient space, we could create a torus. All other closed orientable 2-dimensional manifolds F can be created in a similar manner, using only the spaces $\mathbb{E}^2$, $\mathbb{S}^2$, and $\mathbb{H}^2$. To do this we take X as one of the three spaces $\mathbb{E}^2$, $\mathbb{S}^2$, or $\mathbb{H}^2$ and Γ an appropriate group of isometries acting nicely (i.e. freely, cocompactly, properly discontinuously) on X, so that the quotient space of X/Γ is F. We then say that F is a closed surface *possessing a geometric structure modeled on* X.

The situation is more complicated in three dimensions. Many 3-manifolds do not possess a geometric structure. However, Thurston conjectured (*geometrization conjecture*, see [16] and [15]) that any compact orientable 3-manifold can be cut by disjoint embedded 2-spheres and tori into pieces which, after glueing 3-balls to all boundary spheres, admit geometric structures. This is apparently true as proved by Perelman in [11] and [12]. Also Thurston (see [15] and [16]) shows that if the 3-manifold admits a geometric structure, it must be one of the eight. The eight geometries are $\mathbb{E}^3$, $\mathbb{H}^3$, $\mathbb{S}^3$, $\mathbb{S}^2 \times \mathbb{R}, \mathbb{H}^2 \times \mathbb{R}$, universal cover of $SL_2\mathbb{R}$,

Nil, and Sol.

With this tool kit, without really knowing very much, one can use face pairings – untwisted, twisted, and bitwisted – on a faceted 3-ball to simply create many interesting 3-manifolds. In fact, we can easily create examples of 3-manifolds modeled on each of the eight geometries.

We will next go through each of the eight geometries and create a 3-manifold modeled on each geometry. These examples come from the papers of Cannon, Floyd, and Parry. Many of our examples will involve what they [5] call a *reflection face pairing*. We first choose a graph that subdivides the upper hemisphere of $\partial\mathbb{B}^3$ into faces, and map those faces into the lower hemisphere usually by orthogonal projection. Orthogonal projections map each face to its copy directly beneath it.

7.2 $\mathbb{E}^3$ – Three Torus and Fibonacci Manifold with n=3

The easiest way to construct a Euclidean 3-manifold is to identify opposite faces of a cube by orthogonal projection. The result is the 3-torus.

Also, we can create a Euclidean 3-manifold by a simple twist pairing. This twisted face pairing is a reflection face pairing. The top hemisphere is divided into 3 faces like large slices in a pie. See Figure 7.1. Multipliers are all 1. This manifold is the third cyclic branched cover of $\mathbb{S}^3$ branched over the figure eight knot, which is known to be Euclidean [3]. We will explain in the next chapter why we call this a Fibonacci manifold. The face pairing matrices follow the figure.

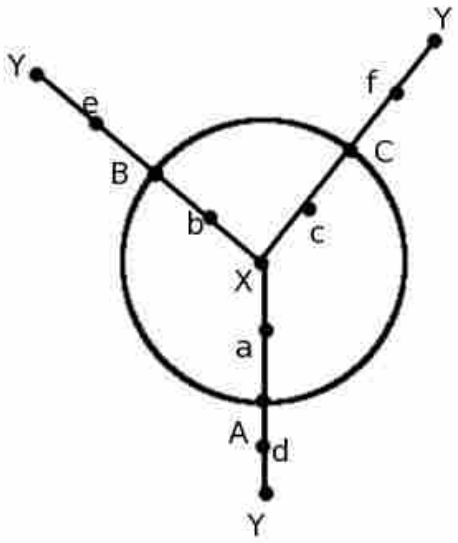

Figure 7.1: Fibonacci 3

$$\begin{pmatrix} B & b & X & a & A & B \\ e & Y & d & A & B & e \end{pmatrix}$$

$$\begin{pmatrix} C & c & X & b & B & C \\ f & Y & e & B & C & f \end{pmatrix}$$

$$\begin{pmatrix} A & a & X & c & C & A \\ d & Y & f & C & A & d \end{pmatrix}$$

Table 7.1: Fibonacci 3 Mappings

To create the Heegaard diagram, we use the method described in secton 5.1. In fact this example is the one used in the explanation of that section, and the Heegaard diagram is as created there. This construction is given again in Figure 7.2. We see 3 annuli. The Heegaard surface S is created by identifying boundary edges with the same initial and terminal vertex. One family of curves is the three orange curves in the center of each annuli. The other family of three curves is the green, the red, and the dark blue simple closed curves passing through all of the annuli. For a review of this construction see Section 5.1.

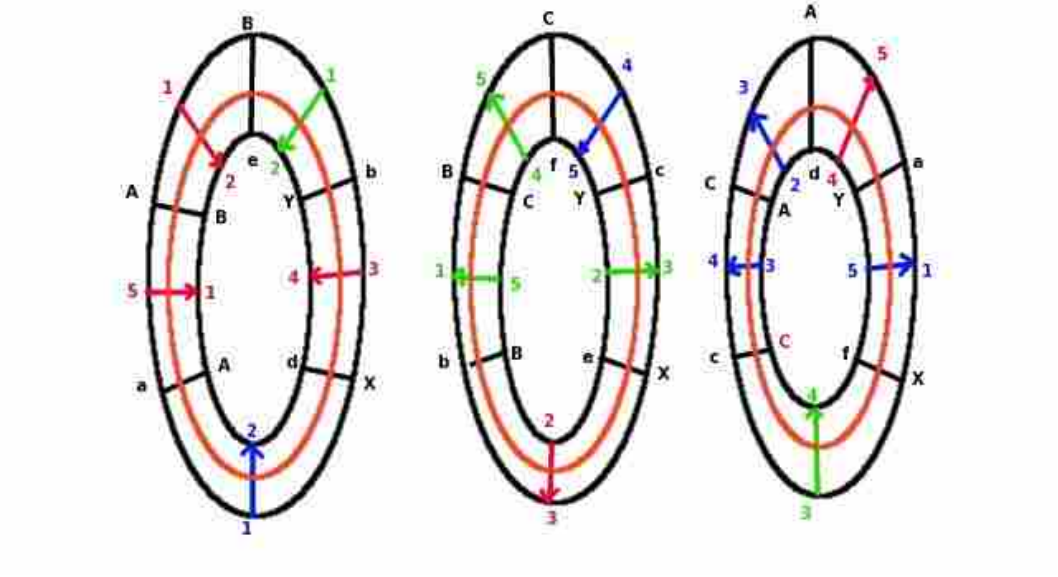

Figure 7.2: Fibonacci 3 Heegaard Diagram

To create the corridor complex link, we follow the process described in Section 5.2. The corridor complex link in this Fibonacci 3, the double pyramid, and the Sieradski 3, are all the same. The corridor complex link demonstrates how similar the basic face pairing structure can be and still result in significantly different manifolds. In Figure 7.3, the light blue circles are the face components and represent the face pairing. Each is in one of two paired faces and has a surgery factor of 0. The other simple closed curves all have surgery factors of 1, which is the twist multiplier for this Fibonacci 3 manifold. Each color orange, violet, dark blue, and green represents an edge cycle. The edges AB, BC, and CA are left fixed by the maps so the green loops become earrings on the face components.

The corridor complex link shows the relationship between the faces and gives an interesting picture of the manifold. We recall that Dehn surgery in $\mathbb{S}^3$ along these curves with

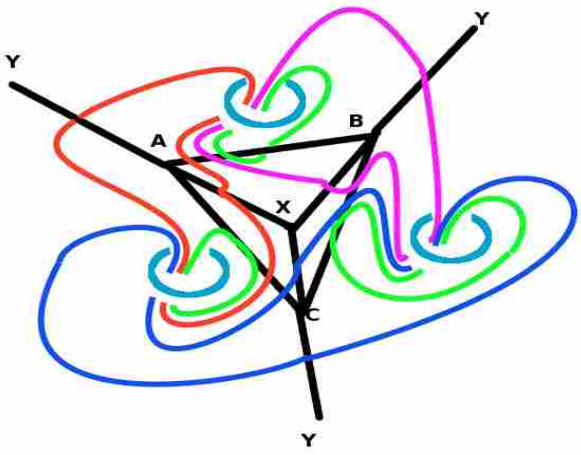

Figure 7.3: Fibonacci 3 Corridor Complex Link

the appropriate mentioned surgery factors (assigned rational numbers) produces the same manifold as the face pairing or the Heegaard splitting. We will see that three of the examples namely, Fibonacci 3, double pyramid, and Sieradski 3, all have this same original 3-ball faces and face pairing. They, however, represent three different geometries, $\mathbb{E}^3, \mathbb{H}^3, and\ \mathbb{S}^3$. The difference in the Dehn surgery is in the surgery factors (rational labels) along the components of the corridor complex link. In the bitwist or twist construction the twisting and edge subdivisions are different in the face pairing. In the Heegaard splitting, the twisting changes the way the pieces of the surface S are put together and changes the curve family paths on S.

7.3 $\mathbb{H}^3$ – Double Pyramid

To create this manifold, we start with a basic downward projection on the double pyramid. See Figure 7.4. The face pairings are shown in the matrices shown in Table 7.2. This

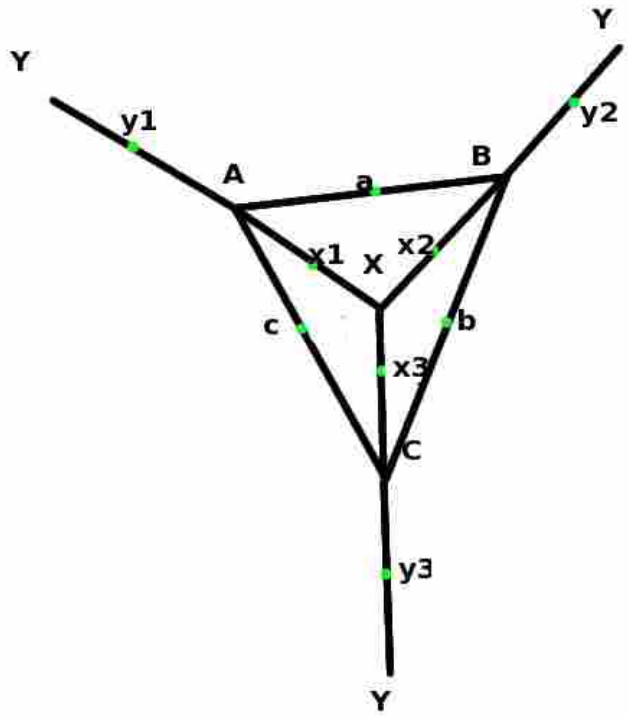

Figure 7.4: Double Pyramid

construction is the 3-ball with 3 radials top and bottom, and orthogonal or straight down projection. We have three edge cycles of length two, and three edge cycles of length one. We use multiplication factors of one on the longer cycles and a factor of two on the length one cycles. This gives us the result shown in Figure 7.4. We know this example is hyperbolic from a calculation of Bill Floyd's, involving SnapPea. Continuing with the twist construction, we use a clockwise twist on each face as shown in table 7.3.

$$\begin{pmatrix} X & A & B \\ Y & A & B \end{pmatrix}$$
$$\begin{pmatrix} X & B & C \\ Y & B & C \end{pmatrix}$$
$$\begin{pmatrix} X & C & A \\ Y & C & A \end{pmatrix}$$

Table 7.2: Basic Double Pyramid Map

$$\begin{pmatrix} X & x1 & A & a & B & x2 & X \\ y1 & A & a & B & y2 & Y & y1 \end{pmatrix}$$
$$\begin{pmatrix} X & x2 & B & b & C & x3 & X \\ y2 & B & b & C & y3 & Y & y2 \end{pmatrix}$$
$$\begin{pmatrix} X & x3 & C & c & A & x1 & X \\ y3 & C & c & A & y1 & Y & y3 \end{pmatrix}$$

Table 7.3: Twisted Double Pyramid Map

Original edge cycles:

$$X\ A \overset{X(1)}{\longrightarrow} Y\ A \overset{X^{-1}(3)}{\longrightarrow} X\ A \qquad mappings : X(1)X^{-1}(3)$$
$$X\ B \overset{X(2)}{\longrightarrow} Y\ B \overset{X^{-1}(1)}{\longrightarrow} X\ B \qquad mappings : X(2)X^{-1}(1)$$
$$X\ C \overset{X(3)}{\longrightarrow} Y\ C \overset{X^{-1}(2)}{\longrightarrow} X\ C \qquad mappings : X(3)X^{-1}(2)$$
$$A\ B \overset{X(1)}{\longrightarrow} A\ B \qquad mappings : X(1)$$
$$B\ C \overset{X(2)}{\longrightarrow} B\ C \qquad mappings : X(2)$$
$$C\ A \overset{X(3)}{\longrightarrow} C\ A \qquad mappings : X(3)$$

Next, we use the new twisted mappings to get new edge cycles, as shown below.

$X\,x1 \overset{X(1)}{\longrightarrow} y1\,A \overset{X^{-1}(3)}{\longrightarrow} A\,c \overset{X^{-1}(3)}{\longrightarrow} c\,C \overset{X^{-1}(3)}{\longrightarrow} C\,x3 \overset{X(2)}{\longrightarrow} y3\,Y \overset{X^{-1}(3)}{\longrightarrow} X\,x1$

$X(1)X^{-1}(3)X^{-1}(3)X^{-1}(3)X(2)X^{-1}(3)$

$$X\,x2\xrightarrow{X(2)}y2\,B\xrightarrow{X^{-1}(1)}B\,a\xrightarrow{X^{-1}(1)}a\,A\xrightarrow{X^{-1}(1)}A\,x1\xrightarrow{X(3)}y1\,Y\xrightarrow{X^{-1}(1)}X\,x2$$

$$X(2)X^{-1}(1)X^{-1}(1)X^{-1}(1)X(3)X^{-1}(1)$$

$$X\,x3\xrightarrow{X(3)}y3\,C\xrightarrow{X^{-1}(2)}C\,b\xrightarrow{X^{-1}(2)}b\,B\xrightarrow{X^{-1}(2)}B\,x2\xrightarrow{X(1)}y2\,Y\xrightarrow{X^{-1}(2)}X\,x3$$

$$X(3)X^{-1}(2)X^{-1}(2)X^{-1}(2)X(1)X^{-1}(2)$$

In order to go from the twist to the surgery description, we construct the corridor complex link, with appropriate surgery coefficients. The corridor complex link is shown in Figure 7.5. Figure 7.6 shows the corridor complex link removed from the 3-ball with the axis of the 3-ball remaining. Figure 7.7 shows the corridor complex link with the appropriate surgery coefficients (designated rational numbers).

The construction of the Heegaard surface and families of curves is done the same way as described in example one and appears in Figure 7.8.

7.4 $\mathbb{S}^2 \times \mathbb{R} - \mathbb{S}^2 \times \mathbb{S}^1$ Upper Lower Hemispheres as Twisted Quad's

This looks like a simple example because of the simple picture shown in Figure 7.9. It is however quite complicated and is described in [6], page 251. The construction has only one face mapping. This mapping takes the inside of the circle to the outside of the circle. Also, the map also causes the line AB to split into the the top and bottom of the circle AC. The top of AC goes to the top of CD and the bottom of AC goes to the bottom of CD.

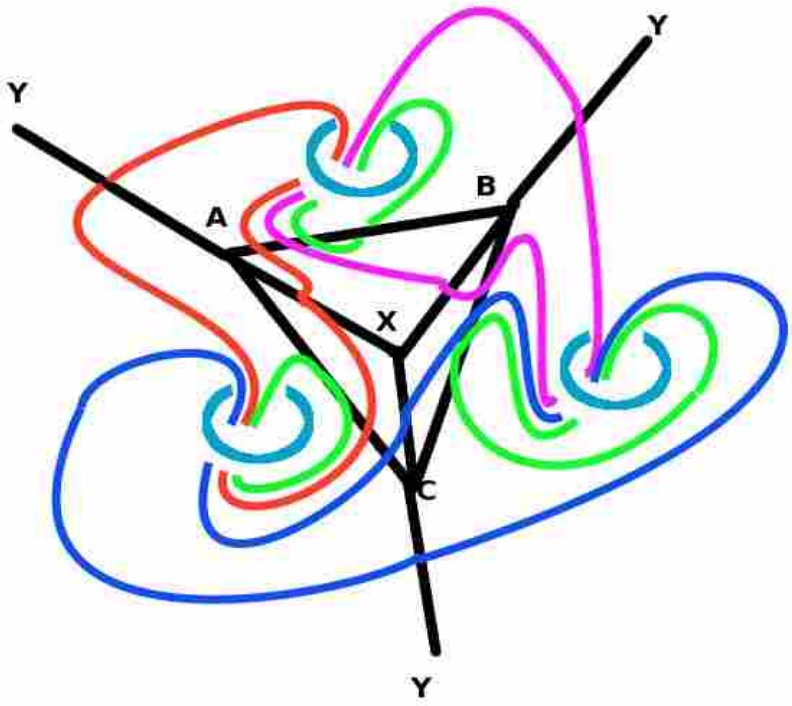

Figure 7.5: Double Pyramid Corridor Complex Link

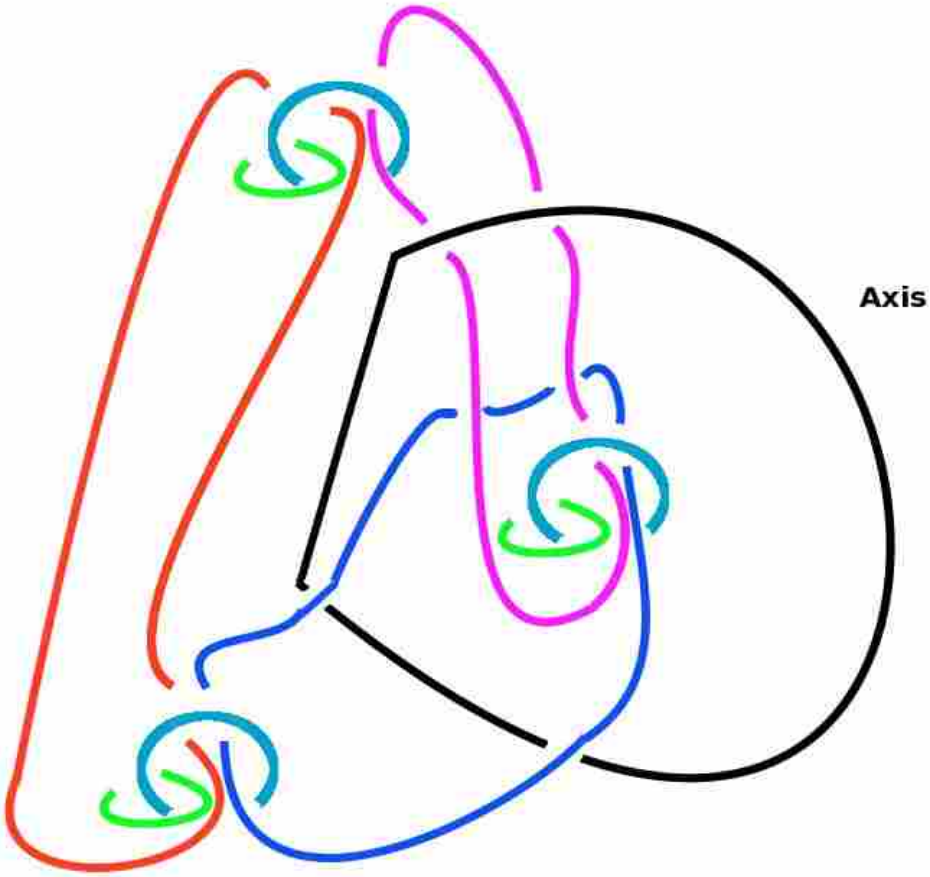

Figure 7.6: Double Pyramid Corridor Complex Link with Axis

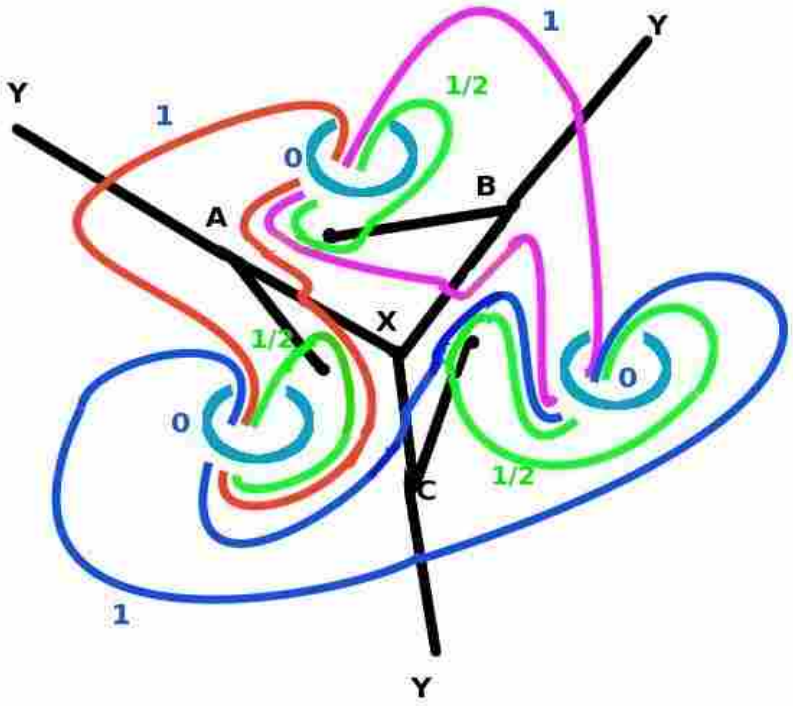

Figure 7.7: Double Pyramid Corridor Complex Link with Surgery Coefficients

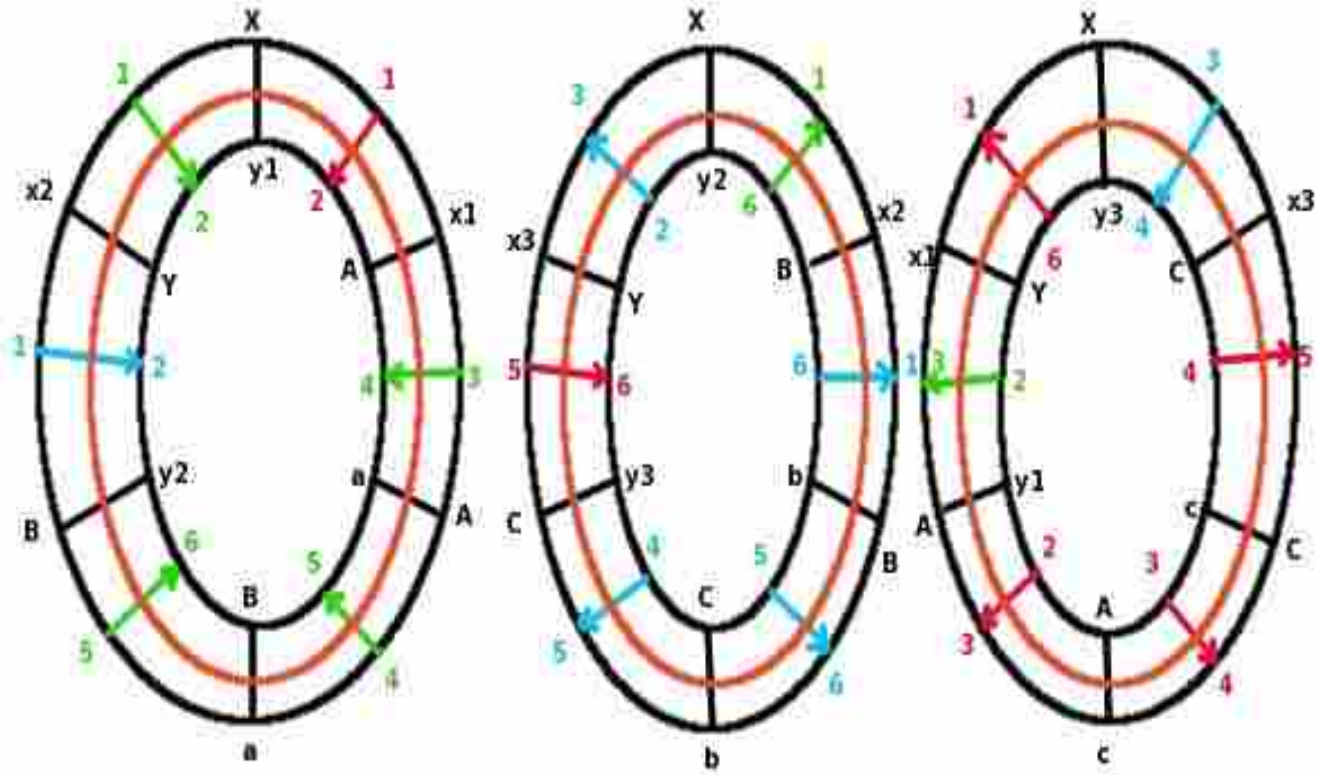

Figure 7.8: Double Pyramid Edge Heegaard Surface

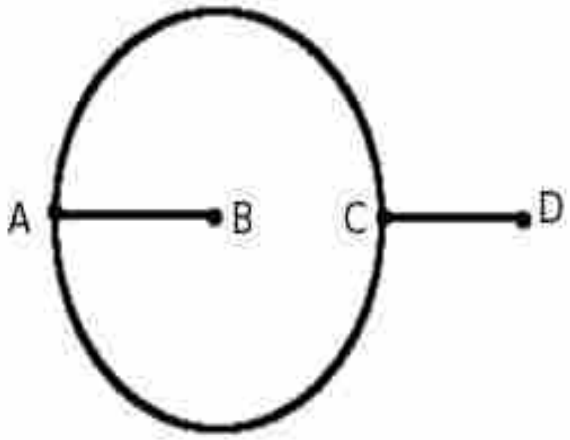

Figure 7.9: Twisted Quadrilaterals on 3-Ball

We apply a multiplier of one. Since the one edge cycle has length 4, we follow the twist construction and subdivide each edge into 4 segments as shown in Figure 7.10. The circle and its interior in Figure 7.9 form the top hemisphere of a 3-ball. The corridor complex link is in Figure 7.11. The surgery coefficient for the face component in blue is 0. The other red edge component has coefficient 1. The Heegaard diagram is in Figure 7.12.

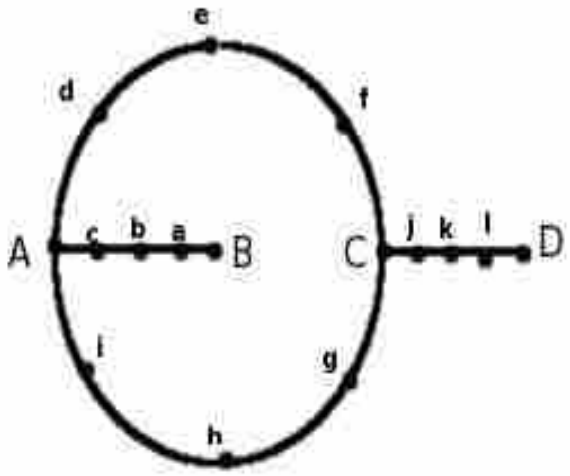

Figure 7.10: Twisted Quadrilaterals with Edges Subdivided

$$\begin{pmatrix} B & a & b & c & A & d & e & f & C & g & h & i & A & c & b & a & B \\ d & e & f & C & j & k & l & D & l & k & j & C & g & h & i & A & d \end{pmatrix}$$

Table 7.4: Adjusted Twisted Quads Mapping

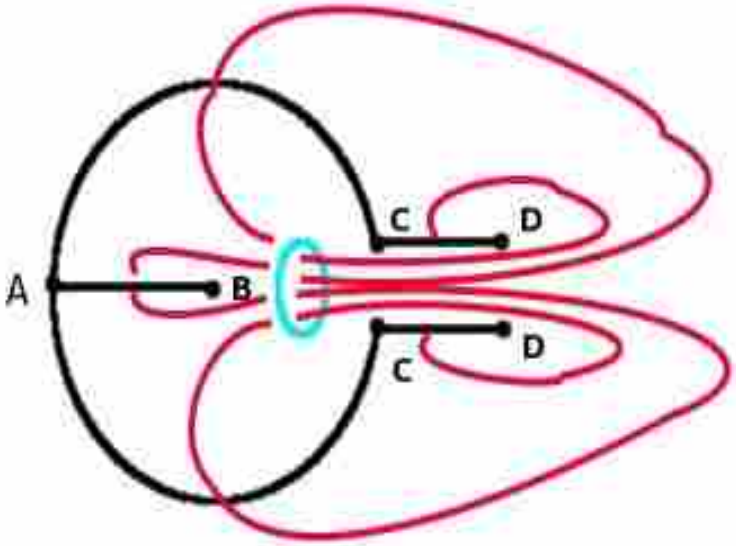

Figure 7.11: Corridor Complex Link on Twisted Quadrilaterals

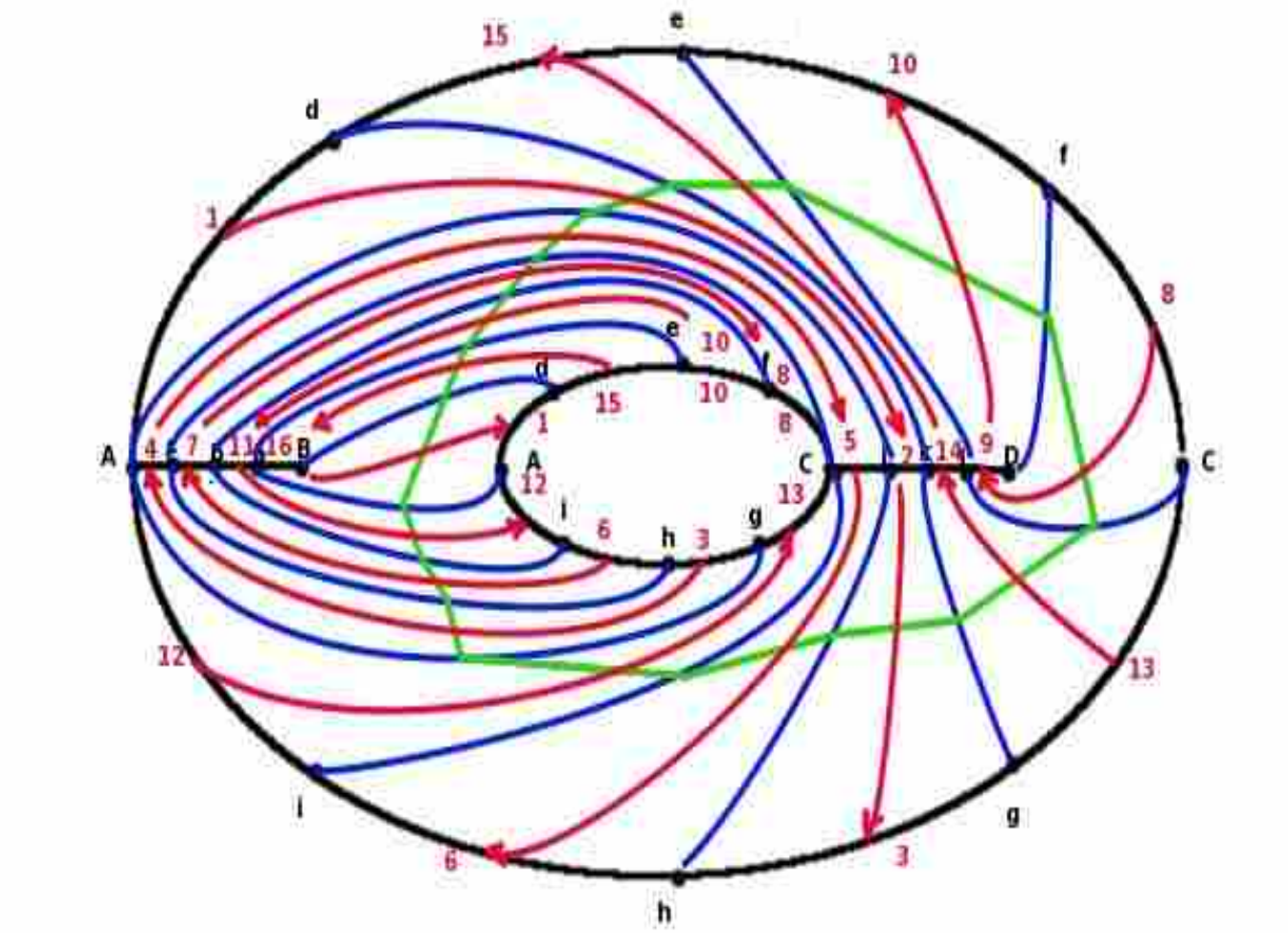

Figure 7.12: Twisted Quadrilaterals Heegaard Diagram

7.5 $\mathbb{S}^3$ – Sieradski with 3 Radials

The reason we call this 3-manifold Sieradski will become clear in chapter eight. This construction is another example of a reflection face pairing with three radials in the top hemisphere making three equal pie-shaped faces. The difference in this 3-pie upper hemisphere

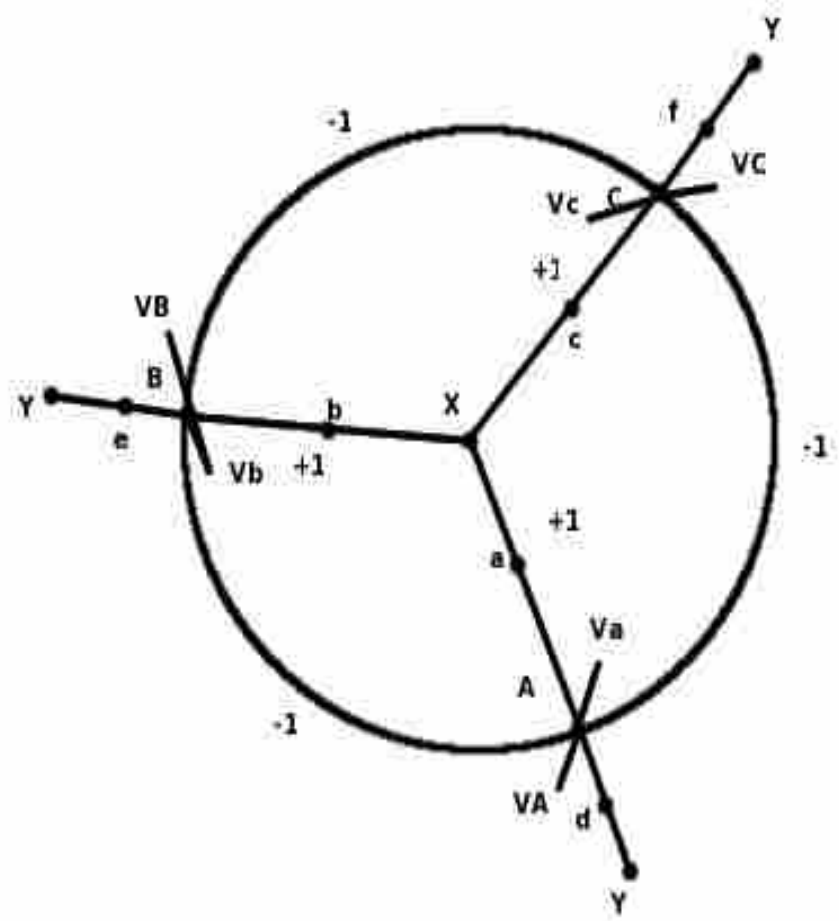

Figure 7.13: Sieradski 3 Faces

construction is that this construction is bitwist with a -1 multiplier on the circle edges and +1 elsewhere [3]. This construction of the 3-ball is shown in Figure 7.13. The adjusted mappings are shown in Table 7.5. The Heegaard diagram is constructed as before and shown in Figure 7.14. The corridor complex link is the same as the double pyramid and is shown in Figure 7.6. The corridor complex link with coefficients is shown in Figure 7.15

$$\begin{pmatrix} Vb & B & b & X & a & A & B & Vb \\ B & e & Y & d & A & VA & A & B \end{pmatrix}$$

$$\begin{pmatrix} Vc & C & c & X & b & B & C & Vc \\ C & f & Y & e & B & VB & B & C \end{pmatrix}$$

$$\begin{pmatrix} Va & A & a & X & c & C & A & Va \\ A & d & Y & f & C & VC & C & A \end{pmatrix}$$

Table 7.5: Adjusted Sieradski 3 Mappings

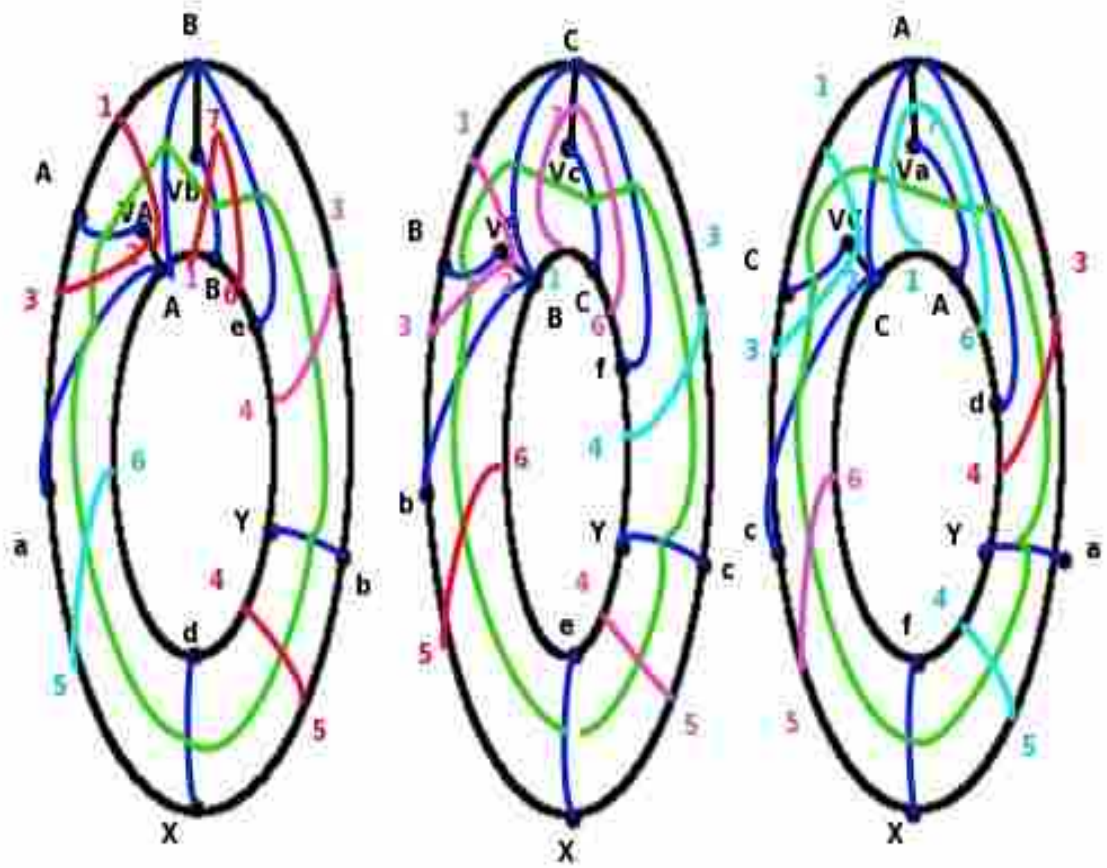

Figure 7.14: Sieradski 3 Heegaard Diagram

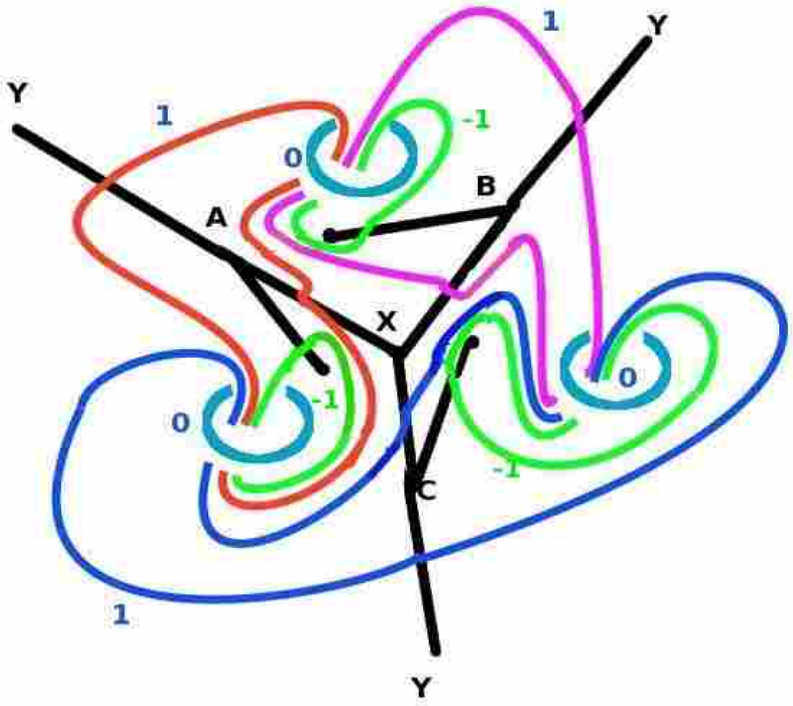

Figure 7.15: Sieradski 3 Corr. Complex Link with Coefficients

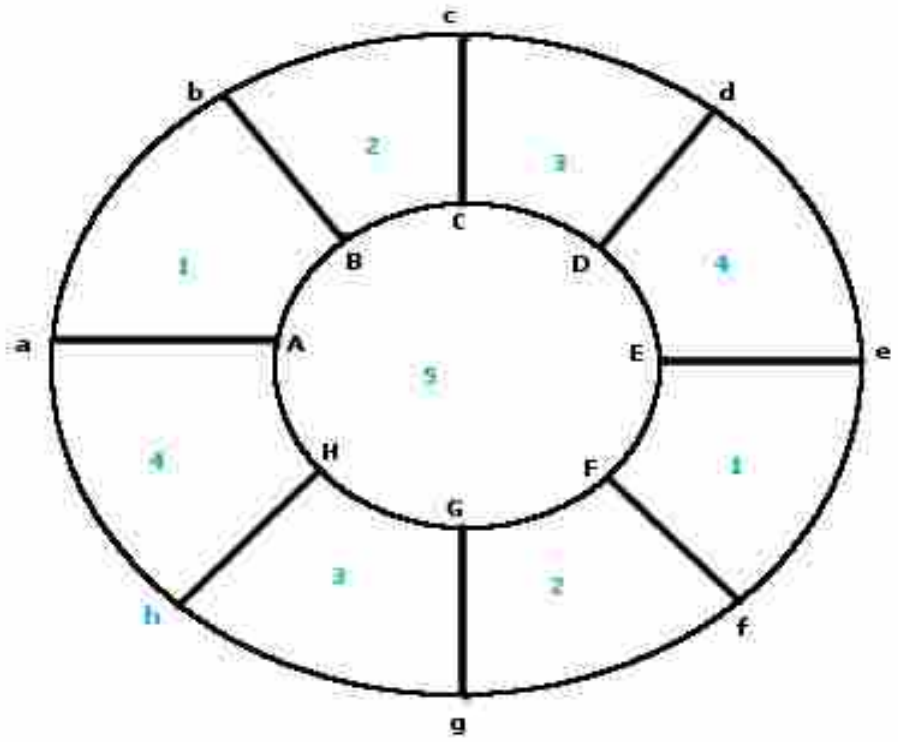

Figure 7.16: Genus 2 Surface $\times\mathbb{S}^1$

7.6 $\mathbb{H}^2 \times \mathbb{R}$ – Genus 2 Surface $\times S^1$

We originally create the genus 2 torus $\times S^1$ by pairing opposite edges of a 8-sided disc and then producting this with $\mathbb{S}^1$, as shown in Figure 7.16. This gives us the five mappings in Table 7.6.

$$\begin{pmatrix} a & b & B & A \\ f & e & E & F \end{pmatrix}$$
$$\begin{pmatrix} b & c & C & B \\ g & f & F & G \end{pmatrix}$$
$$\begin{pmatrix} c & d & D & C \\ h & g & G & H \end{pmatrix}$$
$$\begin{pmatrix} d & e & E & D \\ a & h & H & A \end{pmatrix}$$
$$\begin{pmatrix} A & B & C & D & E & F & G & H \\ a & b & c & d & e & f & g & h \end{pmatrix}$$

Table 7.6: Genus 2 Surface $\times\mathbb{S}^1$

$ab \xrightarrow{X(1)} fe \xrightarrow{X^{-1}(5)} FE \xrightarrow{X^{-1}(1)} AB \xrightarrow{X(5)} ab$

$bc \xrightarrow{X(2)} gf \xrightarrow{X^{-1}(5)} GF \xrightarrow{X^{-1}(2)} BC \xrightarrow{X(5)} bc$

$cd \xrightarrow{X(3)} hg \xrightarrow{X^{-1}(5)} HG \xrightarrow{X^{-1}(3)} CD \xrightarrow{X(5)} cd$

$de \xrightarrow{X(4)} ah \xrightarrow{X^{-1}(5)} AH \xrightarrow{X^{-1}(4)} DE \xrightarrow{X(5)} de$

$Aa \xrightarrow{X(1)} Ff \xrightarrow{X^{-1}(2)} Cc \xrightarrow{X(3)} Hh \xrightarrow{X^{-1}(4)} Ee \xrightarrow{X^{-1}(1)} Bb \xrightarrow{X(2)} Gg \xrightarrow{X^{-1}(3)} Dd \xrightarrow{X(4)} Aa$

Reviewing the vertices, from mapping 5 in Table 7.6, all lower case letters map to the corresponding upper case letters. The last edge cycle shows all letters are related. Hence, all vertices are equivalent. Since we have five faces, five edge cycles, one 3-ball, and one vertex, the Euler characteristic is 0 and this construction makes a 3-manifold.

7.7 Universal Cover of $SL(2\,R)$ – Sieradski Manifold with Seven Radials

This is also known as the Brieskorn manifold M(2,3,7) [3] [9]. To construct this manifold, we use the same constructions as Sieradski 3, except there are 7 pie pieces in the top hemisphere. This is described as a $SL(2,\mathbb{R})$ universal cover in [3].

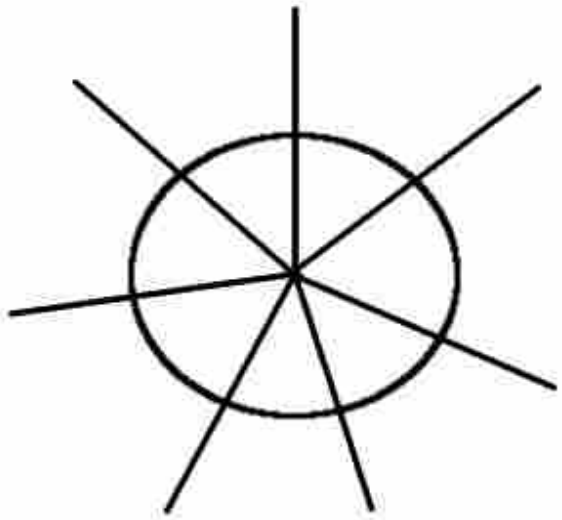

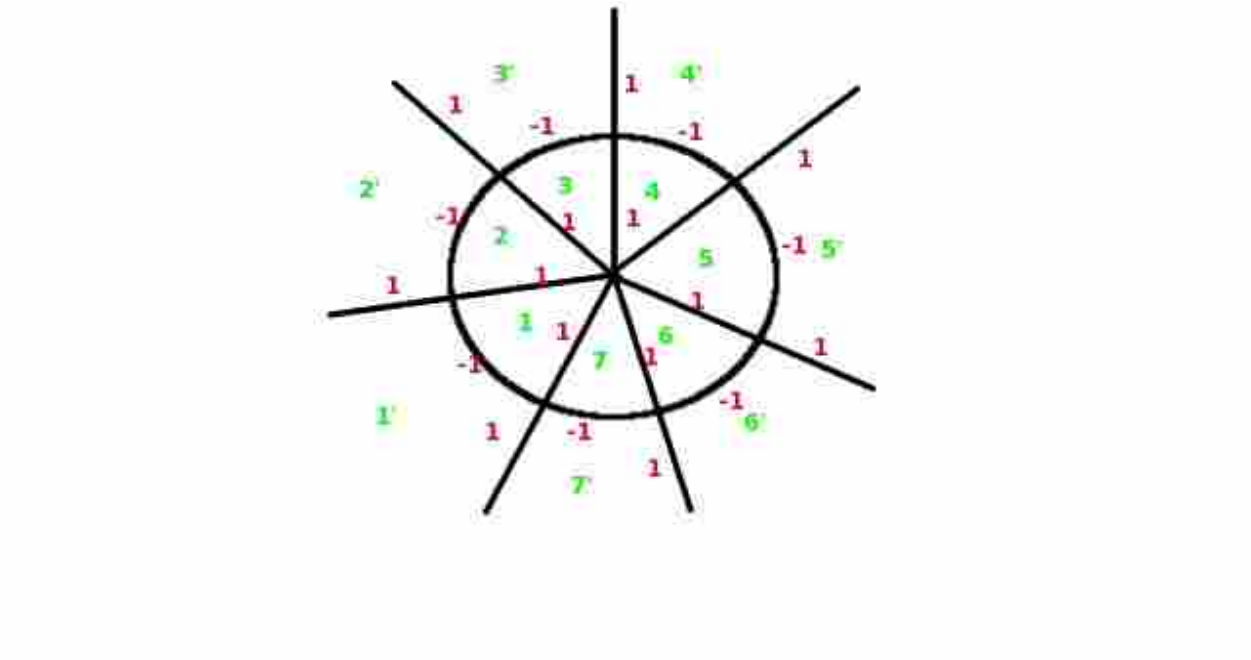

$SL(2,\mathbb{R})$ manifold

The face identifications are shown in green and the multipliers in red.

7.8 NIL – Heisenberg Manifold– Four Digons

To construct this 3-manifold we use an example of the twist construction on a 3-ball, with multiplier of 1. This manifold may also be obtained by Dehn surgery on the Borromean rings with framings (0,0,1)[5], page 30. We start with a face pairing of 4 digons, called lunes shown in Figure 7.17 and 7.18. We take the 3-ball centered at (0,0,0) in $\mathbb{E}^3$. There are two vertices (0,0,1) and (0,0,-1). The orientation reversing mapping ϵ takes each face to its direct opposite. The vertices are unchanged by ϵ. We use a multiplier of 1 on all edge cycles. Since there is only one edge cycle including all four edges, we subdivide each edge into four segments as shown in Figure 7.19. We then apply the twist construction to get mappings shown in Table 7.7. The Heegard surface and diagram are shown in Figures

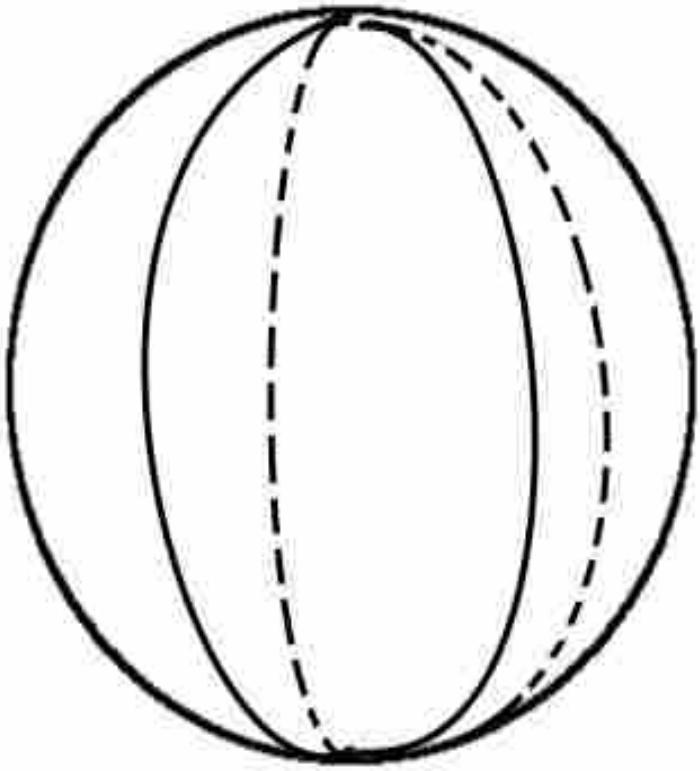

Figure 7.17: Heisenberg Four Lunes 3-Ball

7.20 and 7.21. The colors and number references are the same in both the Heegaard surface and the Heegard diagram. The violet circles are one family of curves and the red and green closed curves form the other family of curves in the Heegard splitting. The corridor complex link is shown in Figure 7.22. The surgery factors for the green face components are 0. The surgery factor for the red edge cycle component is 1.

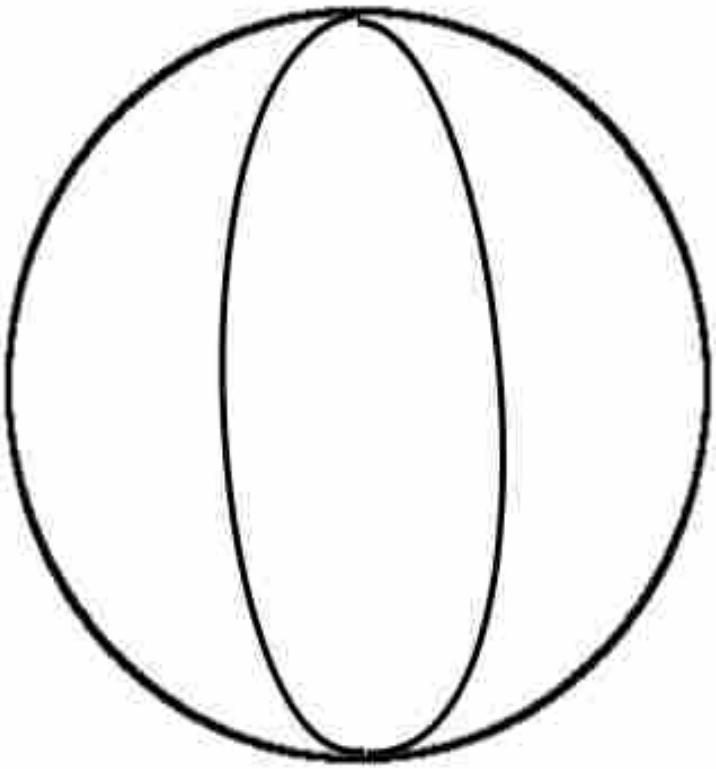

Figure 7.18: Heisenberg 4th Lune as Outside

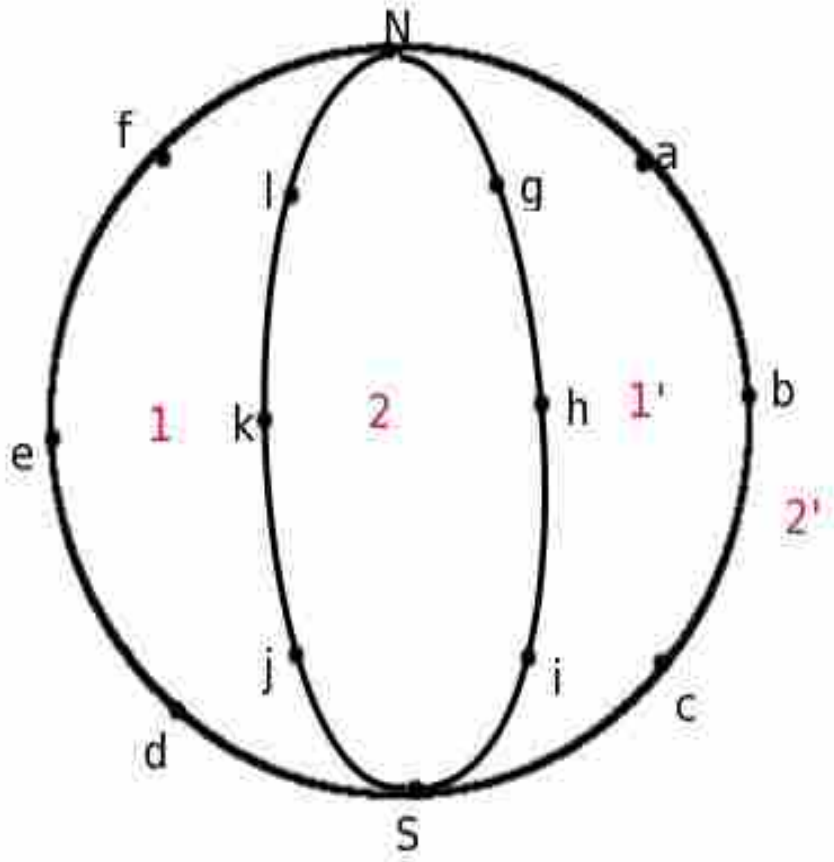

Figure 7.19: Heisenberg Subdivided with Face Mappings

$$\begin{pmatrix} N & l & k & j & S & d & e & f & N \\ g & h & i & S & c & b & a & N & g \end{pmatrix}$$
$$\begin{pmatrix} N & g & h & i & S & j & k & l & N \\ a & b & c & S & d & e & f & N & a \end{pmatrix}$$

Table 7.7: Adjusted Heisenberg Mappings

7.9 SOL - Two Digons and One Triangle on Each Hemisphere

To create this Solv manifold we start with a simple Northern and Southern hemispheres of a 3-ball with the faces divided as in Figure 7.23.

For the face pairing we take the simple downward projection, which leaves all segments on the equator unchanged with edge cycle length as 1. This is another example of a reflection face pairing. The two segments passing through the interior of the upper hemisphere have edge cycle length 2. Following the twist construction, we subdivide each segment into (edge cycle length)×(edge cycle multiplier) subsegments. To make this construction a Sol manifold, we choose all multipliers to be 2 except a 1 for the segment from B to C on the equator. This gives the 3-ball shown in Figure 7.24 with the appropriate edge subdivisions. The Southern hemisphere center has been taken to ∞. The corridor complex link can now be constructed since we know the face pairings and the multipliers. The corridor complex link is shown in Figure 7.25.

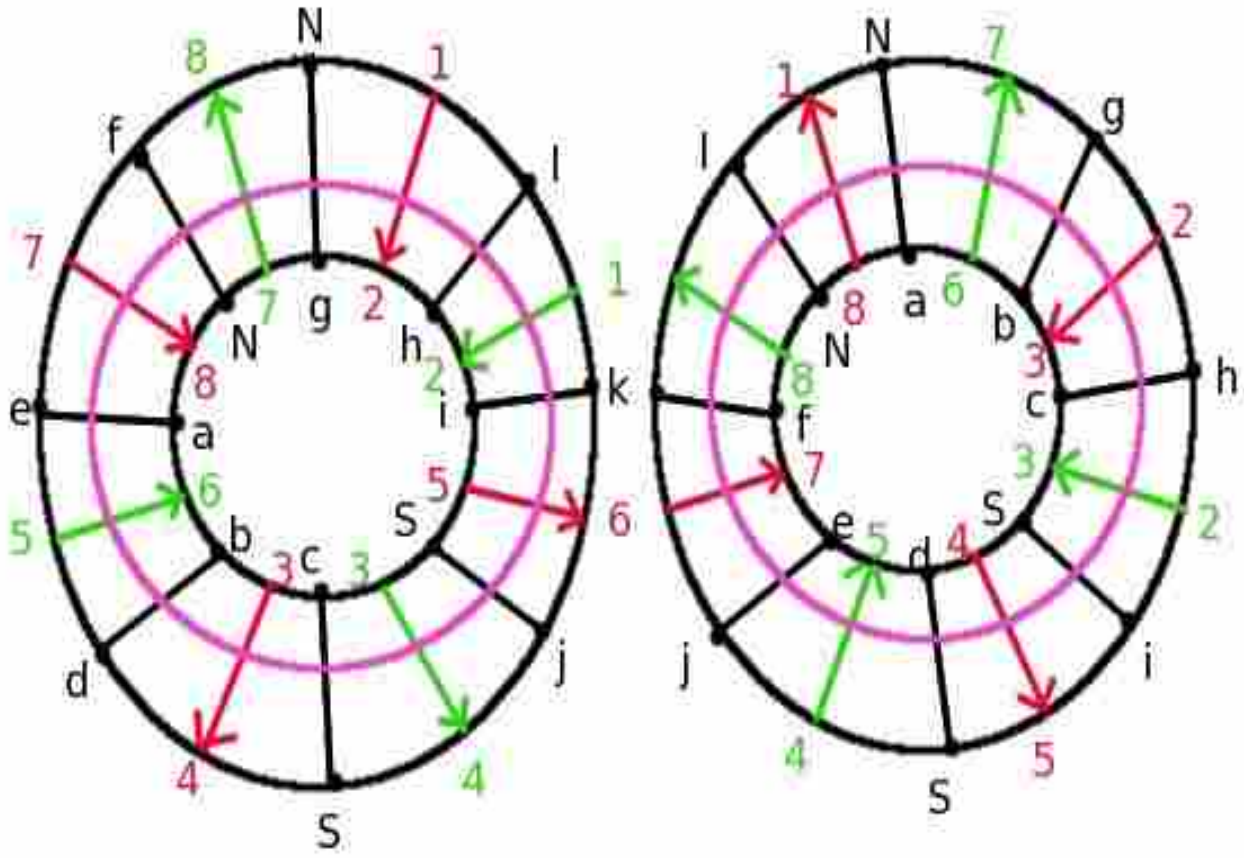

Figure 7.20: Heisenberg Heegaard Diagram

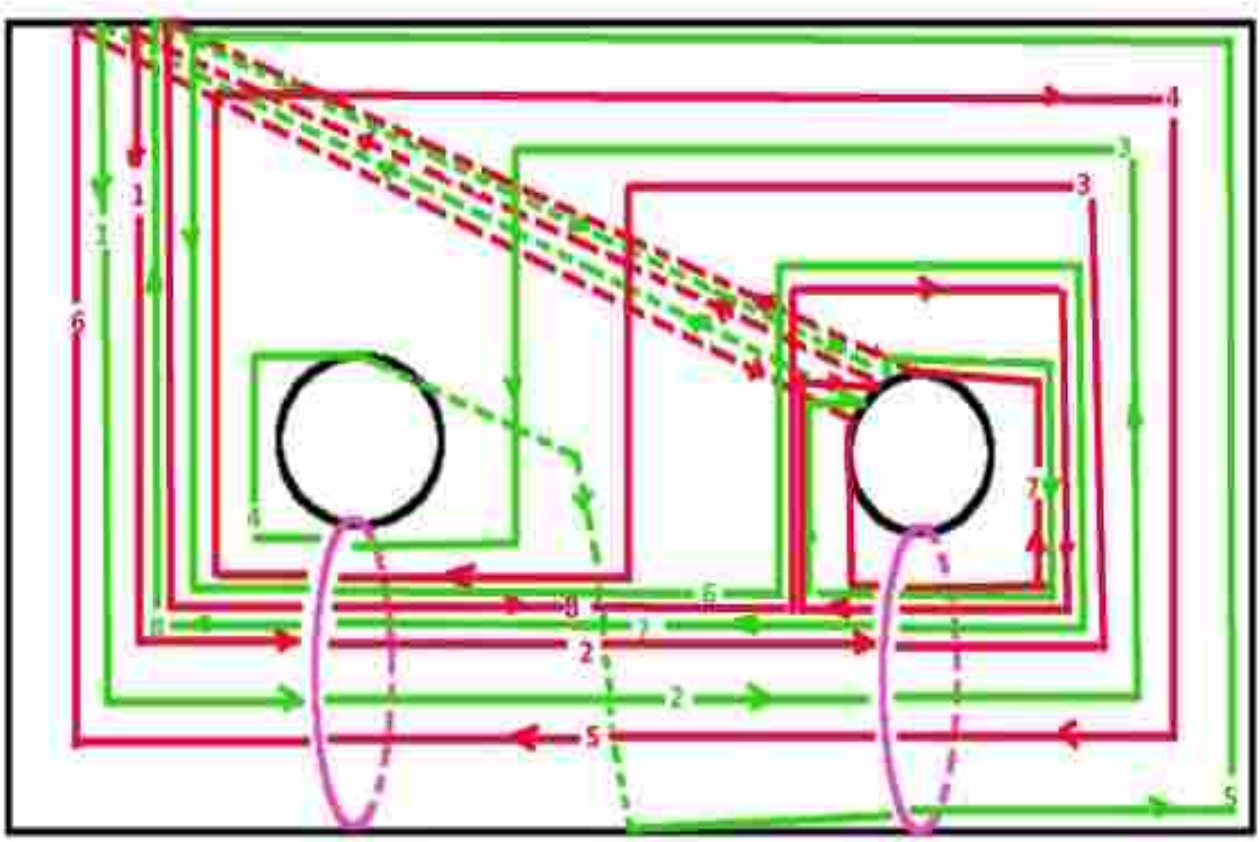

Figure 7.21: Heisenberg Heegaard Surface

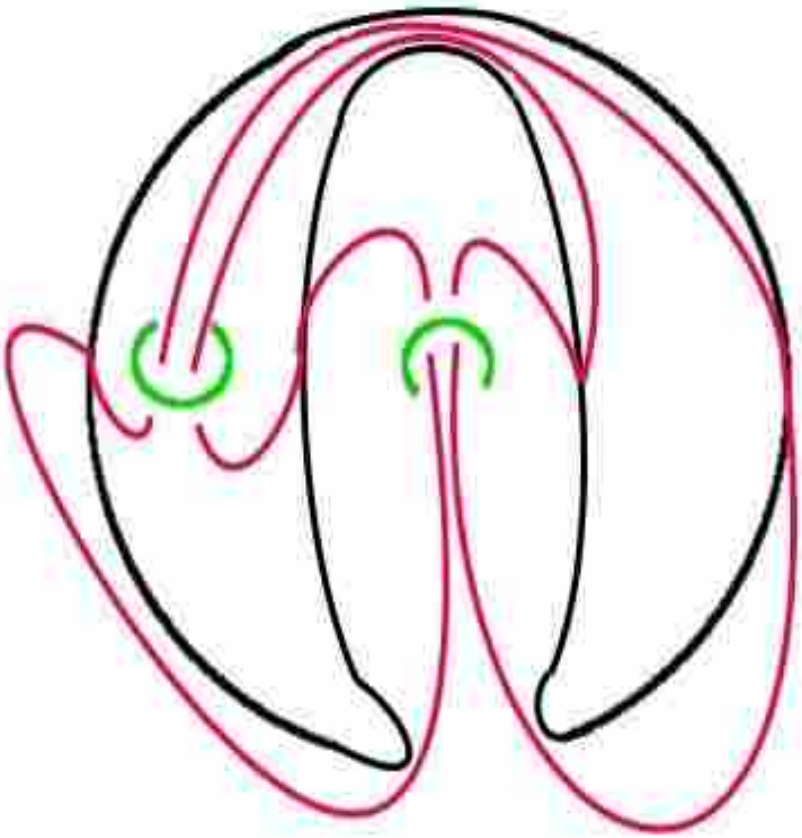

Figure 7.22: Heisenberg Corridor Complex Link

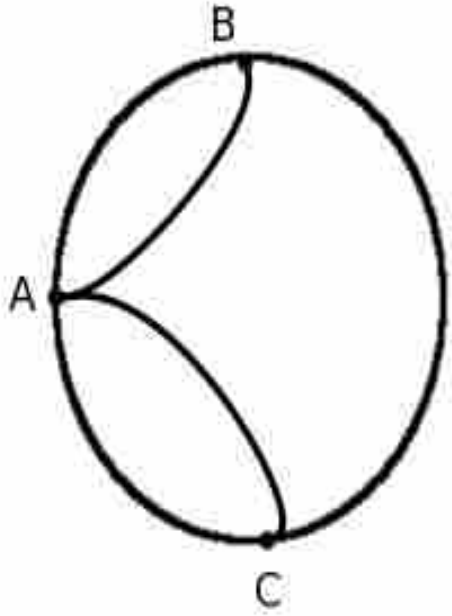

Figure 7.23: Initial Sol Manifold Construction

.

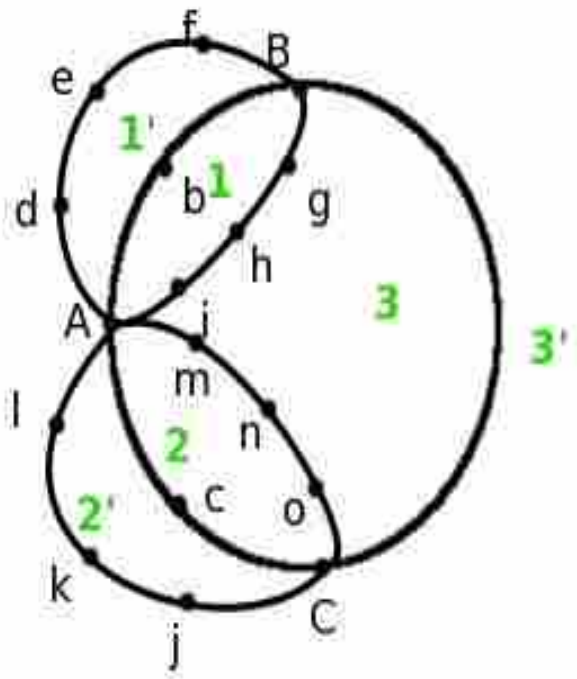

Figure 7.24: Sol Manifold with Segment Subdivisions

.

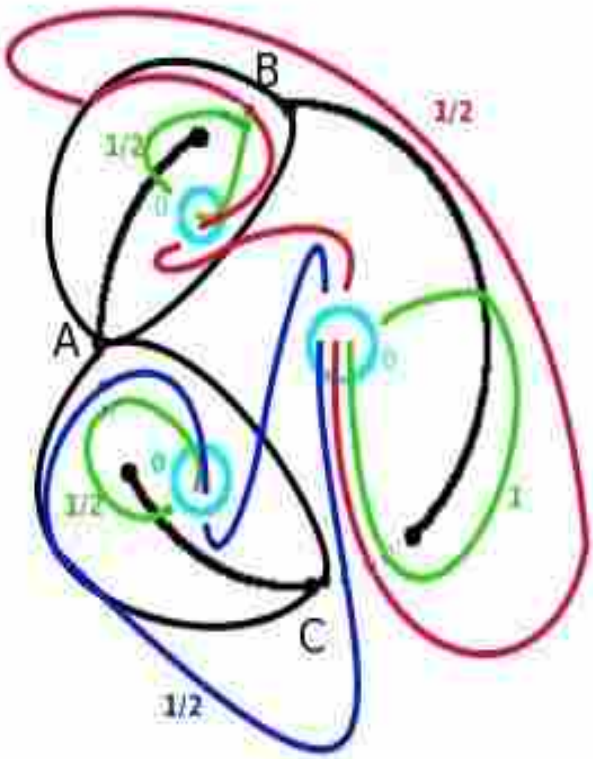

Figure 7.25: Sol Manifold Corridor Complex Link with Factors

.

$$\begin{pmatrix} A & b & B & g & h & i & A \\ b & B & f & e & d & A & b \end{pmatrix}$$
$$\begin{pmatrix} C & c & A & m & n & o & C \\ c & A & L & k & j & C & c \end{pmatrix}$$
$$\begin{pmatrix} C & o & n & m & A & i & h & g & B & C \\ j & k & l & A & d & e & f & B & C & j \end{pmatrix}$$

Table 7.8: Adjusted Sol Mappings

Now we construct the mappings including new vertices. This is Table 7.8.

Next, for edge cycles, looking at face 1, we start with the jA edge. In our chapter 6 on fundamental groups we showed a method to simplify the calculation of the twisted edge cycles using the original edge cycles. Using this approach we would expect the relators of the fundamental group to be: $X^2(1)[X(1)X^{-1}(3)]^2$. Calculating the twisted edge cycles, we get:

$jA \xrightarrow{X(1)} Ab \xrightarrow{X(1)} bB \xrightarrow{X(1)} Bf \xrightarrow{X^{-1}(3)} gh \xrightarrow{X(1)} ed \xrightarrow{X^{-1}(3)} iA$

Which is what was expected. Symmetrically for face 2, we get:$X^2(2)[X(2X^{-1}(3))]^2$ Next for face 3 we get:$[X(3)X^{-1}(2)]^2[X(3)X^{-1}(1)]^2X(3)$ These new edge cycle mappings define the relators for the fundamental group of this manifold.

Next, to create the Heegaard diagram, we create an annulus depicting the mapping of each face. This Heegard diagram is in Figure 7.26.

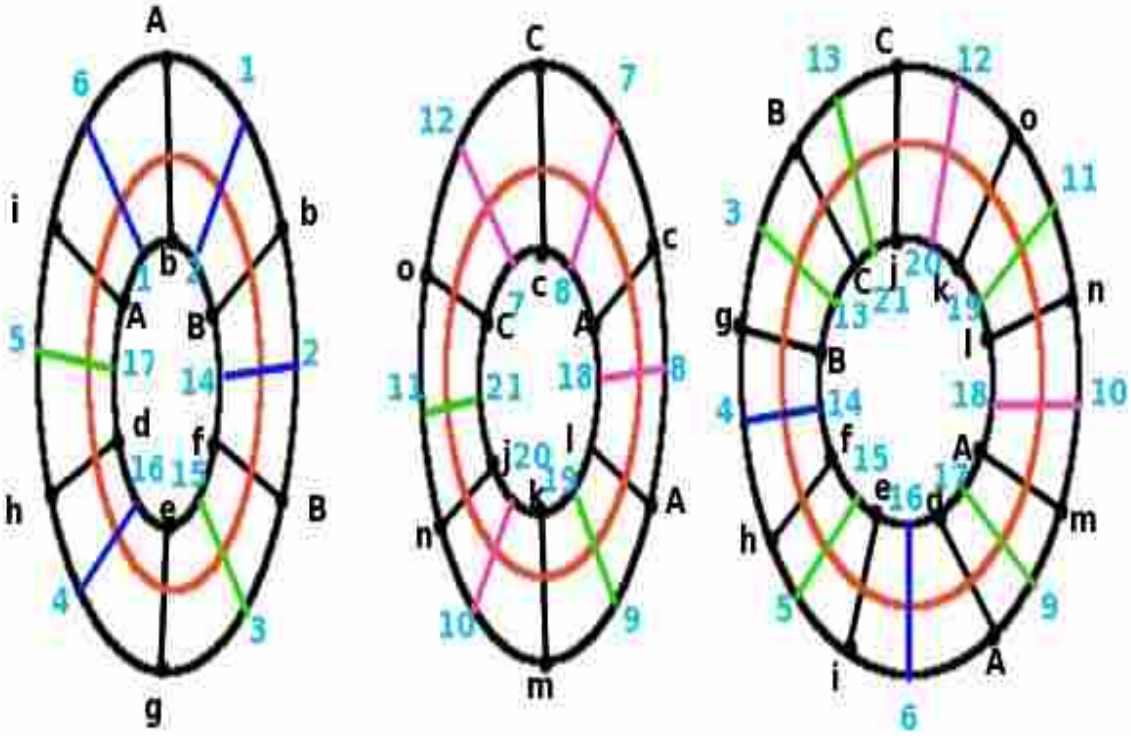

Figure 7.26: Sol Manifold Heegaard Diagram

.

Chapter 8. Sieradski Manifolds, Fibonacci Manifolds, and Cyclic Branched Covers

8.1 Basic Definitions

In this chapter we demonstrate how easy it is to create infinite families of interesting 3-manifolds with simple face pairings. The examples are for the most part reflection face pairings with natural symmetries. We recall the definition of reflection face pairing:

We begin with the simplest possible face pairing on the boundary of the 3-ball. As faces, we take the northern hemisphere (the *top*) and the southern hemisphere (the *bottom*), and, by orthogonal projection, we map each point of the northern hemisphere to that point of the southern hemisphere that is directly beneath it. This pairing can serve as the basis for infinitely many other essentially trivial face pairings if we subdivide the northern hemisphere into multiple faces and carry that cell division onto the southern hemisphere by projection. We orient the faces in the top in the clockwise direction. Compatible orientation on the bottom requires that those faces, as viewed in the figures, be oriented in the counterclockwise direction.

In introducing Sieradski manifolds, we introduce them as examples of the bitwist construction. For more formal and detailed descriptions, see [3] and [5].

For the Sieradski manifolds in particular, we cut the northern hemisphere into slices, like the pieces of a pie. We perform n radial cuts from the north pole to the equator and then project directly down. We cut both the top and the bottom into n slices. It will be important in our analysis to allow the degenerate case where $n = 1$.

The Figure 8.1 illustrates the 4-slice pie. We label the four vertices on the equator by A,

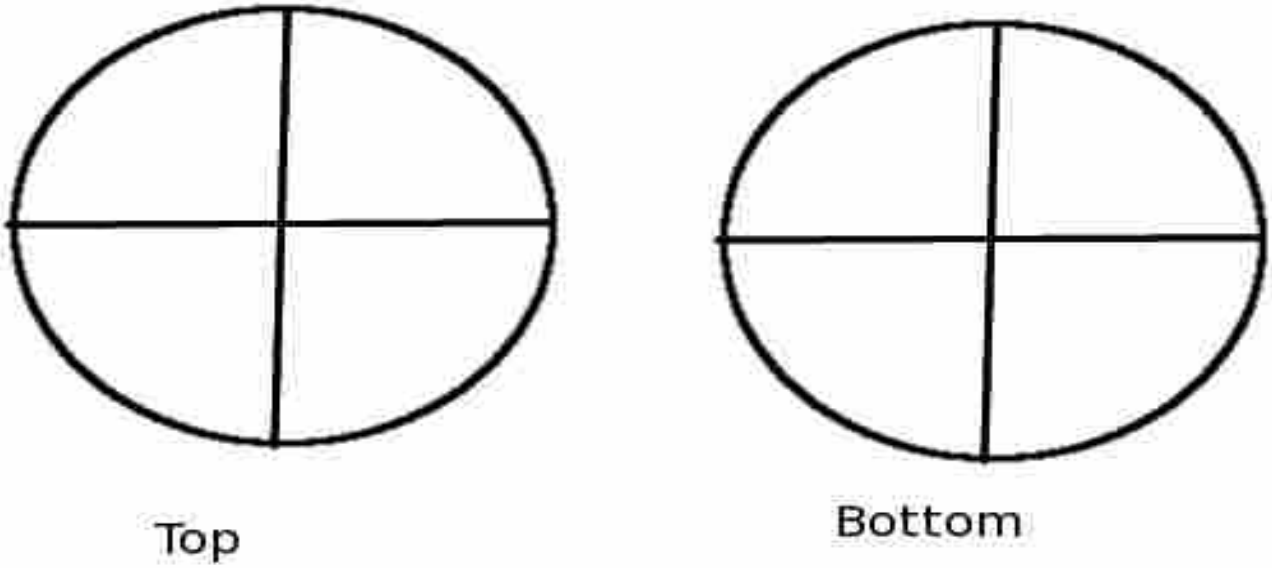

Figure 8.1: Four Slices or Four Radials

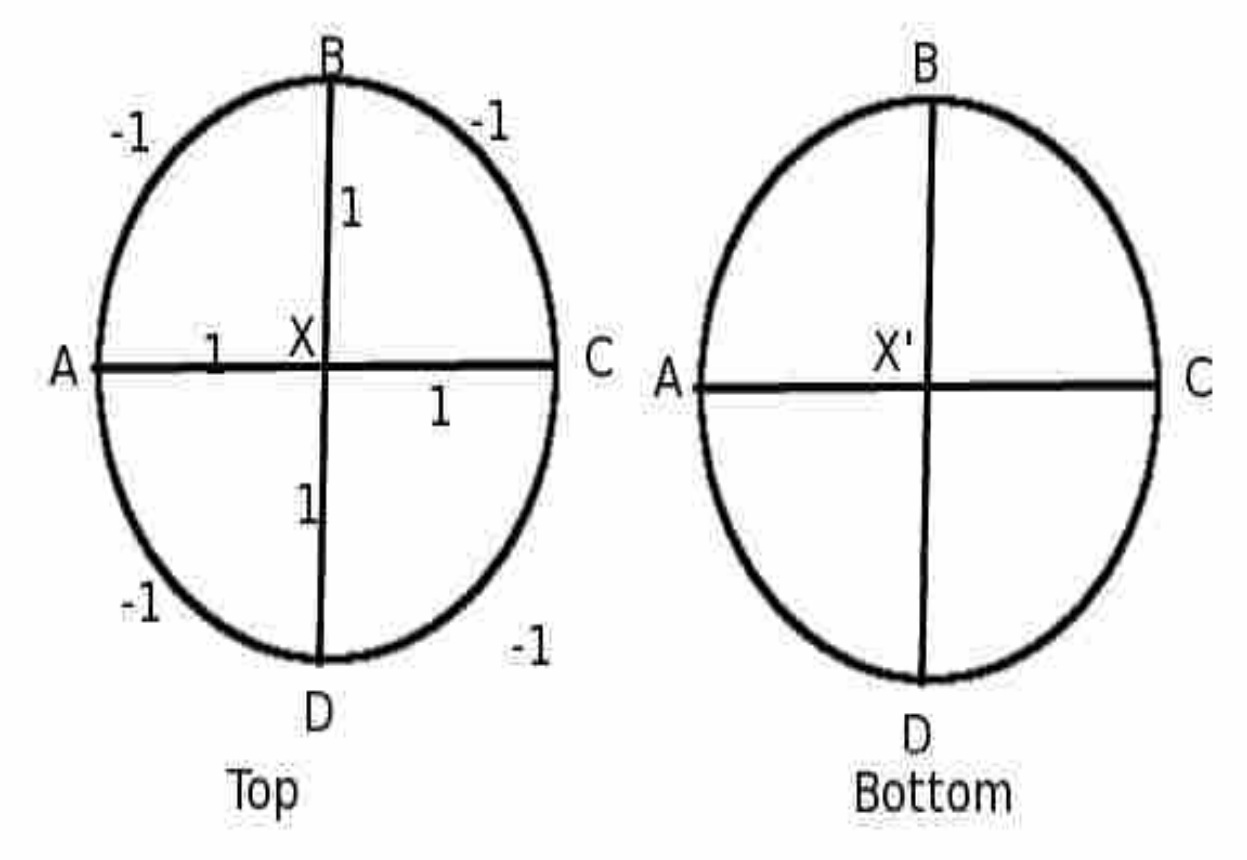

Figure 8.2: Four Slices with Multipliers

B, C, and D. We label the north pole by X and the south pole by X'. This is illustrated in Figure 8.2.

Table 8.1 is the basic face pair mappings defining the images of the vertices, which in turn define the original edges and edge cycles. These mappings have no twisting and simply map directly downward in an orthogonal projection. They are labeled Basic Sieradski maps because they are used as a basis for the twisting introduced in the bitwist construction which produces the actual Sieradski manifolds.

$$\begin{pmatrix} A & B & X \\ A & B & X' \end{pmatrix}$$
$$\begin{pmatrix} B & C & X \\ B & C & X' \end{pmatrix}$$
$$\begin{pmatrix} C & D & X \\ C & D & X' \end{pmatrix}$$
$$\begin{pmatrix} D & A & X \\ D & A & X' \end{pmatrix}$$

Table 8.1: Basic 4-Slice Sieradski

8.2 Bitwist Construction

The Sieradski manifolds are presented as bitwist manifolds by Cannon, Floyd, and Parry, in [3]. We illustrate the construction with the 4-slice pie. Then we will define infinitely many infinite classes of manifolds that generalize the Sieradski manifolds, all of which we call *generalized Sieradski manifolds*. We shall see that the generalized Sieradski manifolds share many of the properties of the Sieradski manifolds that were established in [3].

With the face pairing defined by the 4-slice pie (and more generally for the n-slice pie), the equatorial edges are mapped to themselves by the face pairing, and so are the only edges in their edge cycle. The radial edges have X or X' as an endpoint and therefore have two edges in their edge cycles, matching one edge in the top with one in the bottom.

Following the bitwist construction used in [3], we choose multipliers of -1 for the outside equatorial edges and $+1$ for the inner edges. We also subdivide each edge into a number of segments equal to the the number of elements in the edge cycle times the absolute value of the multiplier, as in Figure 8.3.

Following the procedure in [3], we add a sticker to a top face at a vertex when the vertex is preceded by a negative twist (negative multiplier) and followed by a positive twist (positive multiplier) in the oriented boundary (clockwise) of the face. We label the four new vertices

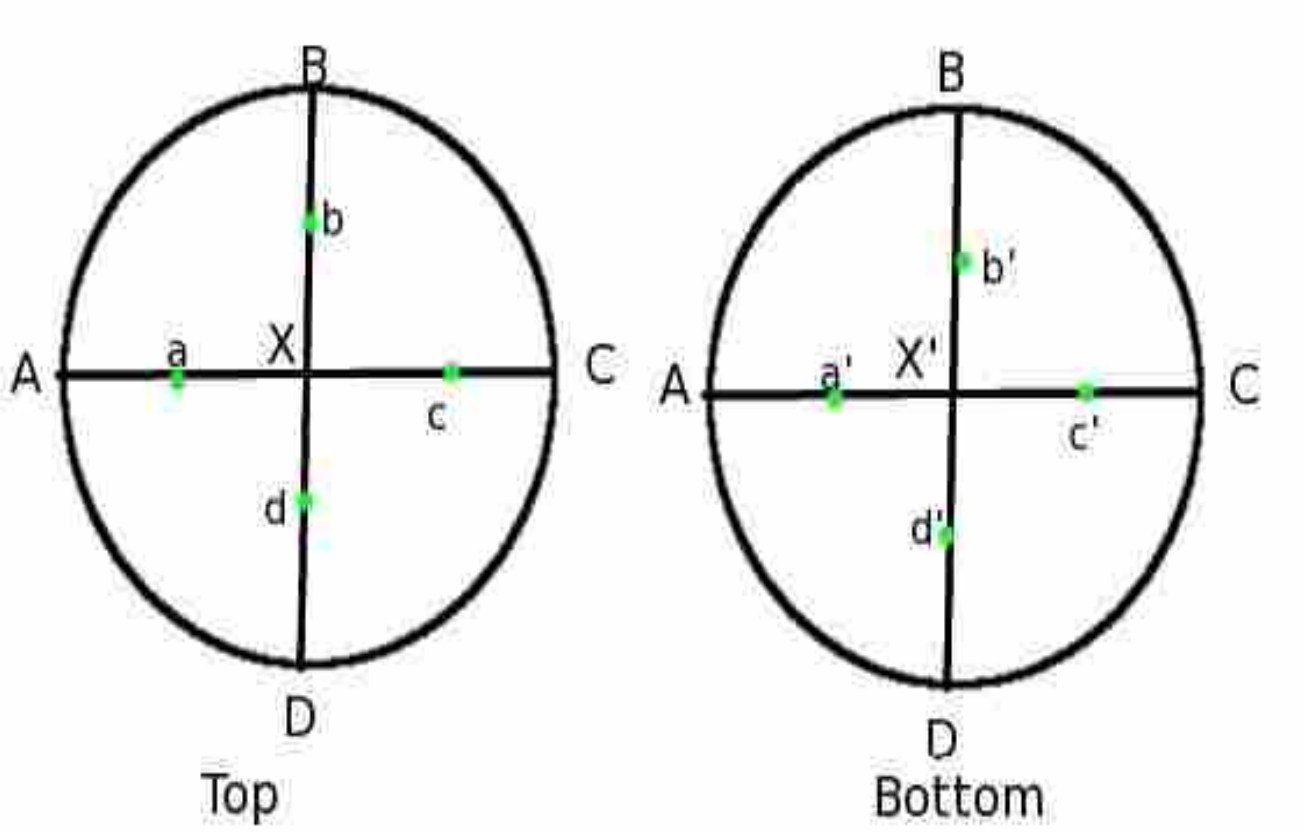

Figure 8.3: Edge Segments Subdivided

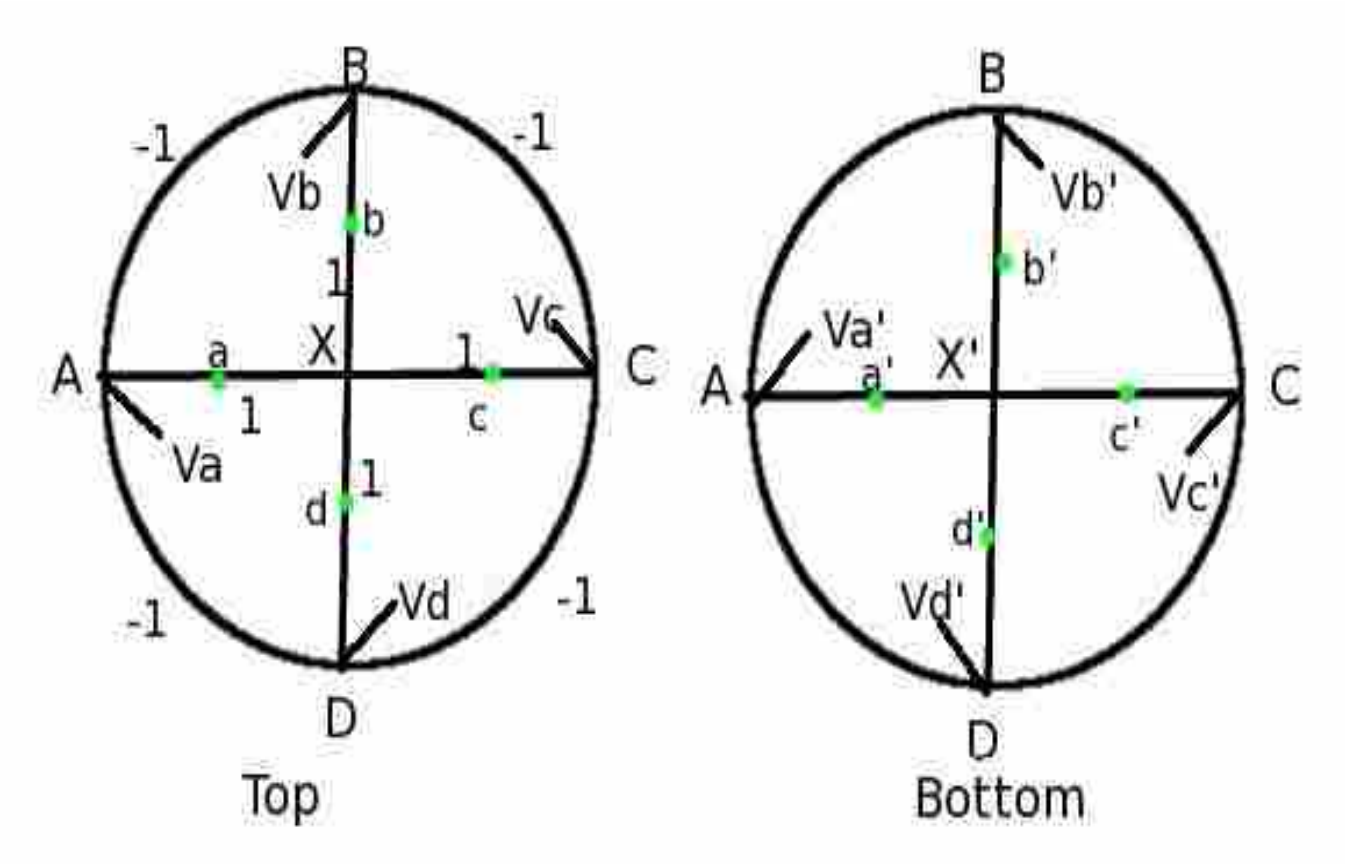

Figure 8.4: Stickers and Twist Factors Added

thus obtained by Va, Vb, Vc, and Vd. Similarly, stickers are added in the bottom at a vertex when the vertex is preceded by a negative twist (negative multiplier) and followed by a positive twist (positive multiplier) in the oriented boundary (counter-clockwise) of the face (Va', Vb', Vc', Vd').

Next, we adjust the face maps of each segment, twisting a segment clockwise if there is a positive twist parameter, and twisting in a counter-clockwise direction for each negative twist parameter. The new face maps are in Table 8.2.

$$\begin{pmatrix} A & Va & A & a & X & d & D & A \\ D & A & a' & X' & d' & D & Vd' & D \end{pmatrix}$$

$$\begin{pmatrix} B & Vb & B & b & X & a & A & B \\ A & B & b' & X' & a' & A & Va' & A \end{pmatrix}$$

$$\begin{pmatrix} C & Vc & C & c & X & b & B & C \\ B & C & c' & X' & b' & B & Vb' & B \end{pmatrix}$$

$$\begin{pmatrix} D & Vd & D & d & X & c & C & D \\ C & D & d' & X' & c' & C & Vc' & C \end{pmatrix}$$

Table 8.2 Adjusted Sieradski 4

As explained in earlier sections, we now apply the tool of bitwist to create a new object by identifying points with their image by these face maps. This creates a quotient space. The bitwist theorem [7] implies that the quotient M of this modified face pairing is a closed 3-manifold. Generators $X(1), X(2), X(3), X(4)$ for the fundamental group of M are represented by the four face pairs, and relators for the fundamental group are given by the edge cycles. Next, we calculate the four edge cycles: We start with the edge from A to Va, denoted AVa. We get
$AVa \xrightarrow{X(1)} DA \xrightarrow{X(1)} Vd'D \xrightarrow{X^{-1}(1)} Dd \xrightarrow{X(4)} d'X' \xrightarrow{X^{-1}(1)} Xa \xrightarrow{X(2)} a'A \xrightarrow{X^{-1}(1)} AVa$. This completes the cycle and equivalence class of the new edge from A to Va. For the next edge, we have:
$Aa \xrightarrow{X(1)} a'X' \xrightarrow{X^{-1}(2)} Xb \xrightarrow{X(3)} b'B \xrightarrow{X^{-1}(2)} BVb \xrightarrow{X(2)} AB \xrightarrow{X(2)} Va'A \xrightarrow{X^{-1}(2)} Aa$, and next,
$Xd \xrightarrow{X(1)} d'D \xrightarrow{X^{-1}(4)} DVd \xrightarrow{X(4)} CD \xrightarrow{X(4)} Vc'C \xrightarrow{X^{-1}(4)} Cc \xrightarrow{X(3)} c'X \xrightarrow{X^{-1}(4)} Xd$, and last
$bB \xrightarrow{X(3)} BVb' \xrightarrow{X^{-1}(3)} CB \xrightarrow{X^{-1}(3)} VcC \xrightarrow{X(3)} Cc' \xrightarrow{X^{-1}(4)} cX \xrightarrow{X(3)} X'b' \xrightarrow{X^{-1}(2)} bB$.

These edge cycles create the relators for the fundamental group π_1.
$X(1)X(1)X^{-1}(1)X(4)X^{-1}(1)X(2)X^{-1}(1) = X(1)X(4)X^{-1}(1)X(2)X^{-1}(1) =$

$X(4)X^{-1}(1)X(2)$

$X(1)X^{-1}(2)X(3)X^{-1}(2)X(2)X(2)X^{-1}(2) = X(1)X^{-1}(2)X(3)$

$X(1)X^{-1}(4)X(4)X(4)X^{-1}(4)X(3)X^{-1}(4) = X(1)X(3)X^{-1}(4) = X(3)X^{-1}(4)X(1)$

$X(3)X^{-1}(3)X^{-1}(3)X(3)X^{-1}(4)X(3)X^{-1}(2) = X^{-1}(4)X(3)X^{-1}(2) = X(2)X^{-1}(3)X(4).$

We see a pattern in the final results, which are the relators for the fundamental group.

$$X(1)X^{-1}(2)X(3)$$

$$X(2)X^{-1}(3)X(4)$$

$$X(3)X^{-1}(4)X(1)$$

$$X(4)X^{-1}(1)X(2)$$

From the four edge cycles, it is an easy matter to illustrate one method of proof for the bitwist theorem. A classical theorem implies that M is a closed manifold if and only if its Euler characteristic is 0 [4], page 7. The quotient M obviously has one 3-cell and four 2-cells. The four edge cycles show that M has four 1-cells. In order to show that the Euler characteristic is 0, it therefore remains only to show that M has exactly one vertex.

Tracing not just the edges, but also the individual vertices in the edge cycles, we see that each edge cycle exhibits two partial vertex orbits, for example the sequence of first vertices $A, D, Vd', D, d', X, a', A$ and the sequence $Va, A, D, d, X', a, A, Va$ of second vertices in the first edge cycle. Since both sequences contain A, all of these vertices are equivalent in the quotient M. The vertex A appears in the first two edge cycles as both a first and second vertex of these vertex sequences. The vertex C appears in the last two as both a first and second vertex. The vertex B appears in sequences 2 and 4. Hence all vertices are equivalent, M has only one vertex, and the Euler characteristic is therefore equall to 0.

It is an easy matter to establish analogous results for the n-slice pie, hence for all of the Sieradski manifolds.

Theorem 8.1. *Let $M(n)$ denote the bitwist quotient obtained from the n-slice pie with mul-*

tipliers -1 *on equatorial edges and* $+1$ *on radial edges. Then* $M(n)$ *is a closed* 3*-dimensional manifold called the* n^{th} *Sieradski manifold. Its fundamental group is generated by elements* $X(1), \ldots, X(n)$ *corresponding to the* n*-pieces of the pie and subject to the* n *relators*

$$X(i-1)X^{-1}(i)X(i+1),$$

$i = 1$ *to* n *with indices calculated modulo* n*.*

Using the tool of bitwist on the simply constructed Sieradski manifolds shows the power of the bitwist tool. Many different manifolds can be generated with this construction. Details of the these manifolds can be found in [3]. The fundamental groups of the first four Sieradski manifolds are (1) $\mathbb{S}^3$, π_1= 1; (2) lens space L(3,1) with π_1=Z_3; (3) π_1= quaternion group of order 8, (4) π_1=binary tetrahedral group.

The fifth Sieradski manifold is the interesting Poincaré homology sphere, with π_1= binary icosahedral group. In [13] we read that Poincaré first conjectured that any homology sphere was homeomorphic to $\mathbb{S}^3$. A homology sphere is a closed 3-manifold with homology groups equal to those of $\mathbb{S}^3$. Soon afterwards he constructed a counterexample which is now called the Poincare homology sphere. He then conjectured the famous *Poincare' conjecture* that any closed, oriented, simply connected 3-manifold is homeomorphic to $\mathbb{S}^3$. The sixth Sieradski manifold is the Heisenberg manifold with $\pi_1 = \{x, y, \mid [x,[x,y]] = [y,[x,y]] = 1\}$. The seventh and above Sieradski manifolds are all based on the geometry of the universal cover of SL(2,$\mathbb{R}$), [3] page 5.

8.3 Generalized Sieradski Manifolds

We now describe *generalized Sieradski manifolds*. We subdivide the northern hemisphere of the 2-sphere $\mathbb{S}^2 = \partial(\mathbb{B}^3)$ with n radial cuts (as with the n-slice Sieradski manifold) and

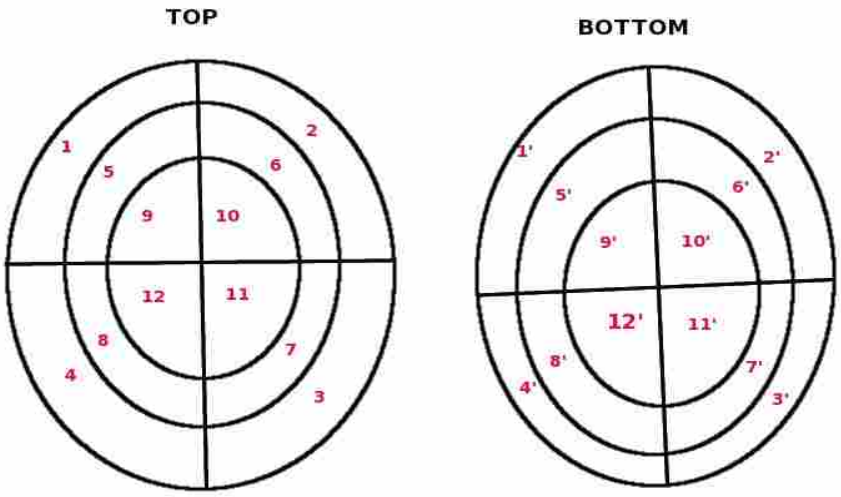

Figure 8.5: Three Circles and Four Radials

with $m-1$ additional circular cuts concentric with the equator boundary so that one sees m circles in the cellular division of that hemisphere. We carry that cell structure to the southern hemisphere by orthogonal projection. An example of this construction is in Figure 8.5. We apply the multiplier $+1$ to all radial edges and the multiplier -1 to all circular edges. The bitwist theorem [7] assures us that the resulting bitwist quotient space $M(m,n)$ is a closed, orientable 3-manifold.

We will first illustrate how to calculate a presentation for the fundamental group of $M(m,n)$. We will then abelianize and calculate the first homology group of $M(m,n)$. Finally, we will show that the manifolds $M(m,n)$ are the branched cyclic covers of $\mathbb{S}^3$ over the 2-braid knots.

8.4 The Fundamental Group of the Generalized Sieradski Manifolds.

Figure 8.6 illustrates the construction for $m=3$ and $n=4$. As indicated in chapter 6 on fundamental groups and homology groups, we need only the original face pairing and the multipliers in order to calculate the groups. But for the moment, we include all of the stickers and subdivisions used in the complete construction. The stickers required by the bitwist construction when circular edge classes are endowed with edge multiplier -1 and radial edge classes are endowed with edge multiplier $+1$, have been added to the figure. Also, the segment subdivisions (the original edge cycle length multiplied by the absolute value of the multiplier) required by the bitwist construction have been added.

In the bitwist construction, edges with multiplier $+1$ are twisted clockwise one edge, while edges with multiplier -1 are twisted counterclockwise one edge. Adjacent edges that are pulled apart by this twisting require an intervening sticker that splits into two edges. Adjacent edges that are pushed together by this twisting are folded into a single sticker.

Figure 8.6 has vertices labeled with multiple colors. Intersections of circles and lines in

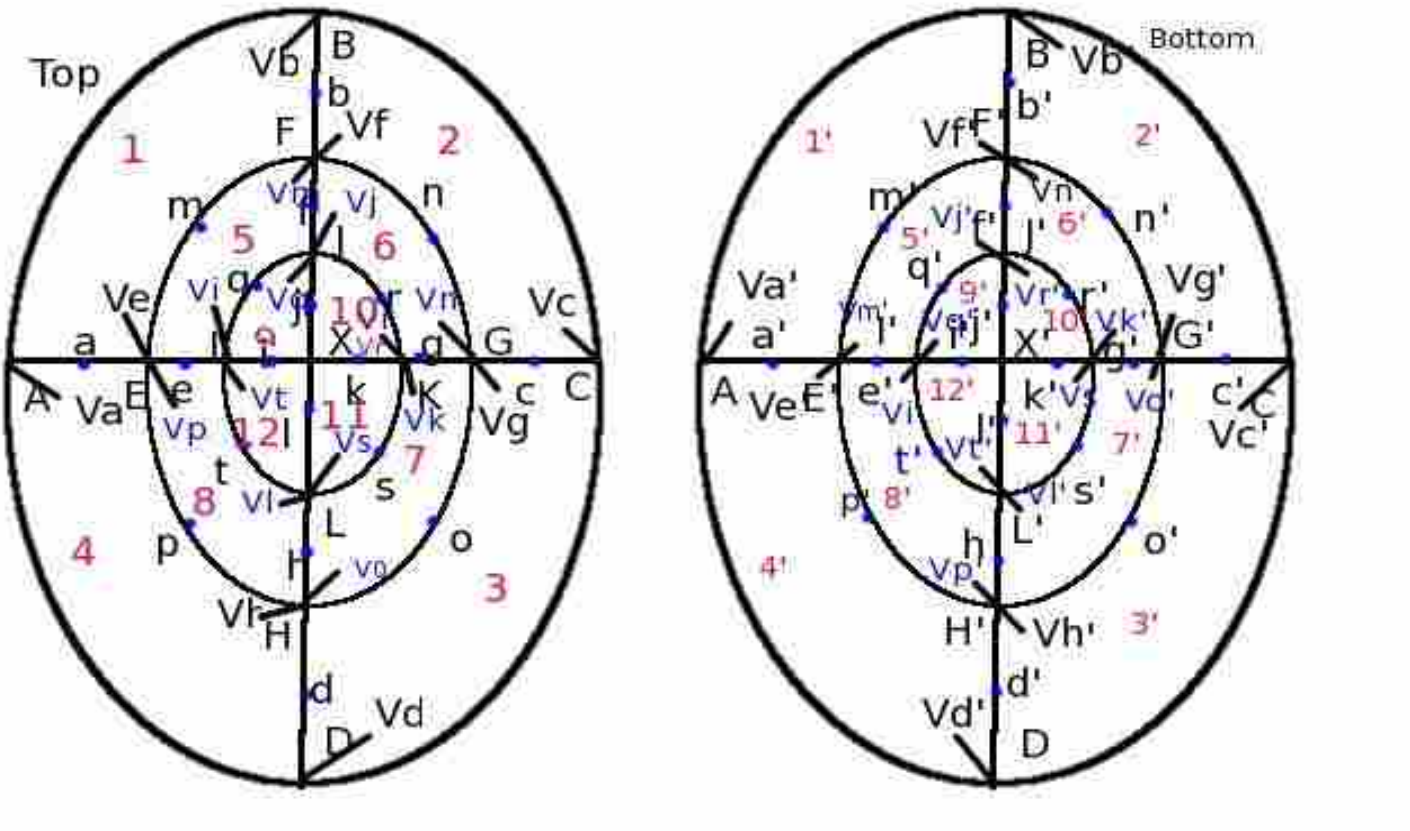

Figure 8.6: Three Circles and Four Radials

the upper hemisphere are labeled with capital letters starting with face number 1, continuing clockwise, to the center which is labeled X. Bottom hemisphere labels have primes. Next, midpoints of straight lines are similarly labeled with lower case letters. Then midpoints of circle segments continue in the same order to be named with the lower case lettering. Finally, the added stickers have endpoints labeled with a V followed by some lower case letter, such as Va. Stickers pointing to the outside take the lower case letter from the vertex from which the sticker originates. Stickers pointing to the inside take the lower case letter from the midpoint of the circle segments on the outside of the vertex.

The resulting face pairing maps are in Table 8.4. Only the face maps required to develop the general relators have been included.

$$\begin{pmatrix} Vb & B & b & F & m & E & Ve & E & a & A & B & Vb \\ B & b' & F' & Vf' & F' & m' & E' & a' & A & Va' & A & B \end{pmatrix}$$

$$\begin{pmatrix} Vc & C & c & G & n & F & Vf & F & b & B & C & Vc \\ C & c' & G' & Vg' & G' & n' & F' & b' & B & Vb' & B & C \end{pmatrix}$$

$$\begin{pmatrix} Va & A & a & E & p & H & Vh & H & d & D & A & Va \\ A & a' & E' & Ve' & E' & p' & H' & d' & D & Vd' & D & A \end{pmatrix}$$

$$\begin{pmatrix} Vm & F & f & J & q & I & Vi & I & e & E & m & F & Vm \\ F' & f' & J' & Vj' & J' & q' & I' & e' & E' & Vm' & E' & m' & F' \end{pmatrix}$$

$$\begin{pmatrix} Vn & G & g & K & r & J & Vj & J & f & F & n & G & Vn \\ G' & g' & K' & Vk' & K' & r' & J' & f' & F' & Vn' & F' & n' & G' \end{pmatrix}$$

$$\begin{pmatrix} Vp & E & e & I & t & L & Vl & L & h & H & p & E & Vp \\ E' & e' & I' & Vi' & I' & t' & L' & h' & H' & Vp' & H' & p' & E' \end{pmatrix}$$

$$\begin{pmatrix} Vq & J & j & X & i & I & q & J & Vq \\ J' & j' & X' & i' & I' & Vq' & I' & q' & J' \end{pmatrix}$$

$$\begin{pmatrix} Vr & K & k & X & j & J & r & K & Vr \\ K' & k' & X' & j' & J' & Vr' & J' & r' & K' \end{pmatrix}$$

$$\begin{pmatrix} Vt & I & i & X & l & L & t & I & Vt \\ I' & i' & X' & l' & L' & Vt' & L' & t' & I' \end{pmatrix}$$

Table 8.4 : Slice Maps

The proof of the bitwist theorem shows that the Euler characteristic is 0 because there is

only one quotient vertex, twelve edge classes, twelve face pairs, and one 3-cell, as the reader can check. It is important to note that the faces are of three types: those having an edge on the equator (equatorial faces), those having a vertex at north or south pole (polar faces), and the remainder (intermediate faces). The edge classes correspond to these faces and create corresponding relators. Here are examples of each class of relators.

Face 1 is an example of a face having an edge on the equator. We start with the edge from Vb to B, denoted VbB. We get

$$VbB \xrightarrow{X(1)} Bb' \xrightarrow{X^{-1}(2)} bF \xrightarrow{X(1)} F'Vf' \xrightarrow{X^{-1}(1)} mF \xrightarrow{X(5)} E'm' \xrightarrow{X^{-1}(1)} VeE \xrightarrow{X(1)}$$
$$E'a' \xrightarrow{X^{-1}(4)} aA \xrightarrow{X(1)} AVa' \xrightarrow{X^{-1}(1)} BA \xrightarrow{X^{-1}(1)} VbB.$$

This gives us:

$$X(1)X^{-1}(2)X(1)X^{-1}(1)X(5)X^{-1}(1)X(1)X^{-1}(4)X(1)X^{-1}(1)X^{-1}(1) = X^{-1}(2)X(5)X^{-1}(4)$$

Next, for an inside face, having a vertex at the north pole, we take face 9, and we start with the edge from Vq to J, denoted VqJ. We get

$$VqJ \xrightarrow{X(9)} J'j' \xrightarrow{X^{-1}(10)} jX \xrightarrow{X(9)} X'i' \xrightarrow{X^{-1}(12)} iI \xrightarrow{X(9)} I'Vq' \xrightarrow{X^{-1}(9)} qI \xrightarrow{X(5)} J'q' \xrightarrow{X^{-1}(9)} VqJ.$$

This gives us,

$$X(9)X^{-1}(10)X(9)X^{-1}(12)X(9)X^{-1}(9)X(5)X^{-1}(9) = X^{-1}(10)X(9)X^{-1}(12)X(5)$$

.

Next, for a middle or intermediate face, we take face 5, and we start with the edge from

Vm to F, denoted VmF. We get

$$VmF \xrightarrow{X(5)} F'f' \xrightarrow{X^{-1}(6)} fJ \xrightarrow{X(5)} J'Vj' \xrightarrow{X^{-1}(5)} qJ \xrightarrow{X(9)} I'q' \xrightarrow{X^{-1}(5)} ViI \xrightarrow{X(5)} I'e' \xrightarrow{X^{-1}(8)}$$
$$eE \xrightarrow{X(5)} E'Vm' \xrightarrow{X^{-1}(5)} mE \xrightarrow{X(1)} F'm' \xrightarrow{X^{-1}(5)} VmF.$$

We then get,

$$X(5)X^{-1}(6)X(5)X^{-1}(5)X(9)X^{-1}(5)X(5)X^{-1}(8)$$
$$X(5)X^{-1}(5)X(1)X^{-1}(5) = X^{-1}(6)X(9)X^{-1}(8)X(1)$$

By simultaneously permuting the indices from 1 to 4 cyclically, 5 to 8 cyclically, and 9 to 12 cyclically, we obtain all of the edge cycles, hence a complete set of defining relators. After simplifications, we obtain the following group presentation in the general case. We have numbered the faces so that the equatorial faces are numbered from 1 to n, the next layer inward from $n+1$ to $2n$, the third layer from $2n+1$ to $3n$, and so forth.

The work above can be significantly simplified recalling the simplification that does not need stickers or subdivision of edge cycles. Instead of the complicated Figure 8.6, we can just use the more simple Figure 8.5. We only need the original face pairing, original edge cycles, and the multipliers. I repeat again the section from the fundamental group calculation. The original face pairing mapping is ϵ and the twist- or bitwist- mapping is δ.

The calculation of the relators W_δ can be further simplified by expressing them in terms of the relators W_ϵ and the multipliers m_i. We will create one relator for each face pair (f, f^{-1}). First we list the edges $e_1, \ldots, e_n$ of f in clockwise order. Define $m(e_i)$ to be the multiplier associated with the edge class containing e_i. Then the relator is

$$W_\epsilon(e_1, f)^{m(e_1)} \cdot W_\epsilon(e_2, f)^{m(e_2)} \cdots W_\epsilon(e_n, f)^{m(e_n)}.$$

For an example of the simpler approach, consider Figure 8.5. The edge cycles of line segments on the equator are length one on the original mappings ϵ. All other edges have edge cycle length two. The equatorial edge cycle consits of X(1), X(2), X(3), or X(4), depending on which equatorial edge we consider. The other edge cycles are simply the face number mapping for the face we are considering, followed by the inverse of the face number mapping on the other side of the edge. I will follow the outline for the relators for faces 1,5, and 9. This will give examples of all three types of faces. For face 1 starting with the edge between faces 1 and 2, we get:

$$[X(1)X^{-1}(2)]^{+1}[X(1)X^{-1}(5)]^{-1}[X(1)X^{-1}(4)]^{+1}[X(1)]^{-1}$$
$$[X(5)X^{-1}(6)]^{+1}[X(5)X^{-1}(9)]^{-1}[X(5)X^{-1}(8)]^{+1}[X(5)X^{-1}(1)]-1$$
$$[X(9)X^{-1}(10)]^{+1}[X(9)X^{-1}(12)]^{+1}[X(9)X^{-1}(5)]^{-1}$$

Note that in writing the edge cycle word, we have a choice as to where to begin, and in which direction to go. The above edge cycles for face r all start with $X(r)$. If the edge cycles is not starting with $X(r)$, start in a different place in the cycle or take the inverse of the cycle word. Next, we simplify to get, again for 1,5, and 9 respectively:

$$X^{-1}(2)X(5)X^{-1}(4) = X^{-1}(r+1)X(r+n)X^{-1}(r-1)$$
$$X^{-1}(6)X(9)X^{-1}(8)X(1) = X^{-1}(r+1)X(r+n)X^{-1}(r-1)X(r-n)$$
$$X^{-1}(10)X(9)X^{-1}(12)X(5) = X^{-1}(r+1)X(r)X^{-1}(r-1)X(r-n)$$

These are the same answers we got before, but with less work. If we want at some point

to do the Heegaard diagrams, the method we have been using requires the full edge divisions with stickers. Calculating with either method, we have the following result:

Theorem 8.2. *Let $M = M(m,n)$ denote the generalized Sieradski manifold with faces in the northern hemisphere bounded by m concentric circles (including the equator) and n radii. Then the fundamental group of M is generated by $m \cdot n$ generators $X(1)$, ..., $X(m \cdot n)$ subject to three types of relators:*

Equatorial relators: $X^{-1}(r+1)X(r+n)X^{-1}(r-1)$, where $r \in [1,n]$ and where $r+1$ and $r-1$ are calculated cyclically within the range $[1,n]$;

Intermediate relators: $X^{-1}(r+1)X(r+n)X^{-1}(r-1)X(r-n)$, where $r \in [1+kn,(k+1)n]$ with $k \in [1,m-2]$ and where $r+1$ and $r-1$ are calculated cyclically within the range $[1+kn,(k+1)n]$.

Polar relators: $X^{-1}(r+1)X(r)X^{-1}(r-1)X(r-n)$, where $r \in [1+(m-1)n, mn]$ and where $r+1$ and $r-1$ are calculated cyclically within that range.

8.5 The First Homology Group of the Generalized Sieradski Manifolds.

The most tantalizing property of the first homology groups of the manifolds $M(m,n)$ is that, for a fixed number m of circles, the groups are periodic as a function of n. Our goal in this section is to calculate these groups precisely. First we will calculate the relators for the homology group as a function of the equatorial relators. This result is illustrated in Tables 8.2 and 8.3. After we have our generalized relators in terms of the n equatorial relators, we will calculate a generalized formula for the first homology group, which formula is stated in Theorem 8.5.4. Next, we will apply this theorem to calculate all homology groups for $m = 1$ to 10, $n = 1$ to 28. This result is shown in Table 8.4

We first abelianize the relators. To generalize these results consider a generalized intermediate face: $X(r+(k+1)n) = X(r+kn-1)X(r+kn+1)X^{-1}(r+(k-1)n)$.

For $k = 1$ we get $X(r+2n) = X(r+n-1)X(r+n+1)X^{-1}(r) = X(r-2)X(r)X(r)X(r+2)X^{-1}(r) = X(r-2)X(r)X(r+2)$

Next assume that for k, $X(r+kn) = X(r-k)X(r-k+2)...X(r+k-2)X(r+k)$.

Then we get $X(r+(k+1)n) = X(r+kn-1)X(r+kn+1)X^{-1}(r+(k-1)n) =$

$X(r-k-1)X(r-k+1)..X(r+k-1)X(r-k+1)X(r-k+3)...X(r+k+1)$

$[X(r-k+1)X(r-k+3)...X(r+k-3)X(r+k-1)]^{-1} = X(r-k-1)X(r-k+1)...X(r+k+1)$

So, our formula for an intermediate face relator works for all k, $X(r+kn) = X(r-k)X(r-k+2)...X(r+k-2)X(r+k)$. Looking on for a general formula for the relators, we start with the general polar relator for face $r+(m-1)n$, which equals:

$X(r+(m-1)n-1)X^{-1}(r+(m-1)n)X(r+(m-1)n+1)X^{-1}(r+(m-2)n) =$

$X(r-m+1-1)X(r-m+2)...X(r+m-4)X(r+m-1-1)$

$[X(r-(m-1))X(r-m+3)...X(r+m-3)X(r+m-1)]^{-1}$

$X(r-m+1+1)X(r-m+4)...X(r+m-3+1)X(r+m-1+1)$

$[X(r-m+2)X(r-m+4)...X(r+m-4)X(r+m-2)]^{-1} =$

$X(r-m)X^{-1}(r-m+1)X(r-m+2)X^{-1}(r-m+3)X(r-m+4)...X^{-1}(r+m-1)X(r+m)$

Then, we vary r cyclically from 1 to n to generate all of the relators and keep the index of the relators cyclicly in the range from 1 to n. From the generalized intermediate face relators, we have shown that particular intermediate face mappings can be considered to be functions of the face maps of faces further from the center, i.e. outside the circle which bounds the face on the outside. Thus all relators can be written as functions of the face maps on the outside edges which have an equatorial edge. Therefore, all function maps in the relators as calculated above range cyclicly from 1 to n.

If we take as an example m=2; n=4, we get Table 8.2, or, in general m=m and n=n, Table 8.3

If we take the first two relators in Table 8.3, we multiply them to get $X(1)X(2m+2) = id.$ or $X(1) = X^{-1}((2m+2) \mod n)$. Extending for r in the range of 1 to n, we can then, start

with a face mapping, take the index number associated to that map and add $2m+1 \mod n$ to obtain a map equal to the inverse of the original map. Add $4m+4$, to the index of a map (mod n) to obtain a map equal to the original map. These results are stated in lemma 8.5.1 and corollary 8.5.2.

Lemma 8.5.1. *Considering the face maps as discussed, we see that* $X(r) = X^{-1}(r+2m+1)$

Corollary 8.5.2. $X^{(-1)^p}(r) = X(r + p(2m+1))$

The following lemma is a commonly known useful result.

Lemma 8.5.3. *In the subgroups of* $\mathbb{Z}/n\mathbb{Z}$ $(= \mathbb{Z}_n)$*, the subgroup generated by* $2m+1 \mod n$ *is equal to the group generated by the greatest common divisor of* $2m+1$ *and* n*, written as* $gcd(2m+1, n)$.

Theorem 8.5.4. *Let* $g = gcd(2m+1, n)$*. If* n *is odd, then* $H_1[m,n] = \mathbb{Z}_2^{g-1}$*, if* n *is even,* $H_1[m,n] = \mathbb{Z}^{g-1} \oplus \mathbb{Z}_{(2m+1)/g}$.

Proof. If n is odd, then g divides n and must also be odd. From corollary 8.5.2 we see that for each r, the maps equal to $X(r)$ or its inverse, are maps indexed by the coset Hr, where H is the group generated by $2m+1$, which equals the group generated by g. This group also has odd order. Therefore when we cycle through the group by lemma 8.5.1, we eventually return to r, and we have $X(r) = X^{-1}(r)$. Thus each element in the homology group has order 2. From the first row of $2m+1$ generators in Table 8.3, we see that the g distinct generators are repeated an odd number of times leaving just one set, since the homology

group is abelian and the elements of order 2 cancel. Therefore, the relator shows that any one of these g elements can be expressed in terms of the other $g-1$, leaving $g-1$ elements of order 2 in the relator.

If, on the other hand, n is even, the order of the subgroup H of $\mathbb{Z}/n\mathbb{Z}$ generated by g is even, since the order of H times g equals n, and g must be odd, dividing $2m+1$. When we cycle through the collection of maps equal to$X(r)$, we return to $X(r) = X(r)$, not forcing all elements to be of order 2, as in the n is odd case. As we cycle through the group generated by g with g odd, we note that the face maps indexed by odd integers are inverses of those indexed by even integers. For example, if $2m+1 = 5$ we would have $X(1) = X^{-1}(6) = X(11)$, etc. Our first relator would then be X(1) $X^{-1}(2)...X(g)[X^{-1}(g+1) = X(1)]X^{-1}(2)...etc.$ The first g relators would be repeated with the same signs as above until there are $2m+1$ entries. The other relators with proper substitutions are the same as the first, which becomes $[X(1)X^{-1}(2)...X(g)]^{(2m+1)/g}$. To finish, we do a change of variable introducing y as $X(1)...X(g)$. We then have one relator as $y^{(2m+1)/g}$, with $g-1$ other free variables (as functions of y and the other variables). □

In Table 8.4 we summarize the results of applying Theorem 8.5.4. There are many cyclic results both by n, the number of radials, and by m, the number of concentric circles in the upper hemisphere.

$$\begin{pmatrix} X(1) & X^{-1}(2) & X(3) & X^{-1}(4) & X(1) \\ X(2) & X^{-1}(3) & X(4) & X^{-1}(1) & X(2) \\ X(3) & X^{-1}(4) & X(1) & X^{-1}(2) & X(3) \\ X(4) & X^{-1}(1) & X(2) & X^{-1}(3) & X(4) \end{pmatrix}$$

Table 8.2: Relators as Rows for m=2; n=4

$$\begin{pmatrix} X(1) & X^{-1}(2) & X(3) & . & . & . & X^{-1}(2m) & X(2m+1) \\ X(2) & X^{-1}(3) & X(4) & . & . & . & X^{-1}(2m+1) & X(2m+2) \\ . & . & . & . & . & . & . & . \\ X(n) & X^{-1}(1) & X(2) & . & . & . & X^{-1}(2m-1) & X(2m) \end{pmatrix}$$

Table 8.3: General Relators as Rows for m=m; n=n

	$m=1$	2	3	4	5	6	7	8	9	10
$n=1$	0	0	0	0	0	0	0	0	0	0
2	$\mathbb{Z}_3$	$\mathbb{Z}_5$	$\mathbb{Z}_7$	$\mathbb{Z}_9$	$\mathbb{Z}_{11}$	$\mathbb{Z}_{13}$	$\mathbb{Z}_{15}$	$\mathbb{Z}_{17}$	$\mathbb{Z}_{19}$	$\mathbb{Z}_{21}$
3	$\mathbb{Z}_2^2$	0	0	$\mathbb{Z}_2^2$	0	0	$\mathbb{Z}_2^2$	0	0	$\mathbb{Z}_2^2$
4	$\mathbb{Z}_3$	$\mathbb{Z}_5$	$\mathbb{Z}_7$	$\mathbb{Z}_9$	$\mathbb{Z}_{11}$	$\mathbb{Z}_{13}$	$\mathbb{Z}_{15}$	$\mathbb{Z}_{17}$	$\mathbb{Z}_{19}$	$\mathbb{Z}_{21}$
5	0	$\mathbb{Z}_2^4$	0	0	0	0	$\mathbb{Z}_2^4$	0	0	0
6	$\mathbb{Z}^2$	$\mathbb{Z}_5$	$\mathbb{Z}_7$	$\mathbb{Z}^2 \oplus \mathbb{Z}_3$	$\mathbb{Z}_{11}$	$\mathbb{Z}_{13}$	$\mathbb{Z}^2 \oplus Z_5$	$\mathbb{Z}_{17}$	$\mathbb{Z}_{19}$	$\mathbb{Z}^2 \oplus \mathbb{Z}_7$
7	0	0	$\mathbb{Z}_2^6$	0	0	0	0	0	0	$\mathbb{Z}_2^6$
8	$\mathbb{Z}_3$	$\mathbb{Z}_5$	$\mathbb{Z}_7$	$\mathbb{Z}_9$	$\mathbb{Z}_{11}$	$\mathbb{Z}_{13}$	$\mathbb{Z}_{15}$	$\mathbb{Z}_{17}$	$\mathbb{Z}_{19}$	$\mathbb{Z}_{21}$
9	$\mathbb{Z}_2^2$	0	0	$\mathbb{Z}_2^8$	0	0	$\mathbb{Z}_2^2$	0	0	$\mathbb{Z}_2^2$
10	$\mathbb{Z}_3$	$\mathbb{Z}^4$	$\mathbb{Z}_7$	$\mathbb{Z}_9$	$\mathbb{Z}_{11}$	$\mathbb{Z}_{13}$	$\mathbb{Z}^4 \oplus \mathbb{Z}_3$	$\mathbb{Z}_{17}$	$\mathbb{Z}_{19}$	$\mathbb{Z}_{21}$
11	0	0	0	0	$\mathbb{Z}_2^{10}$	0	0	0	0	0
12	$\mathbb{Z}^2$	$\mathbb{Z}_5$	$\mathbb{Z}_7$	$\mathbb{Z}^2 \oplus \mathbb{Z}_3$	$\mathbb{Z}_{11}$	$\mathbb{Z}_{13}$	$\mathbb{Z}^2 \oplus \mathbb{Z}_5$	$\mathbb{Z}_{17}$	$\mathbb{Z}_{19}$	$\mathbb{Z}^2 \oplus \mathbb{Z}_7$
13	0	0	0	0	0	$\mathbb{Z}_2^{12}$	0	0	0	0
14	$\mathbb{Z}_3$	$\mathbb{Z}_5$	$\mathbb{Z}^6$	$\mathbb{Z}_9$	$\mathbb{Z}_{11}$	$\mathbb{Z}_{13}$	$\mathbb{Z}_{15}$	$\mathbb{Z}_{17}$	$\mathbb{Z}_{19}$	$\mathbb{Z}^6 \oplus \mathbb{Z}_3$
15	$\mathbb{Z}_2^2$	$\mathbb{Z}_2^4$	0	$\mathbb{Z}_2^2$	0	0	$\mathbb{Z}_2^{14}$	0	0	$\mathbb{Z}_2^2$
16	$\mathbb{Z}_3$	$\mathbb{Z}_5$	$\mathbb{Z}_7$	$\mathbb{Z}_9$	$\mathbb{Z}_{11}$	$\mathbb{Z}_{13}$	$\mathbb{Z}_{15}$	$\mathbb{Z}_{17}$	$\mathbb{Z}_{19}$	Z_{21}
17	0	0	0	0	0	0	0	$\mathbb{Z}_2^{16}$	0	0
18	$\mathbb{Z}^2$	$\mathbb{Z}_5$	$\mathbb{Z}_7$	$\mathbb{Z}^2 \oplus \mathbb{Z}_3$	$\mathbb{Z}_{11}$	$\mathbb{Z}_{13}$	$\mathbb{Z}^2 \oplus \mathbb{Z}_5$	$\mathbb{Z}_{17}$	$\mathbb{Z}_{19}$	$\mathbb{Z}^2 \oplus \mathbb{Z}_7$
19	0	0	0	0	0	0	0	0	$\mathbb{Z}_2^{18}$	0
20	$\mathbb{Z}_3$	$\mathbb{Z}^4$	$\mathbb{Z}_7$	$\mathbb{Z}_9$	$\mathbb{Z}_{11}$	$\mathbb{Z}_{13}$	$\mathbb{Z}^4 \oplus \mathbb{Z}_3$	$\mathbb{Z}_{17}$	$\mathbb{Z}_{19}$	$\mathbb{Z}_{21}$
21	$\mathbb{Z}_2^2$	0	$\mathbb{Z}_2^6$	$\mathbb{Z}_2^2$	0	0	$\mathbb{Z}_2^2$	0	0	$\mathbb{Z}_2^{20}$
22	$\mathbb{Z}_3$	$\mathbb{Z}_5$	$\mathbb{Z}_7$	$\mathbb{Z}_9$	$\mathbb{Z}^{10}$	$\mathbb{Z}_{13}$	$\mathbb{Z}_{15}$	$\mathbb{Z}_{17}$	$\mathbb{Z}_{19}$	$\mathbb{Z}_{21}$
23	0	0	0	0	0	0	0	0	0	0
24	$\mathbb{Z}^2$	$\mathbb{Z}_5$	$\mathbb{Z}_7$	$\mathbb{Z}^2 \oplus \mathbb{Z}_3$	$\mathbb{Z}_{11}$	$\mathbb{Z}_{13}$	$\mathbb{Z}^2 \oplus \mathbb{Z}_5$	$\mathbb{Z}_{17}$	$\mathbb{Z}_{19}$	$\mathbb{Z}^2 \oplus \mathbb{Z}_7$
25	0	$\mathbb{Z}_2^4$	0	0	0	0	$\mathbb{Z}_2^4$	0	0	0
26	$\mathbb{Z}_3$	$\mathbb{Z}_5$	$\mathbb{Z}_7$	$\mathbb{Z}_9$	$\mathbb{Z}_{11}$	$\mathbb{Z}^{12}$	$\mathbb{Z}_{15}$	$\mathbb{Z}_{17}$	$\mathbb{Z}_{19}$	$\mathbb{Z}_{21}$
27	$\mathbb{Z}_2^2$	0	0	$\mathbb{Z}_2^8$	0	0	$\mathbb{Z}_2^2$	0	0	$\mathbb{Z}_2^2$
28	$\mathbb{Z}_3$	$\mathbb{Z}_5$	$\mathbb{Z}^6$	$\mathbb{Z}_9$	$\mathbb{Z}_{11}$	$\mathbb{Z}_{13}$	$\mathbb{Z}_{15}$	$\mathbb{Z}_{17}$	$\mathbb{Z}_{19}$	$\mathbb{Z}^6 \oplus \mathbb{Z}_3$

Table 8.4: Homology Groups by Circles (=m) and Radials (=n) in Top Hemisphere

Lemma 8.5.5. *gcd*(a, b) =*gcd*$(a, (b) \mod a)$ =*gcd*$((a) \mod b, b)$

Proof. Suppose g divides a and b, then g divides $a \mod b$ since $a \mod b = a + s(b)$ for s an integer. If g divides b and $a \mod b$, then g divides a, since $a = a \mod b + s(b), s$ an integer. By symmetry g divides a and b if and only if g divides a and $b \mod a$. □

Theorem 8.5.6. *Let m and n be as defined above. Then for a fixed m, $g = gcd(2m + 1, n)$ is cyclic in n. For fixed n, $g = gcd(2m + 1, n)$ is cyclic in m.*

Proof. By lemma 8.5.5, $g = gcd(2m + 1, n) = gcd(2m + 1, n \mod (2m + 1)) = gcd((2m + 1) \mod n, n)$ □

Theorem 8.5.7. *Let m and n be as defined above. Then for a fixed m, $H_1[m, n]$ is cyclic in n, with a period of $4m + 2$.*

Proof. g =gcd$(2m+1, n)$ is cyclic in n, of period $2m+1$, but if n is odd, then $H_1[m, n] = \mathbb{Z}_2^{g-1}$, and, if n is even, $H_1[m, n] = \mathbb{Z}^{g-1} \oplus \mathbb{Z}_{(2m+1)/g}$. So even though g is cyclic in n of period $2m + 1$, $H_1[m, n]$ has a different formula for odd and even n, and since $2m + 1$ is odd, we need a cycle of $4m + 2$ values of n, to be certain we have completed the cycle of values for $H_1[m, n]$. □

Theorem 8.5.8. *Let m and n be as defined above. Then for any fixed even n, $H_1[m, n]$ is not cyclic in m, and we can create infinitely many different 3-manifolds by varying m. However for any fixed odd n, $H_1[m, n]$ is cyclic.*

Proof. If n is even, $H_1[m, n] = \mathbb{Z}^{g-1} \oplus \mathbb{Z}_{(2m+1)/g}$. So even though g is cyclic in n, $H_1[m, n]$ will vary as $(2m + 1)/g$ varies. Thus we can create infinitely many values for $H_1[m, n]$ by increasing m. Since $H_1[m, n]$ is a topological invariant, we have created infinitely many different manifolds. If on the other hand, n is odd, $H_1[m, n] = \mathbb{Z}_2^{g-1}$ and varies cyclicly with g. □

8.6 Sieradski Manifolds as Cyclic Branched Covers of Knots

We will first define branched covers. For additional background consult Prasolov and Sossinki in [13].

Definition 8.3. Let M^3 and N^3 be 3-dimensional manifolds. A continuous map $p : M^3 \xrightarrow{p} N^3$ is said to be a *branched covering* if there exists a one-dimensional subcomplex L^1 in N^3 whose inverse image $p^{-1}(L^1)$ is a one-dimensional subcomplex in M^3 and p restricted to $M^3 - p^{-1}(L^1)$ is a covering. M^3 is called the *covering manifold*, N^3 the *base manifold* and L^1 is the *branching set*.

So, in the 3-dimensional case, we delete a one-dimensional subcomplex to get a covering. We recall that our Sieradski manifold starts as a 3-ball with top and bottom hemispheres divided into pie-shaped pieces by radials. We create the manifold by the bitwist construction quotient space. If we take an axis through the center of the 3-ball and extend to infinity on both ends of the axis, the axis creates a large circle. If our manifold has n radials, we rotate $1/n$ th of a turn and identify image points with their original points. The result is the Sieradski manifold, with only one radial, as shown in Figure 8.7.

This rotation of $2\pi/n$ is an action of the cyclic group of order n acting on the manifold. Therefore, the original manifold with n radials, is a cyclic branched cover of the manifold of one radial (1-slice pie), branched over the axis through the 3-ball.

We know that any closed 3-manifold can be created by cutting out tori and sewing them back to the holes they created, but with different homeomorphisms [6]. Also, in [6] page 278, we note that if we create the proper corridor complex link in $\mathbb{S}^3$ from a face pairing manifold and perform Dehn surgery on the corridor complex link with the appropriate surgery coefficients, we create the same manifold from which the corridor complex link was constructed.

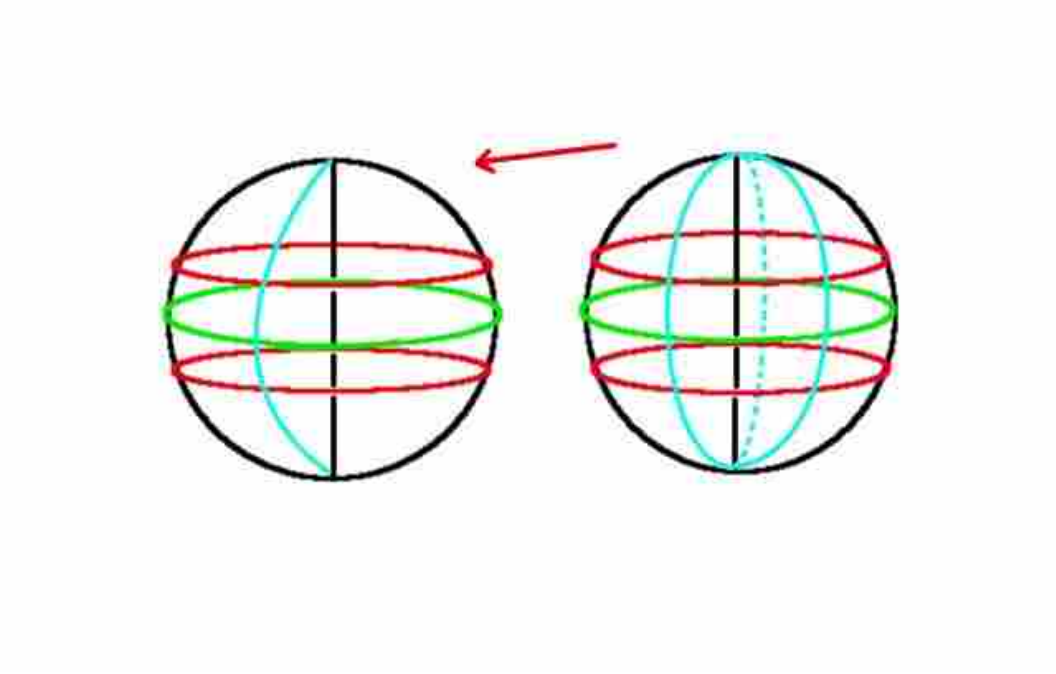

Figure 8.7: n-Slice (right) to 1-Slice(left)

To analyze this branched cover, start with a Sieradski manifold with just one circle and n radials. Next, identify points by rotating 1/n th of a turn. This results in Figure 8.8. The original Sieradski manifold is an n-fold branched cover of Figure 8.8 (with identifications), branched over the axis. Next, create the corridor complex link on this figure. Surgery on the corridor complex link with surgery coefficients of 0 on the face components, and the appropriate coefficients on the edge cycles, which in this case are the bitwist factors of -1 and +1, results in the original manifold.

In Figure 8.8 we remove the corridor complex link and the axis from the 3-ball. We recall also that twist moves from [13] page 106 can be done without changing the resulting manifold. Continuing in the same figure, we do a +1 twist on the green circle which has a -1 surgery coefficient, which causes the green circle to disappear (as shown by arrow II) and the coefficient on the blue circle to change to +1, as described in [13].

Next, perform a -1 twist around the dark blue circle, as shown by arrow III, twisting the red circle, but not changing the surgery coefficient. Continuing in Figure 8.9, straighten

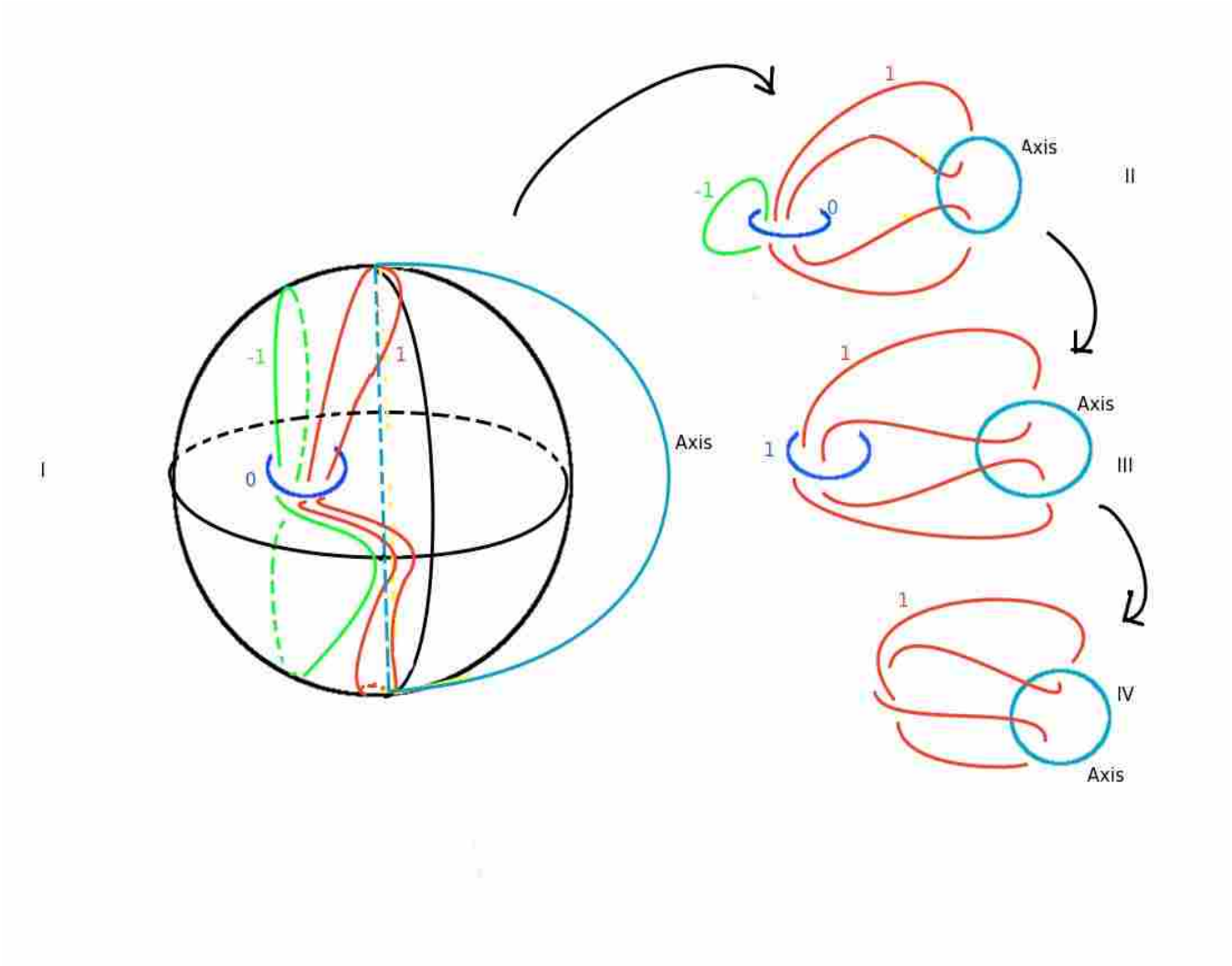

Figure 8.8: 1 Slice Pie

out the red link component, causing the axis to be twisted (not a twist move). In this same figure, do a -1 twist on the red circle, twisting the axis. Finally, untangle the axis a bit, and by moving over the top middle arc, we have a trefoil. The final result shows that our original Sieradski manifold with one circle and n radials, is an n-fold cyclic branched cover of $\mathbb{S}^3$, branched over the trefoil knot.

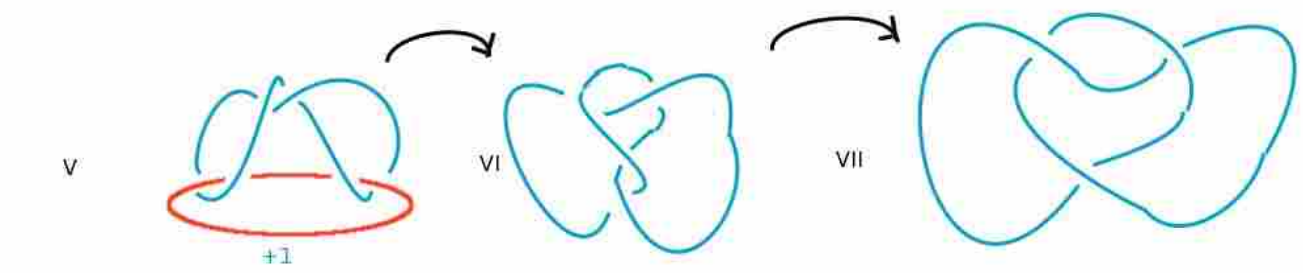

Figure 8.9: Twist to Trefoil

In the same manner, as we generalized the first homology groups in the case where additional circles or so-called pies were added, we want to generalize the knot which is the branching set over which the Sieradski manifold is a cyclic branched cover of $\mathbb{S}^3$.

We start with a simple example of an additional circle and construct the corridor complex link. This is shown in Figure 8.10. In preparation for the generalization, look at the green closed curve. One end circles around M, which is one end of the original axis, and the opposite end of the green curve goes around D, the other end of the axis. We are looking at a 3-ball from the top, with the bottom opened up. D is directly below M. The green circle represents the edge cycle of line segment AM being mapped to CD (AM - CD edge cycle) and then mapped back. The AB - CB edge cycle creates the same result, going around the two ends of the axis.

The edge cycles connecting the straight lines in the Sieradski manifold, then, cause the edge cycle components to loop around each end of the axis. What about the circles edges? First of all, the equator which passes through B on Figure 8.10 maps to itself. This creates an earring hanging on the face component of the only face map effecting this circle. The other circles are mapped by the two face mappings on either side of those circles. The two face components are neighbors, and the edge cycle component has one end around one face component and the other around its neighbor face component.

In Figure 8.10, the green and the purple loops are the straight line edge cycle components, which loop around the ends of the axis. The dark red is the earring going to the equator, and the red is the edge cycle between the circles through C and through A. This red edge cycle component hooks the two face components together.

What happens with more than two pies or representative circles? Figure 8.11 has 4 maps, or 4 circles, looking at the upper and lower hemisphere. To make it easier to track the cycle components, we have represented the circles by rectangles. The result is the same as in the

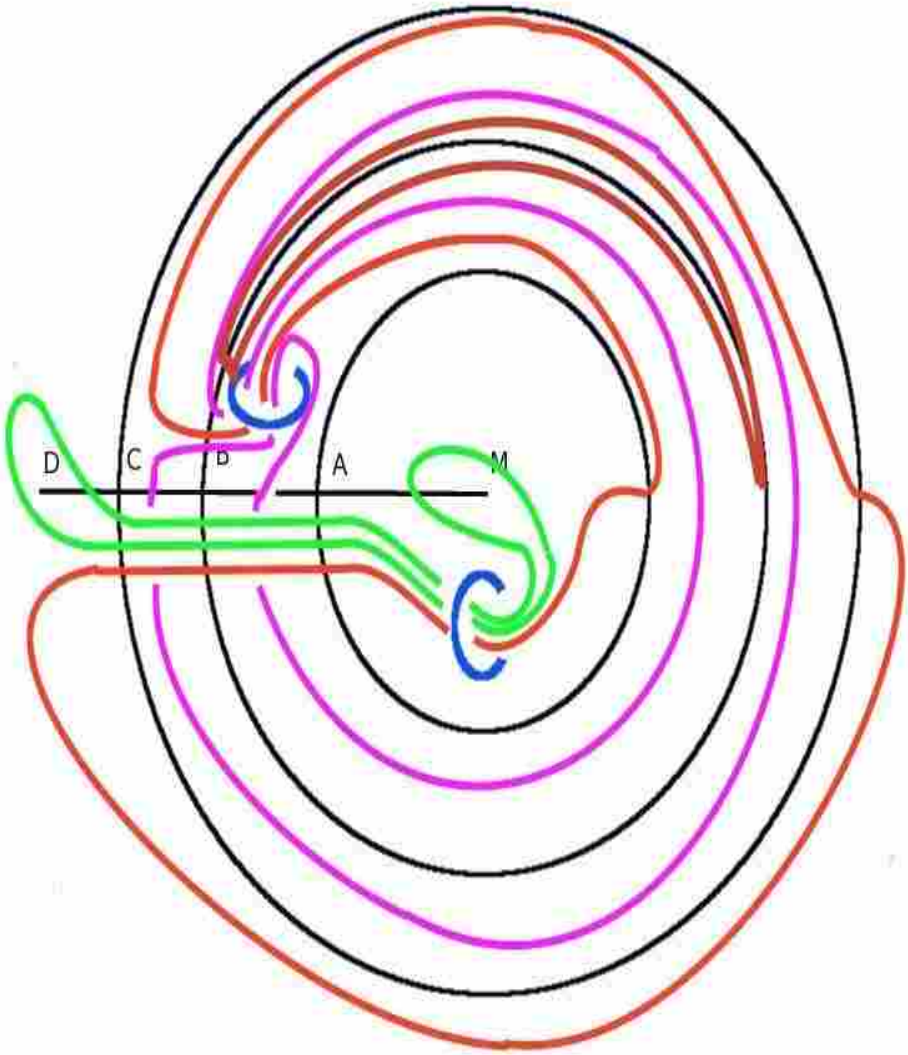

Figure 8.10: Two Pies 1 Slice

previous figure. The cycles between straight line are loops through the face component, with ends of loops around the ends of the axis. In the surgery diagram, created from the corridor complex link, the straight line cycles will have surgery factor of +1. The equator makes an earring in the last face component, and the other circles create edge cycle components which loop neighboring face components together. The circle components will have surgery factor of -1. Face components will have surgery factor 0.

If one has m pies or circles in hemispheres, the result on the various line and circle edge cycle components is the same. In Figure 8.12, we see the generalized corridor complex link, removed from the 3-ball.

Now that we have constructed the general corridor complex link for m circles in the top hemisphere (and 1 slice or radial), we recall that we can do twist moves without changing the resulting manifold. We proceed with twists, first on the -1 factor circles, then +1's, and finally, removing the face components circles working left to right. Remember, as explained above, a -1 surgery factor circle in the corridor complex link, is removed by a +1 twist. A +1 factor circle is removed by -1 twist. In the figures after Figure 8.12, the caption below the figure explains the change from the previous figure.

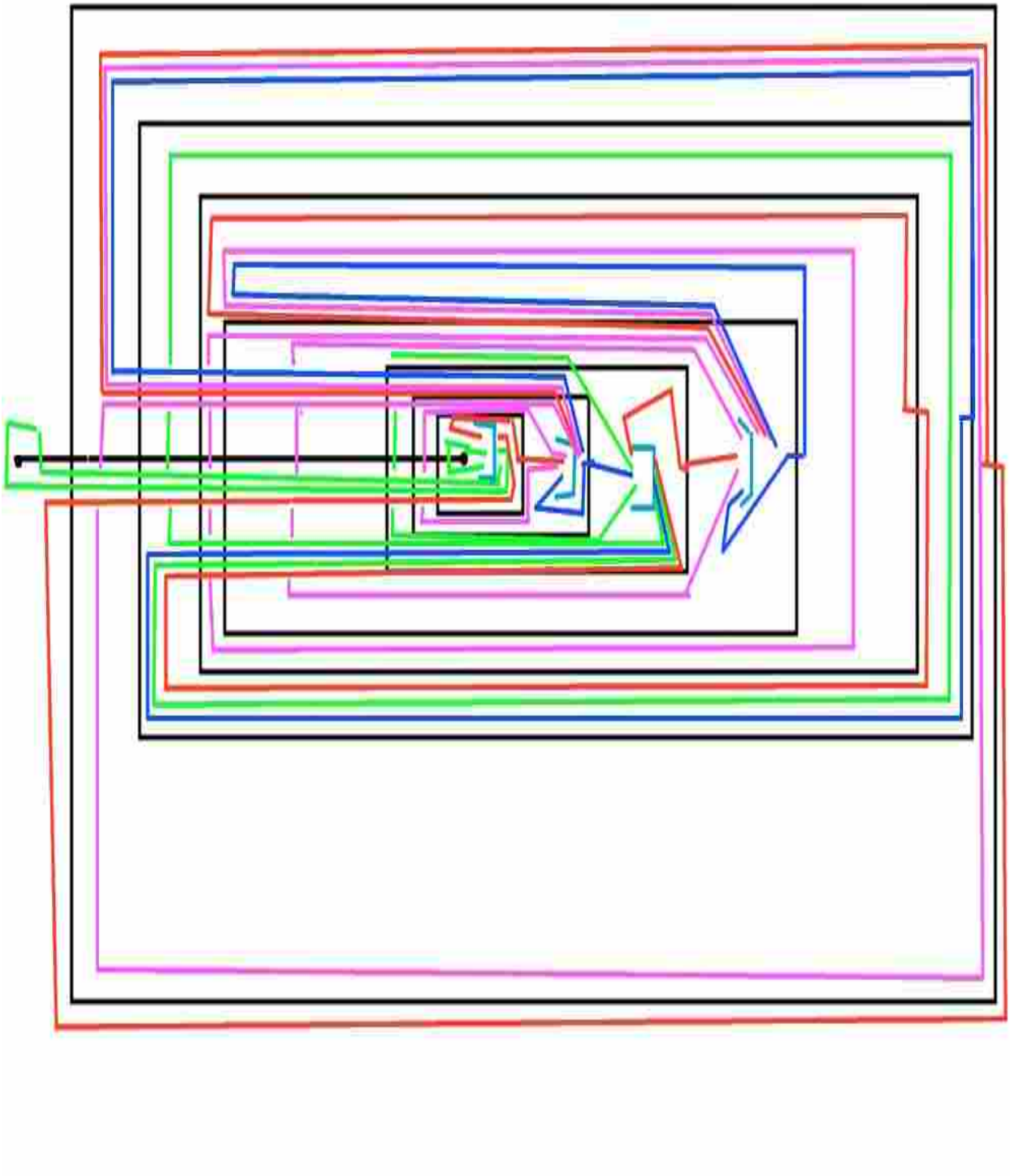

Figure 8.11: Four Circles and One Radial

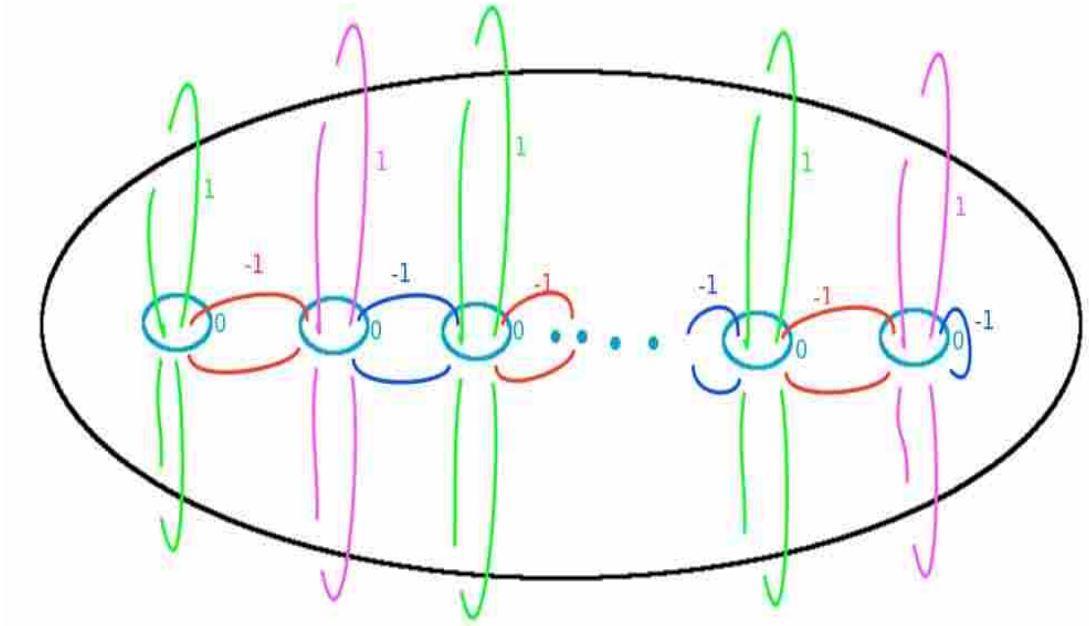

Figure 8.12: Sieradski- CCL- a

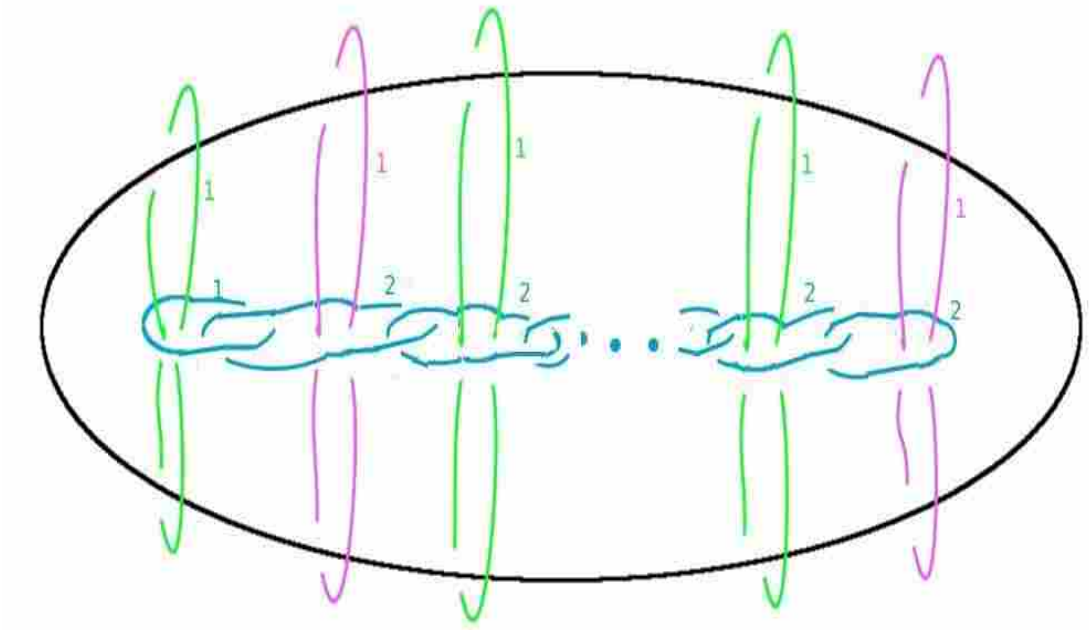

Figure 8.13: Sieradski- CCL- b: +1 Twist on All -1 Components

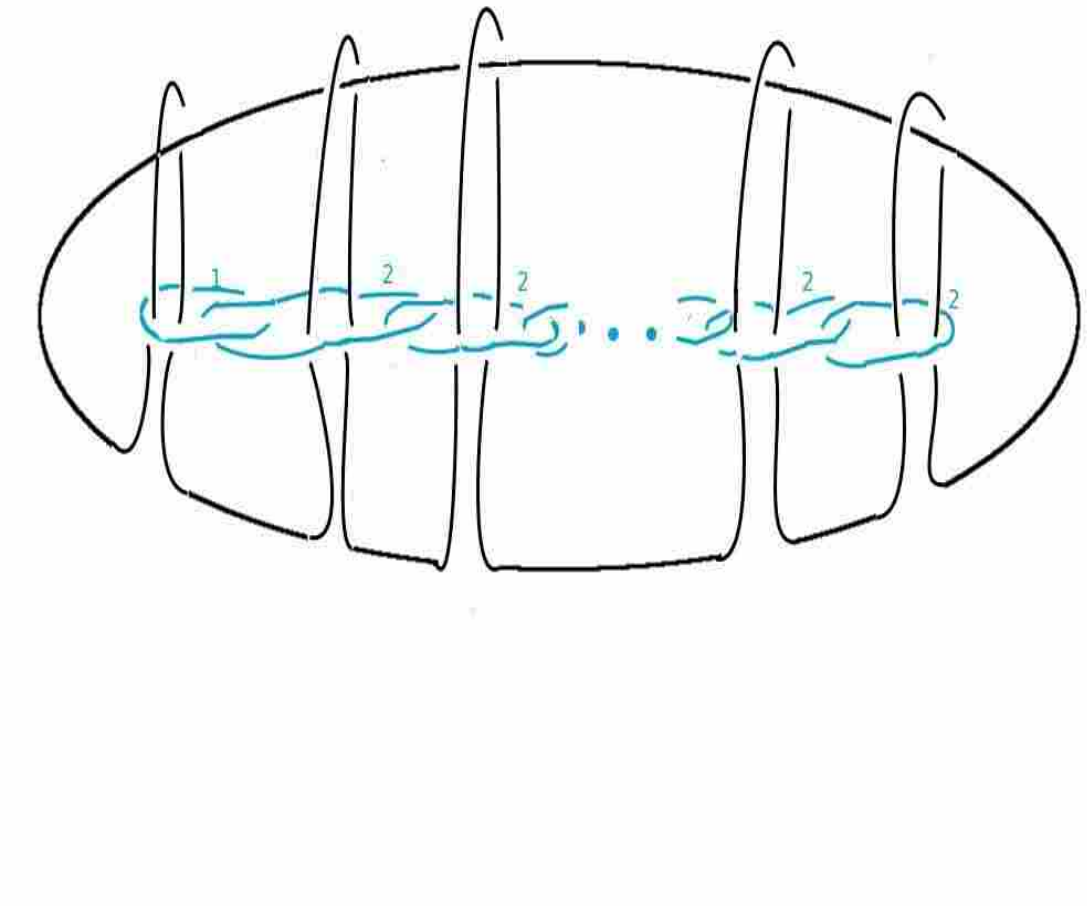

Figure 8.14: Sieradski- CCL- c:-1 Twist on Circle Loops around Axis

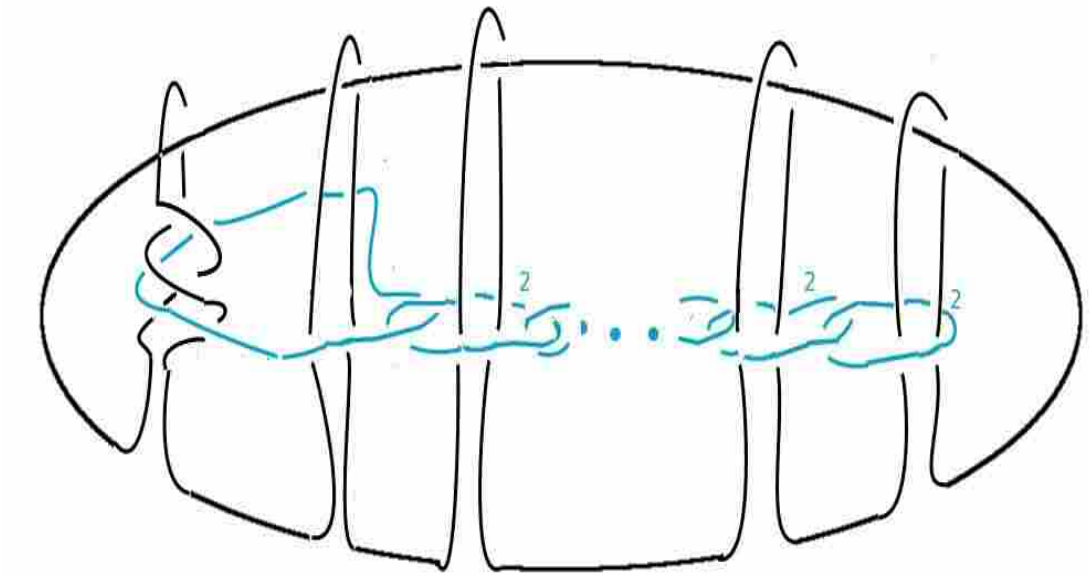

Figure 8.15: Sieradski- CCL- d: -1 Twist on +1 Face Component

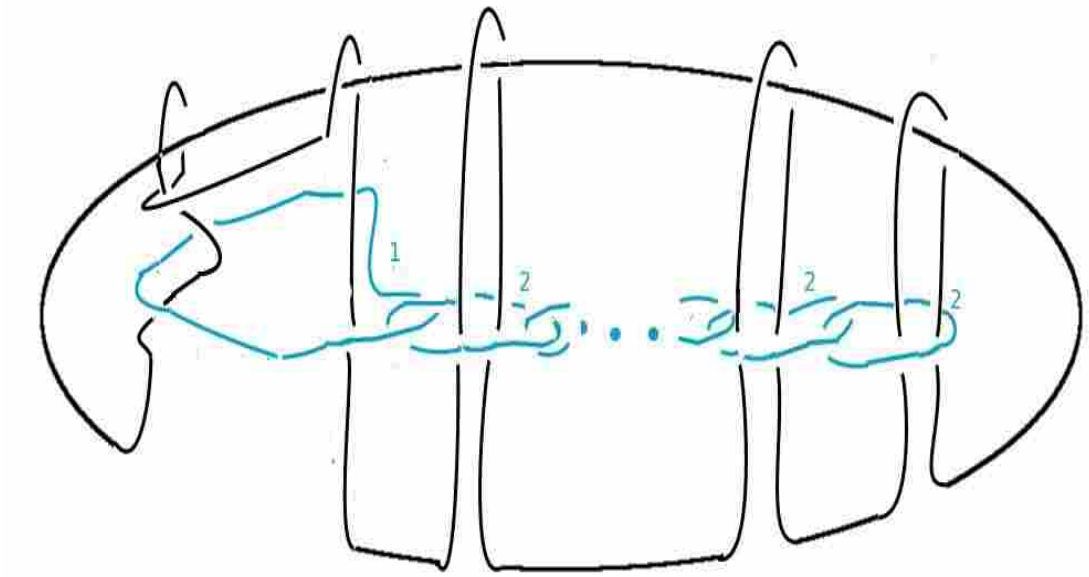

Figure 8.16: Sieradski- CCL- e: Lift Out Rectangle

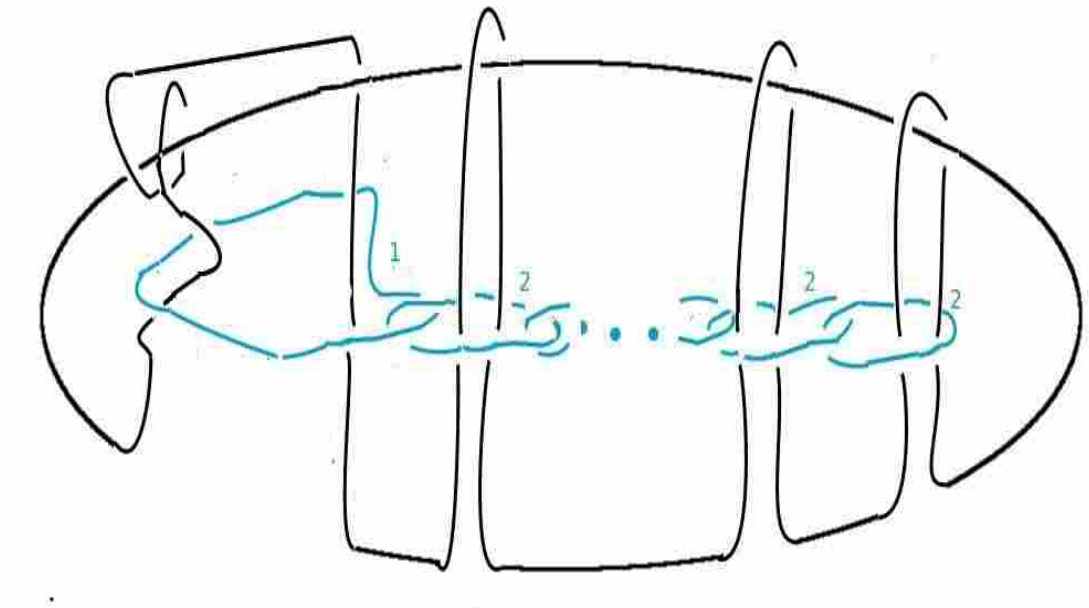

Figure 8.17: Sieradski- CCL- e1: Lift Segment over Axis

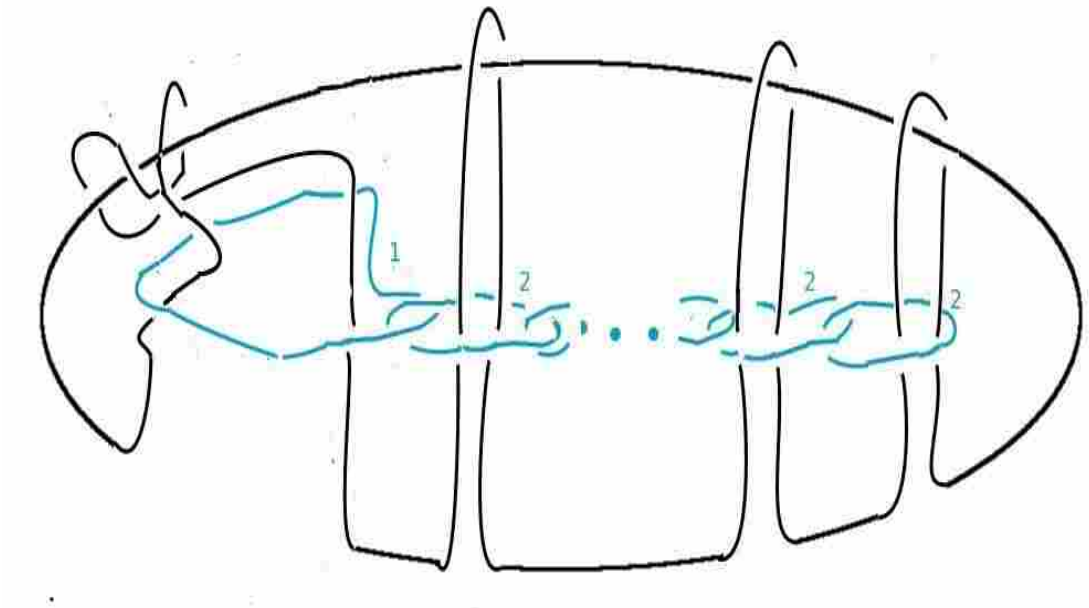

Figure 8.18: Sieradski- CCL- e2: Lower Segment behind Axis

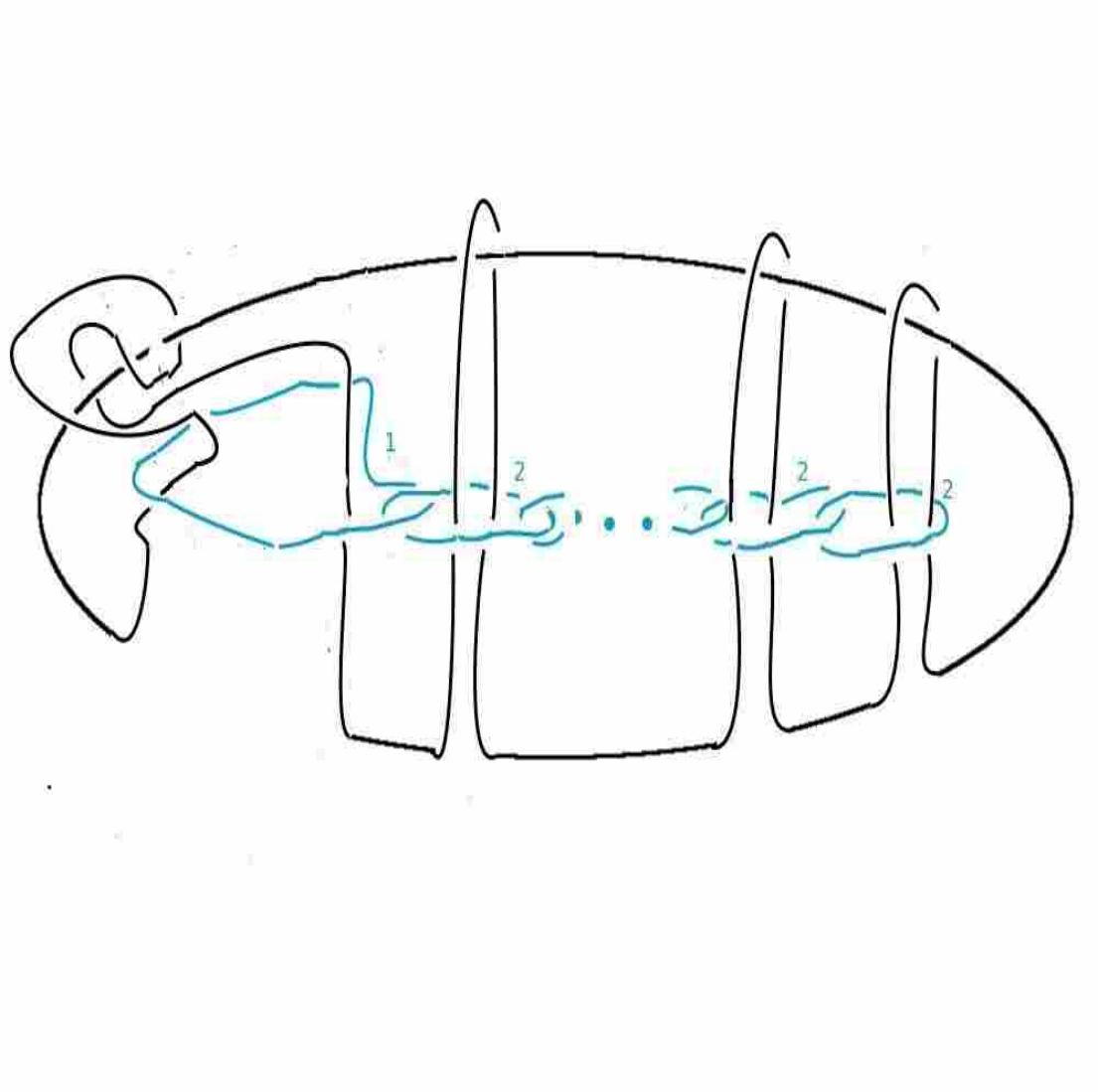

Figure 8.19: Sieradski- CCL- e3: Move Segment to Left

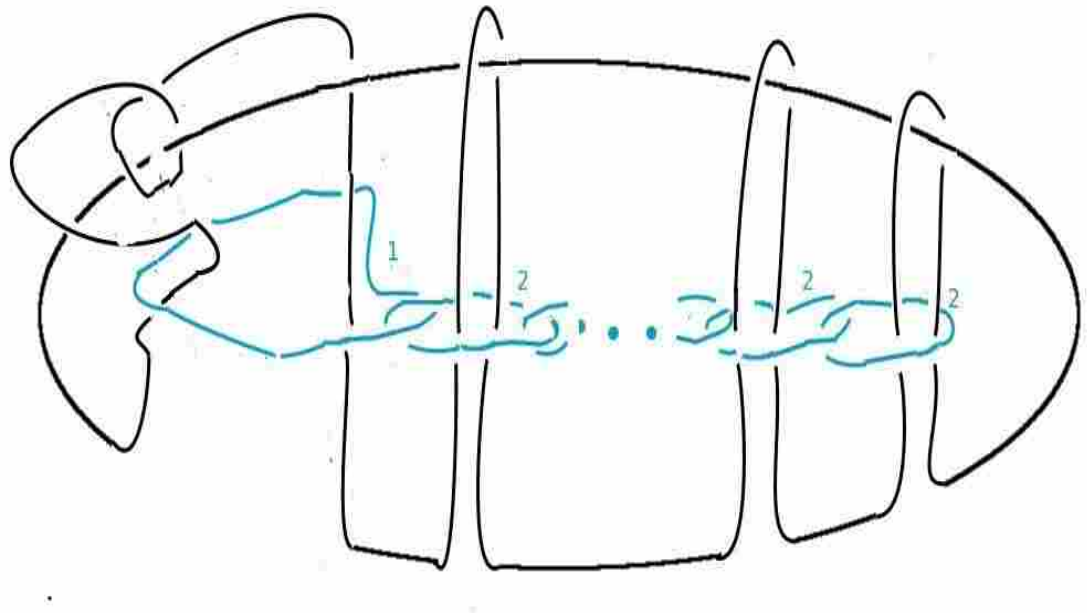

Figure 8.20: Sieradski- CCL- e4: Lift Segment behind Axis

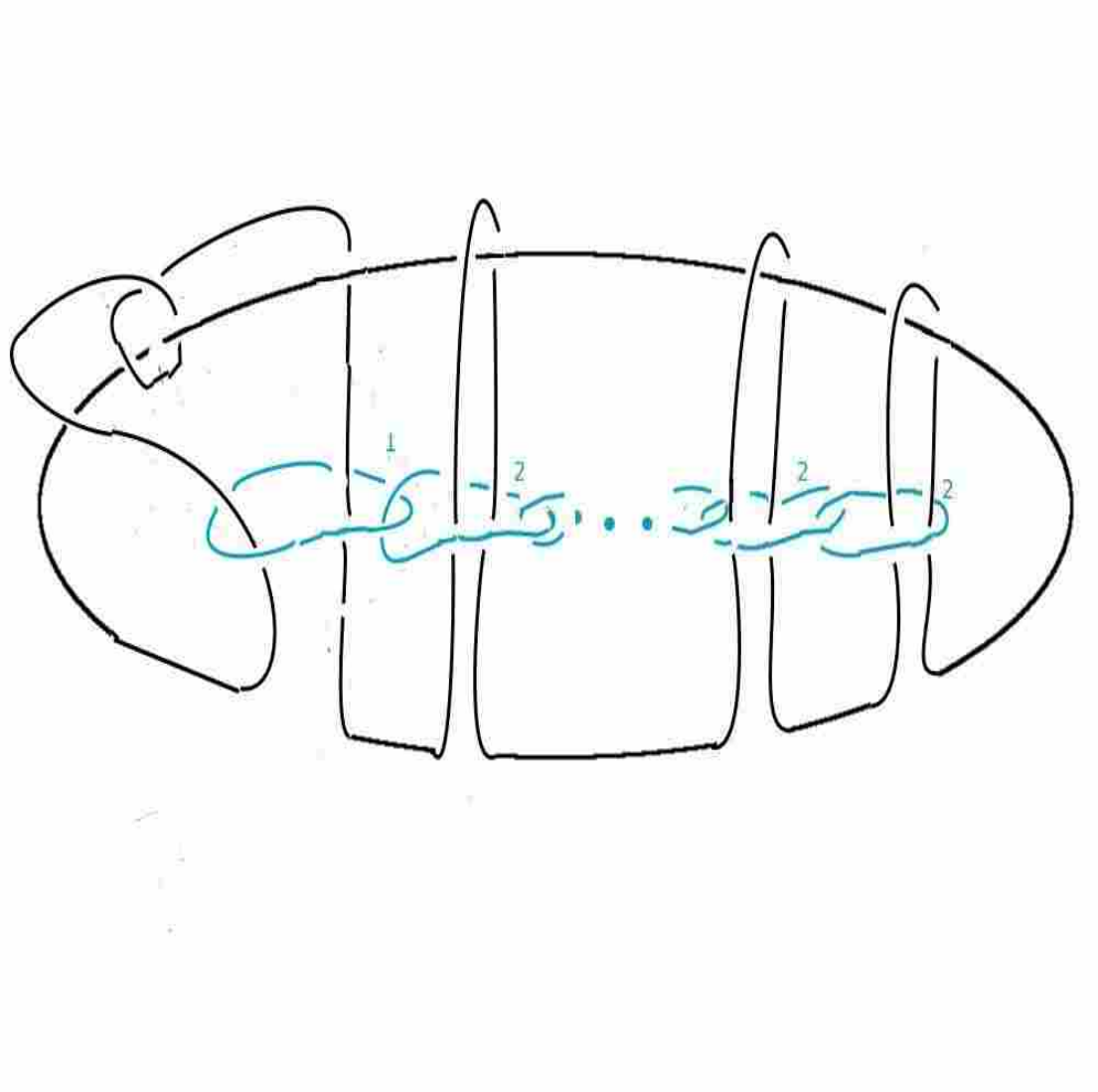

Figure 8.21: Sieradski- CCL- e5: Move +1 Face Component down

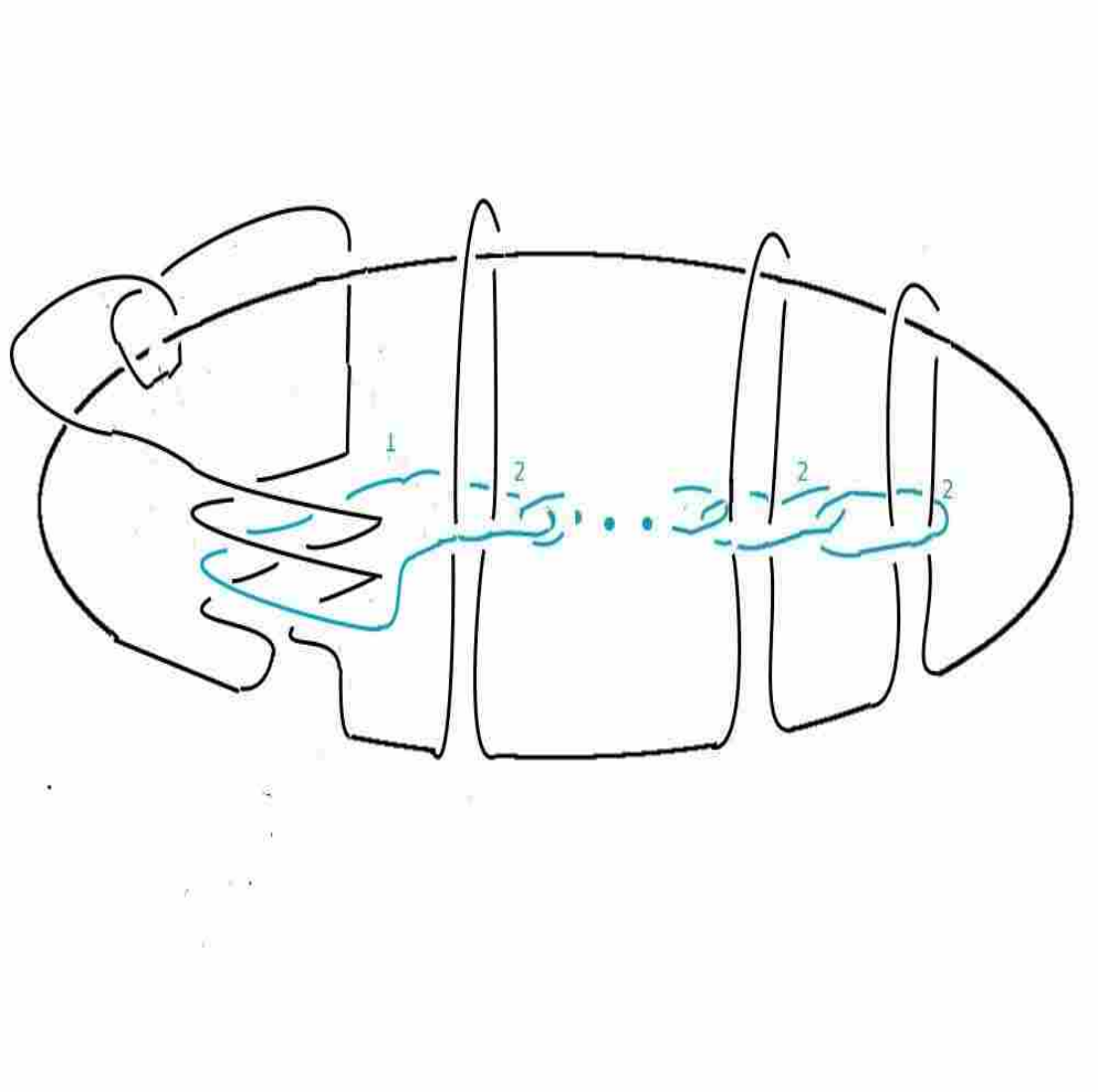

Figure 8.22: Sieradski- CCL- f: -1 Twist on +1 Face Component

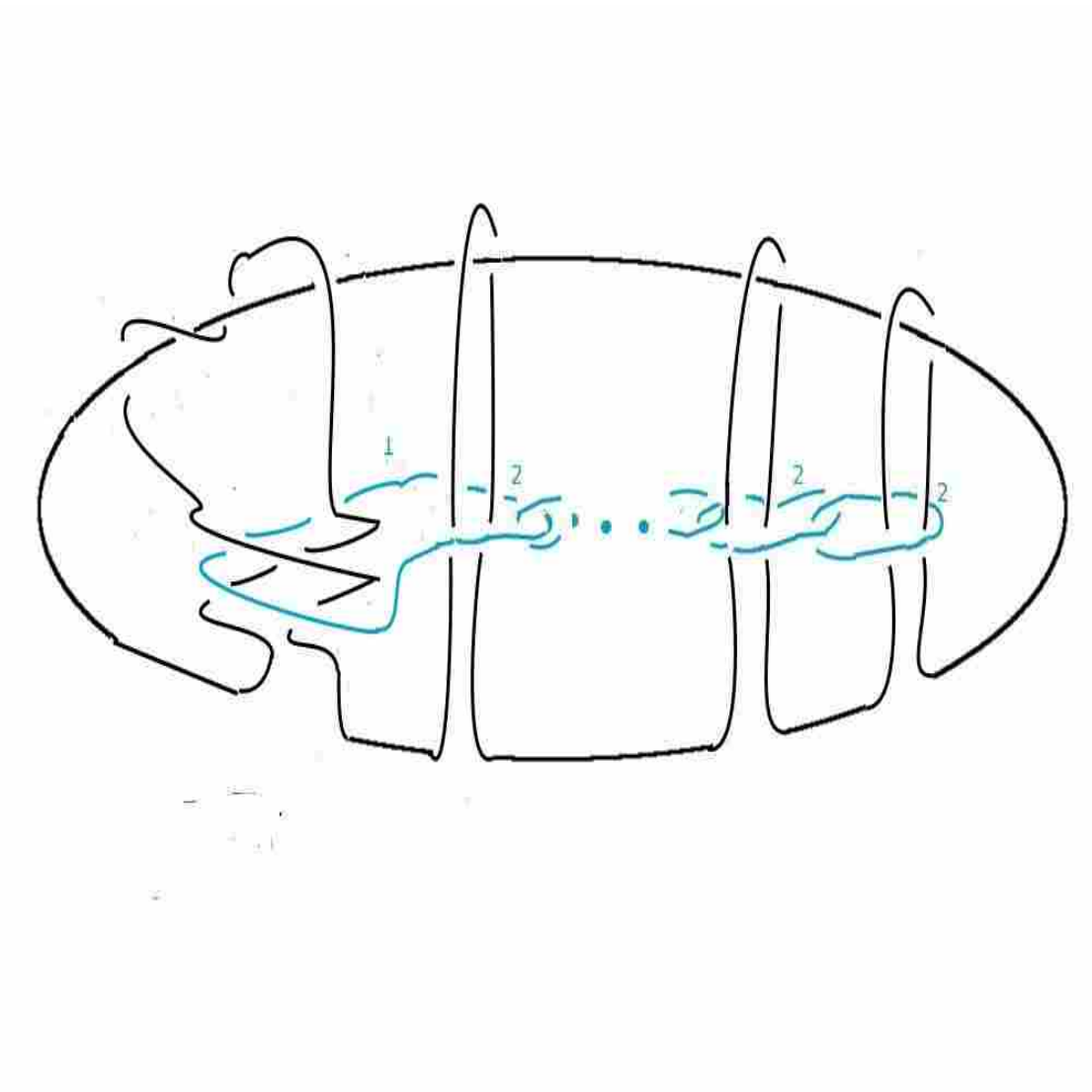

Figure 8.23: Sieradski- CCL- g: Last Loop above Axis Moves Right

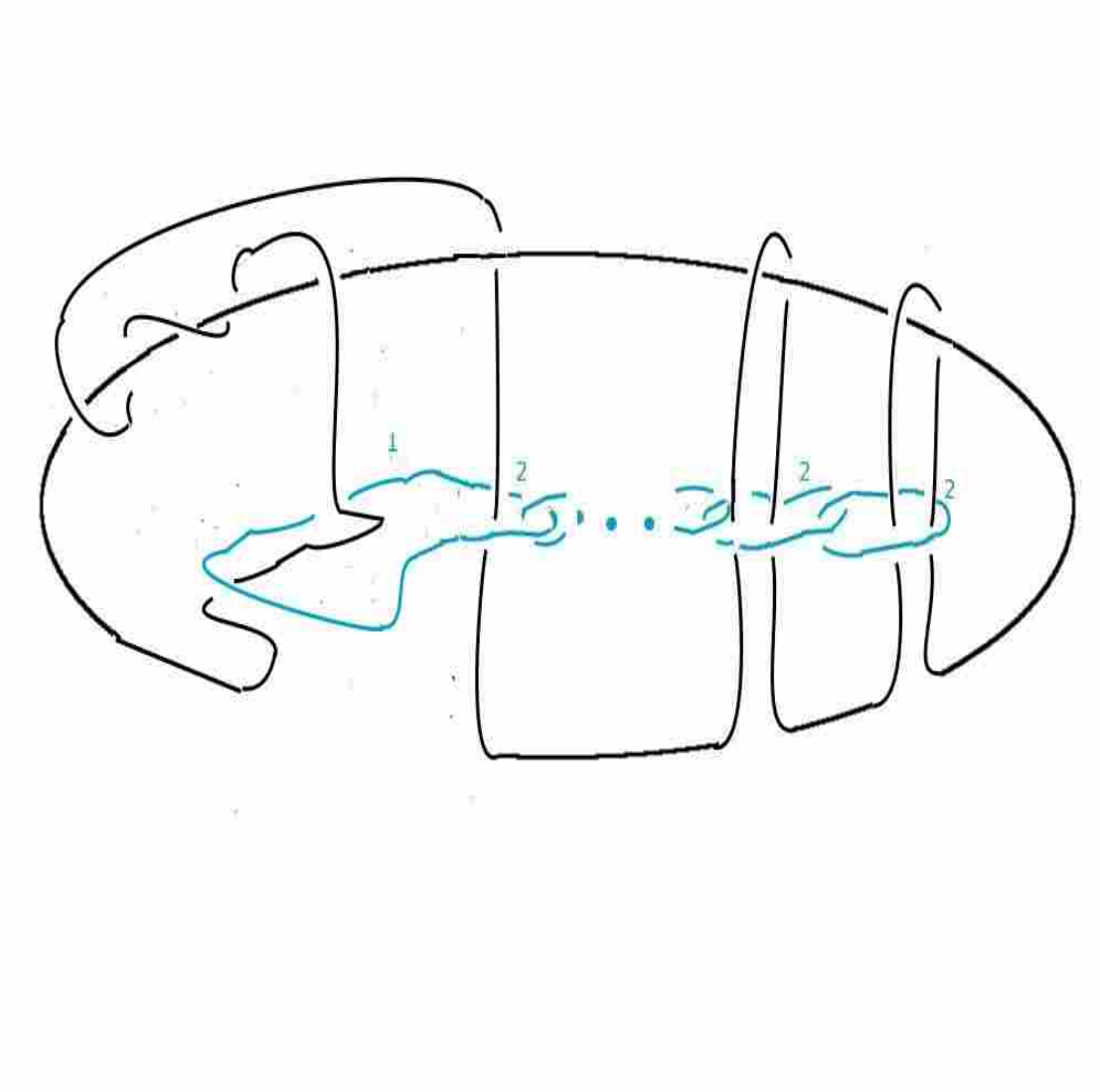

Figure 8.24: Sieradski- CCL- h: Lift Out Rectangle

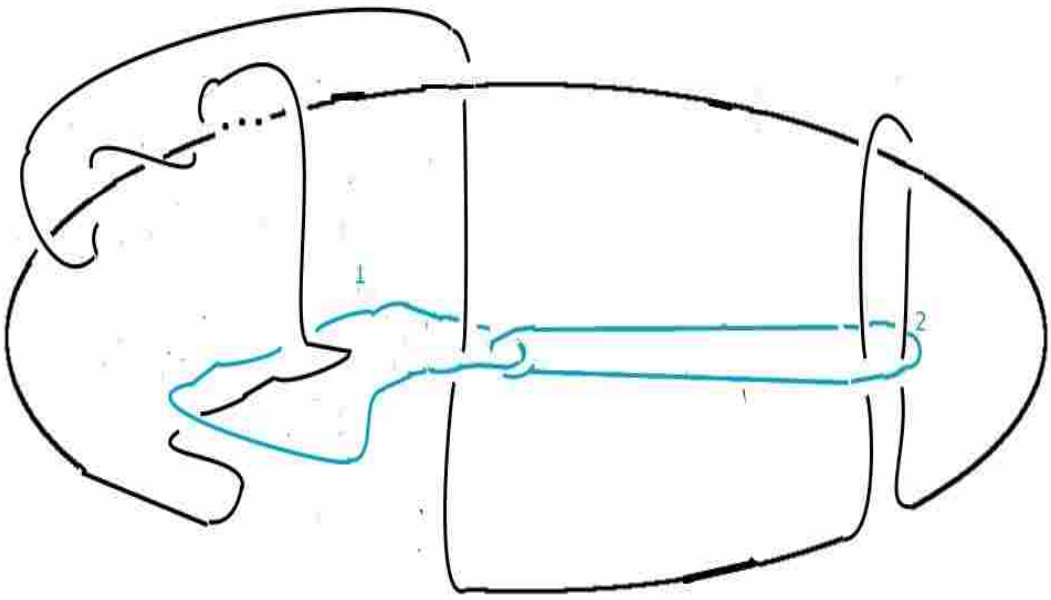

Figure 8.25: Sieradski- CCL- i: Move Dots to Upper Axis

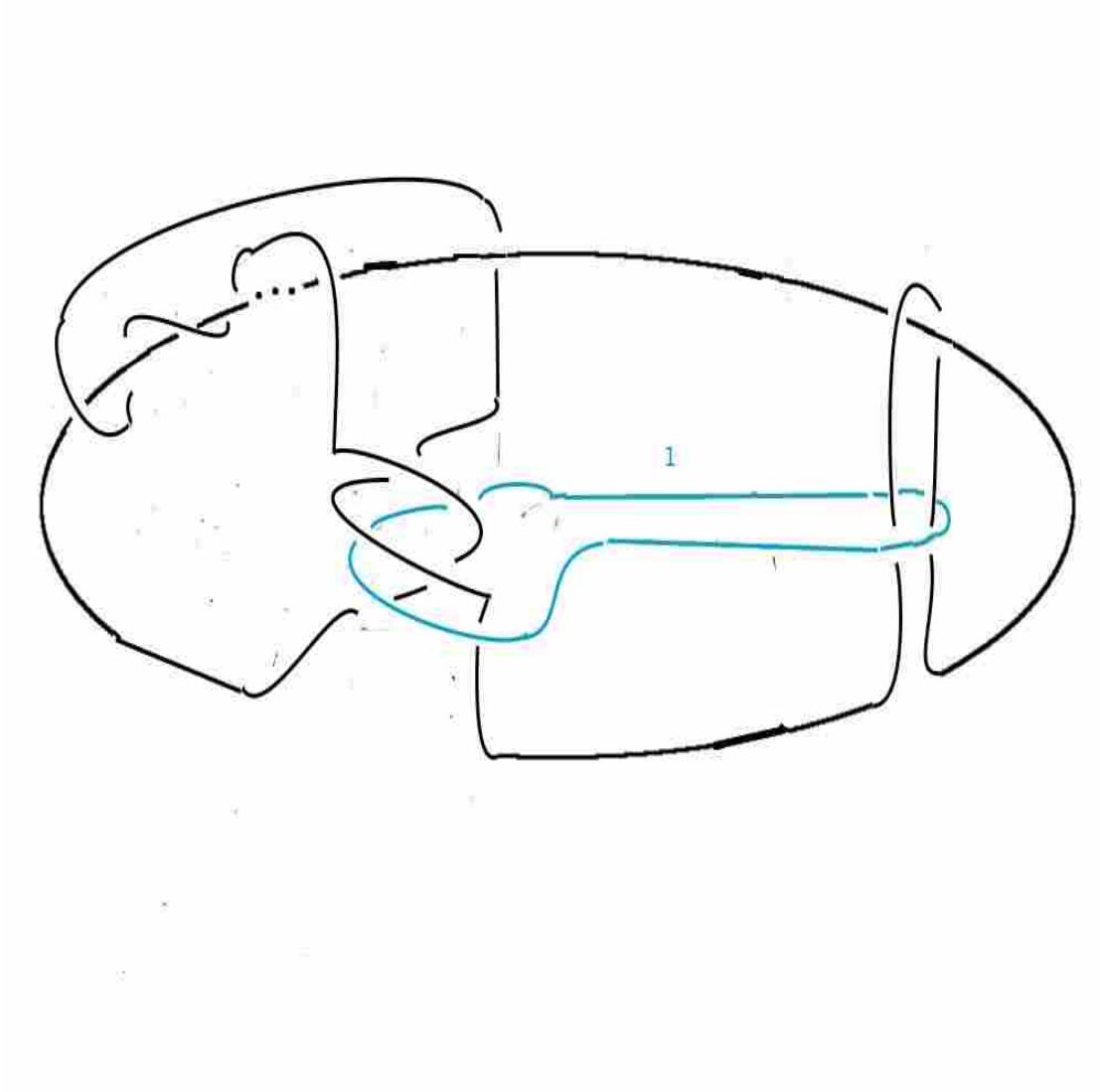

Figure 8.26: Sieradski- CCL- j: -1 Twist on +1 Face Component

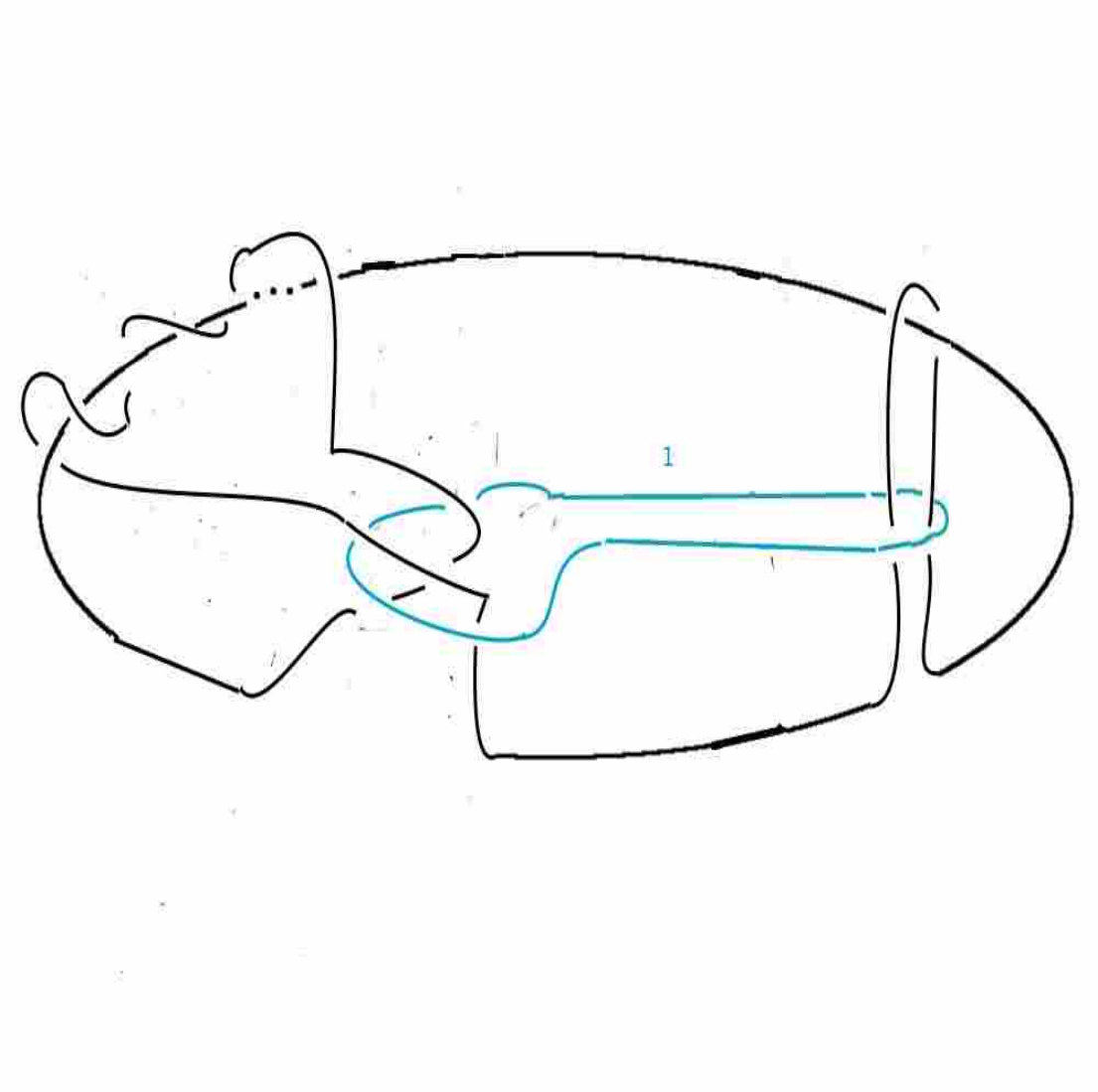

Figure 8.27: Sieradski- CCL- k: Move Upper Loop Down behind Axis

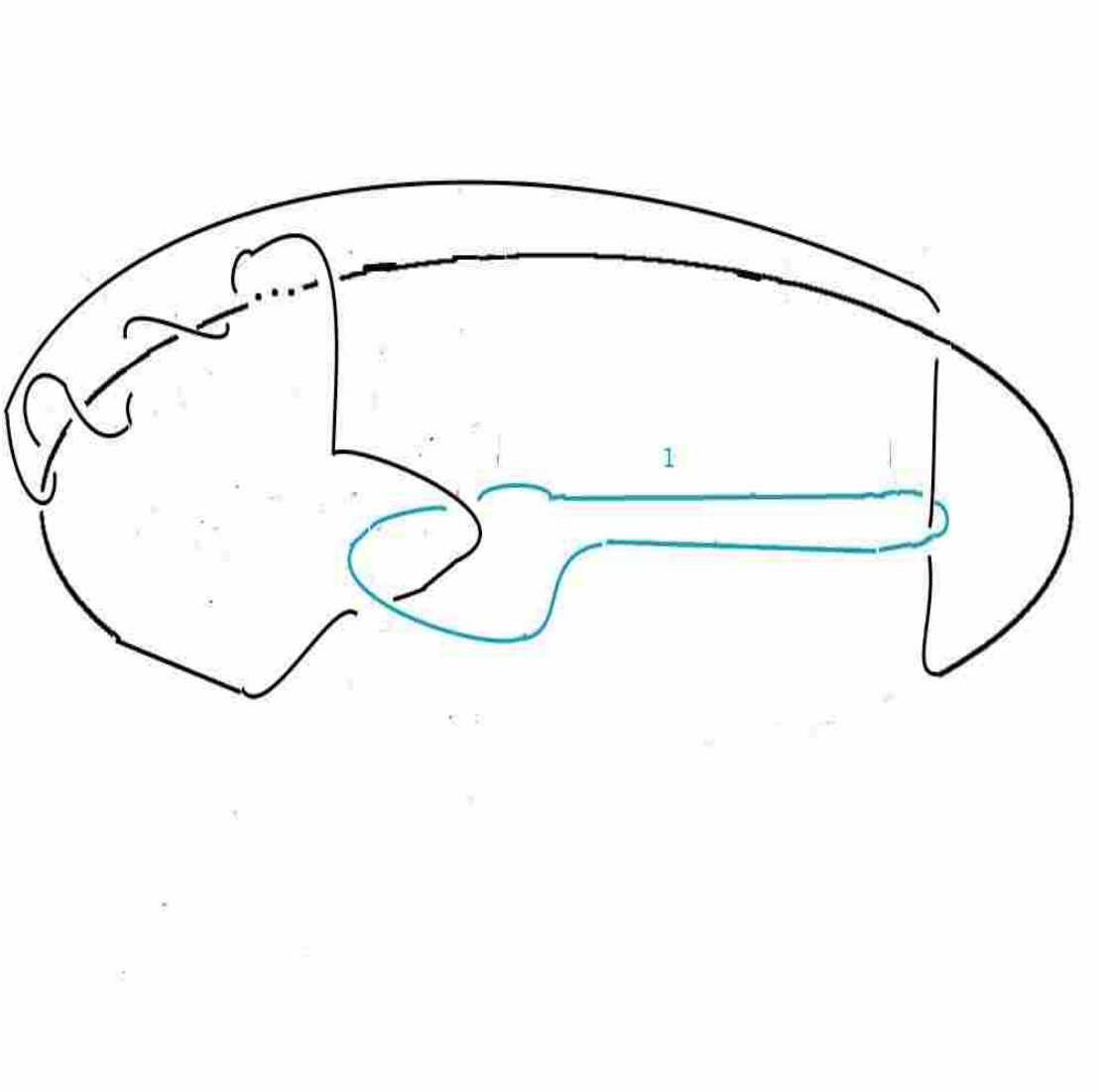

Figure 8.28: Sieradski- CCL- l: Lift Out Rectangle

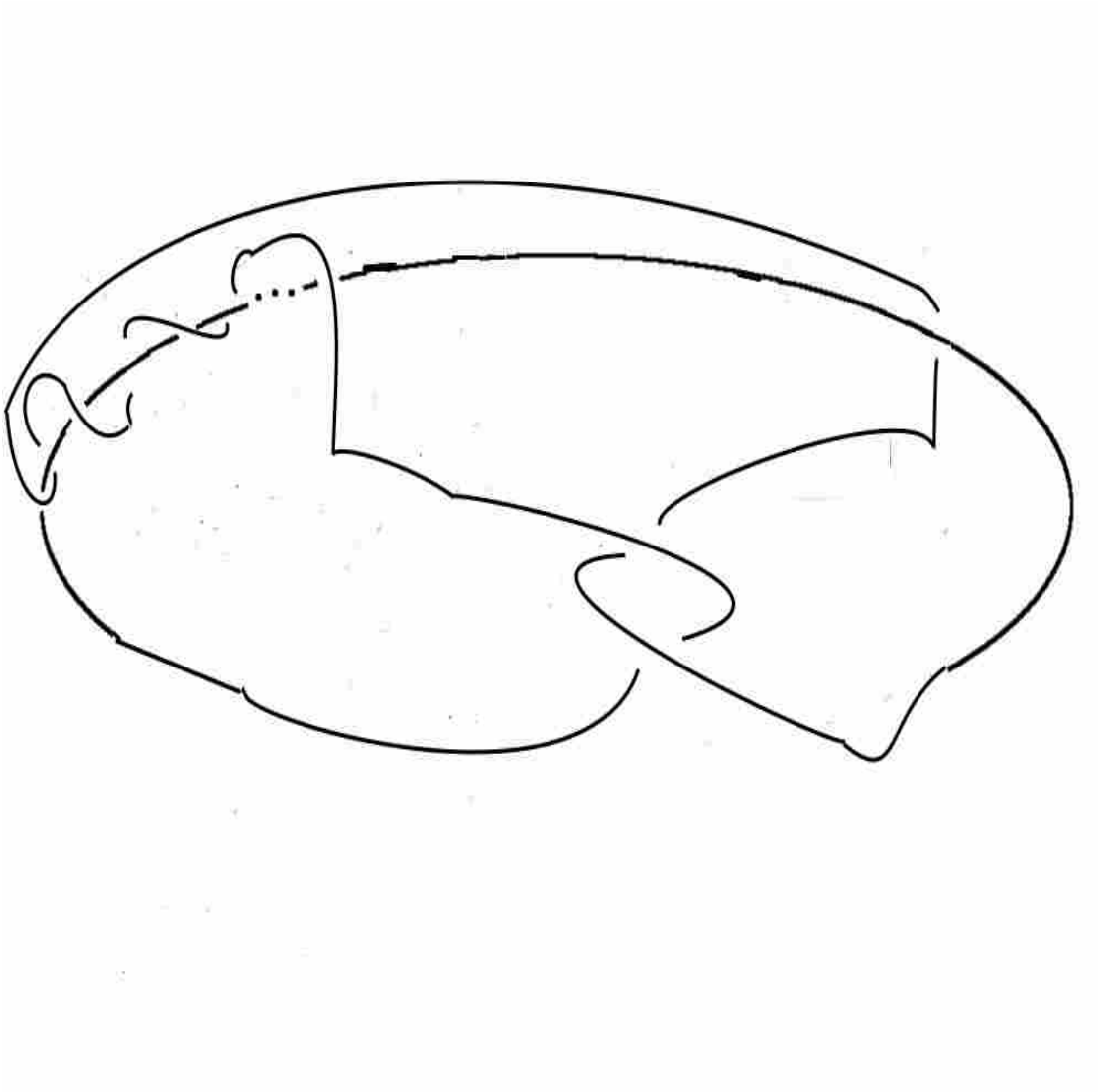

Figure 8.29: Sieradski- CCL- m: -1 Twist on +1 Face Component

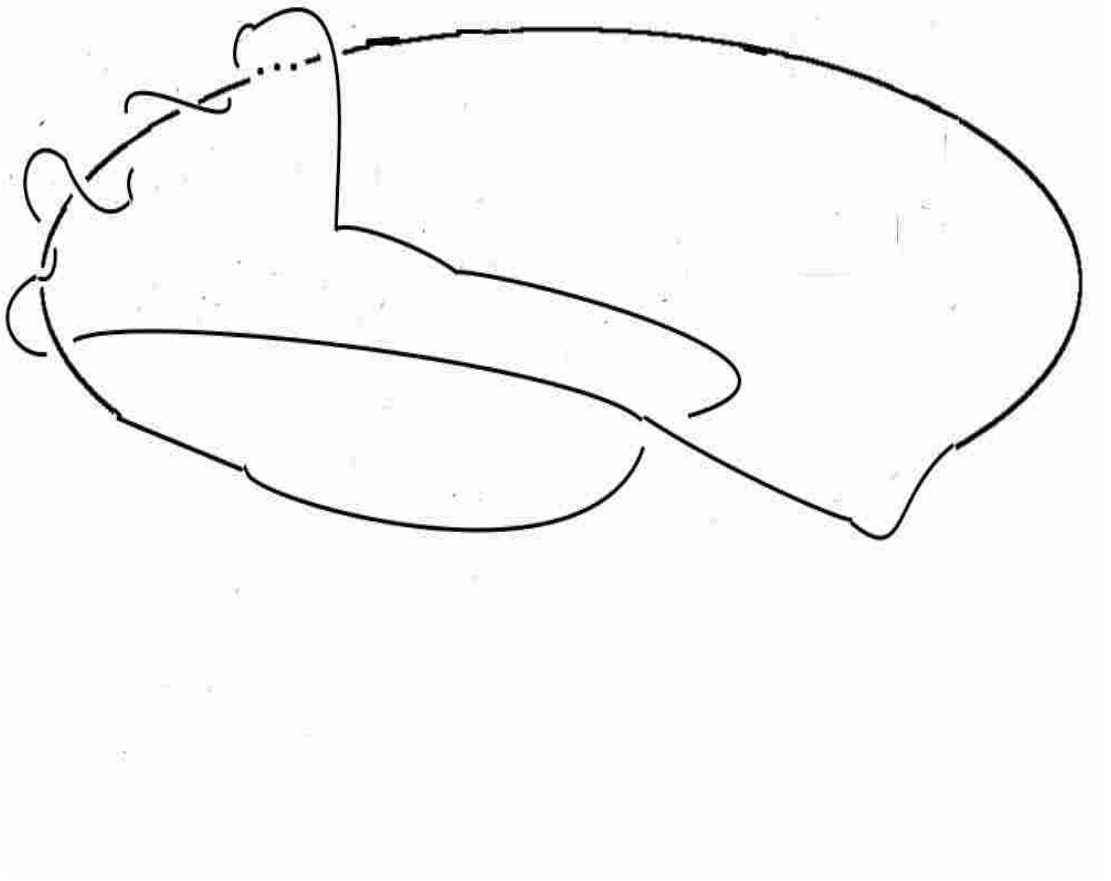

Figure 8.30: Sieradski- CCL- n: Bring Down Loop above Axis

For one pie or circle, we got a trefoil knot. Generalizing to m pies or circles in the hemisphere, we get a closed two braid with additional twists for each pie or circle.

We might also ask, what would be the result of changing the -1 twist factor on the circle edges to be a +1? In [3] it is said that the Sieradski manifolds are changed to the Fibonacci manifolds by this change. Which knot would result from this change? If we start again with the corridor complex link, we get Figure 8.31. We proceed as we just did except we replace the -1 factors with +1.

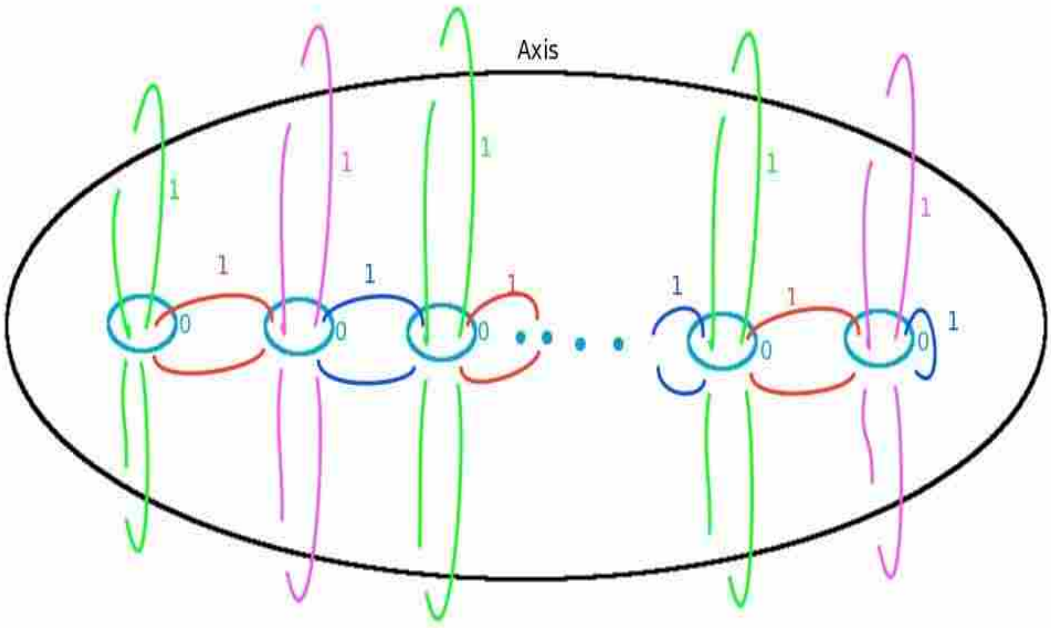

Figure 8.31: Regular Twist- CCL- a: -1 Factors Changed to +1

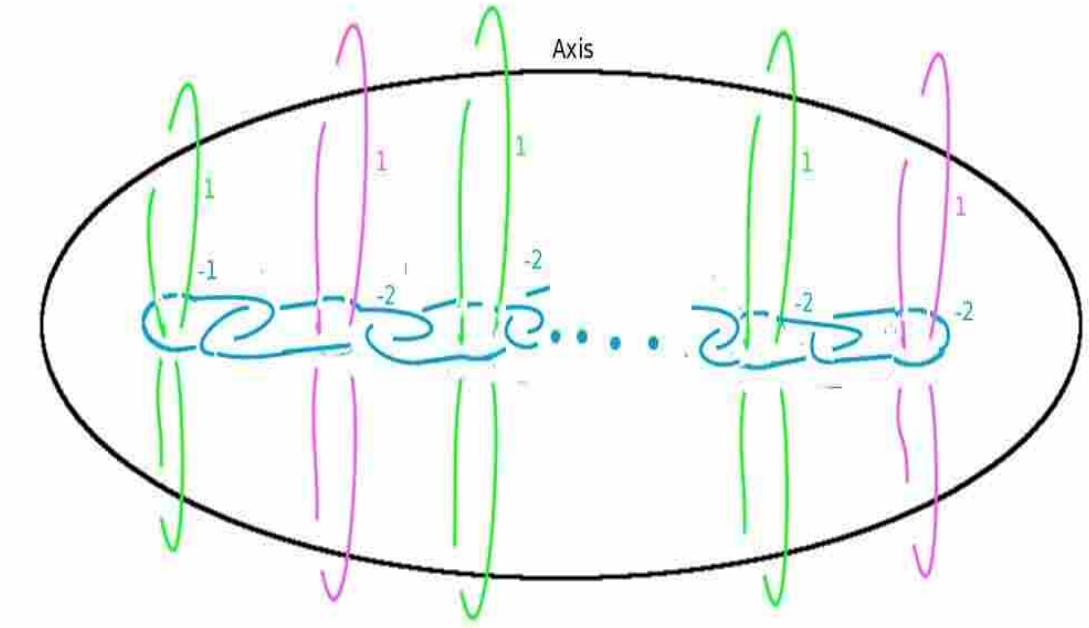

Figure 8.32: Regular Twist- CCL-b: -1 Twist on Circle Components

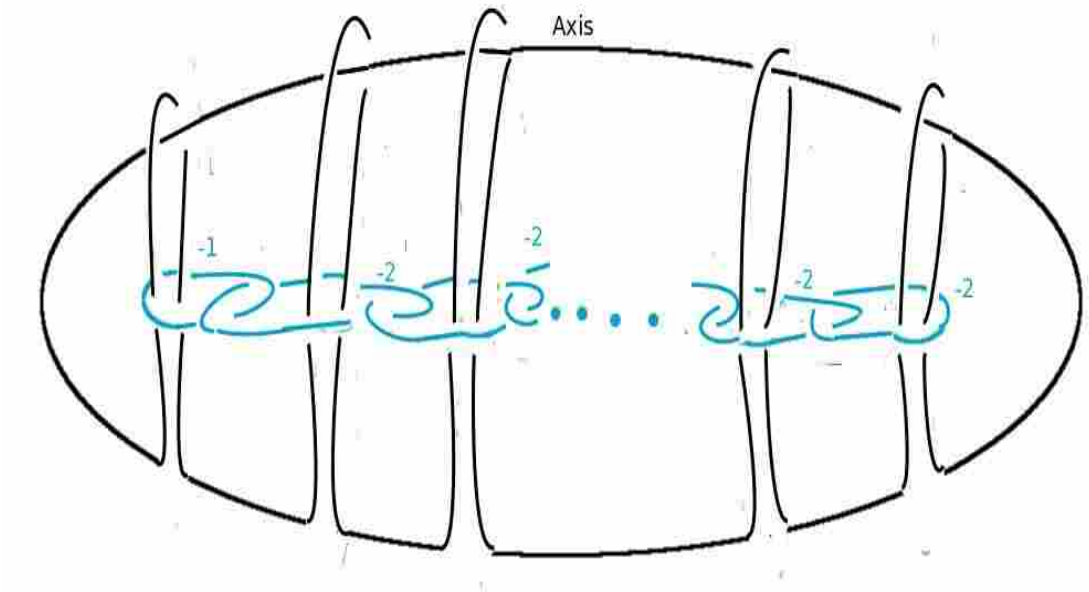

Figure 8.33: Regular Twist- CCL-c: -1 Twist on +1 Components

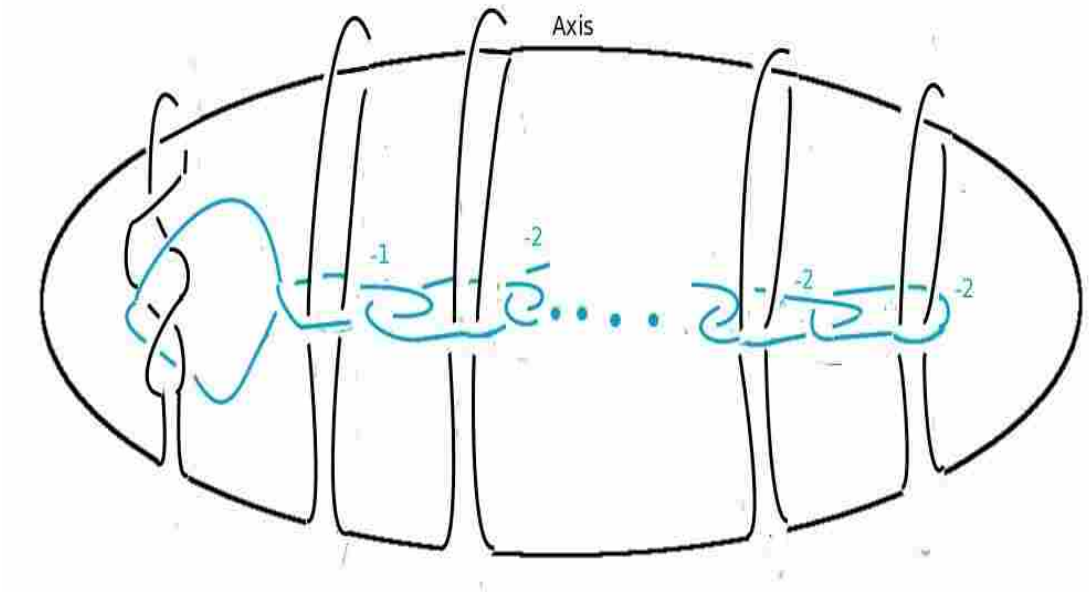

Figure 8.34: Regular Twist- CCL-d: +1 Twist on -1 Component

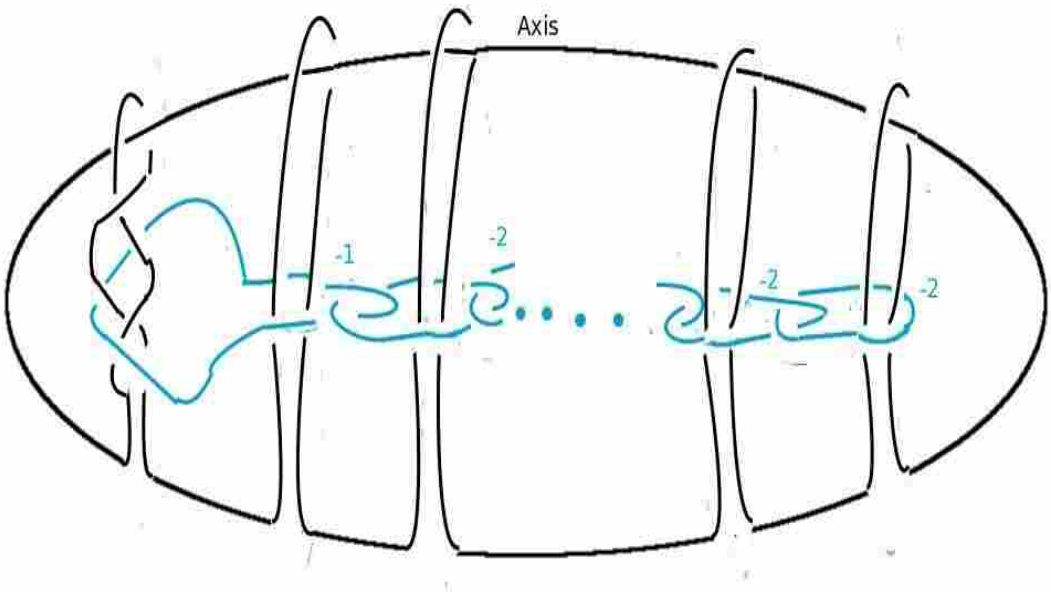

Figure 8.35: Regular Twist- CCL-e: Untwist -1 Component

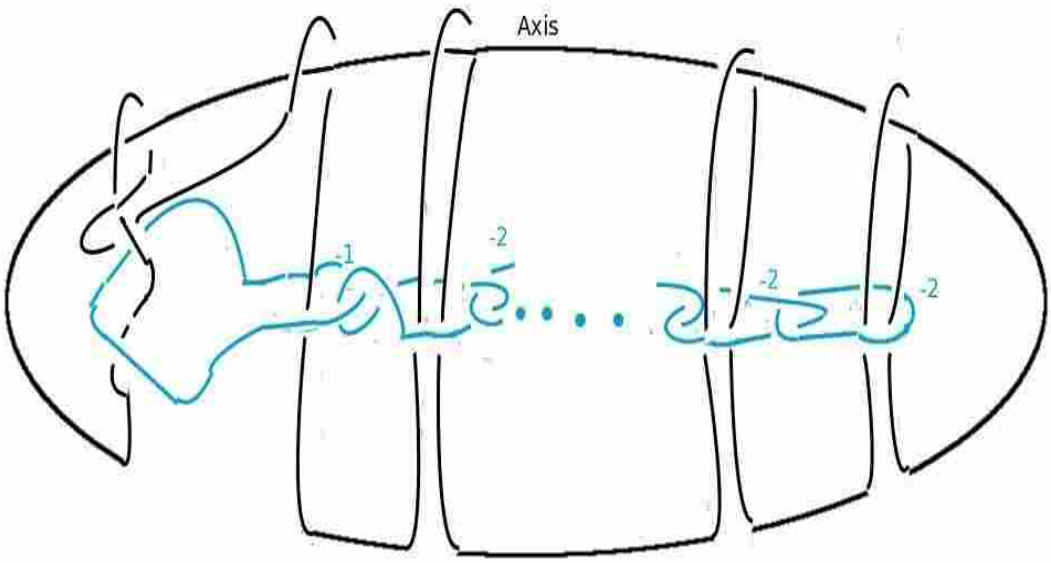

Figure 8.36: Regular Twist- CCL-f: Lift Out Rectangle

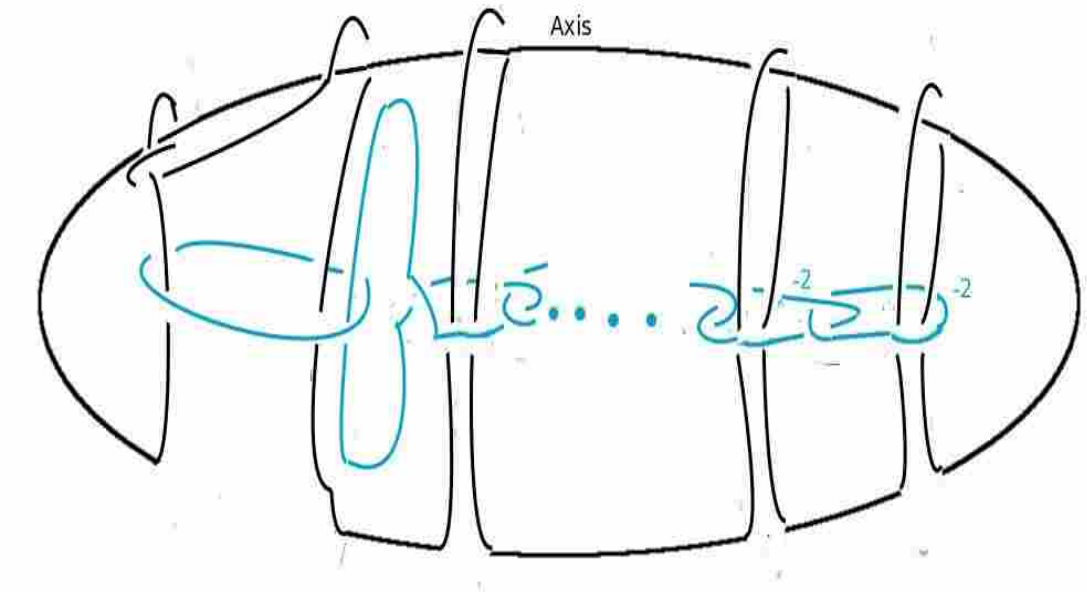

Figure 8.37: Regular Twist- CCL-g: Simplify Two Left Blue Circles

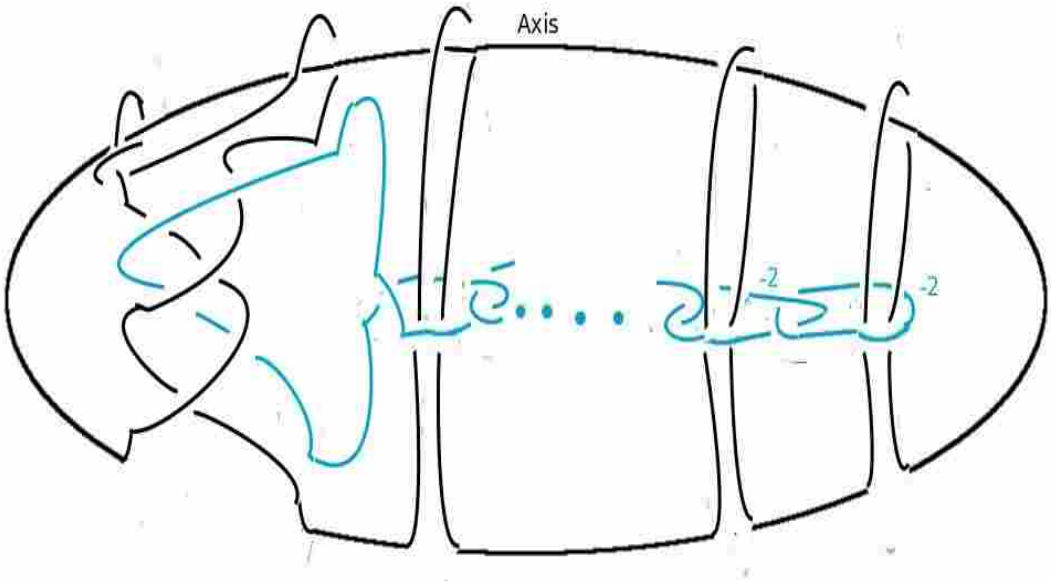

Figure 8.38: Regular Twist- CCL-h: +1 Twist on -1 Component

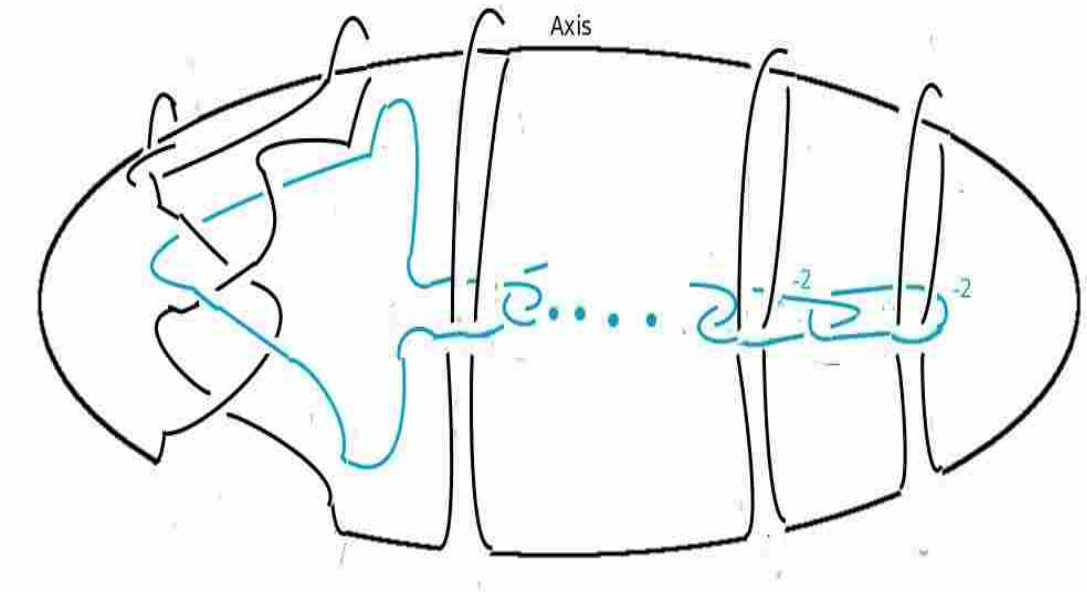

Figure 8.39: Regular Twist- CCL-i: Untwist Left Blue Circle

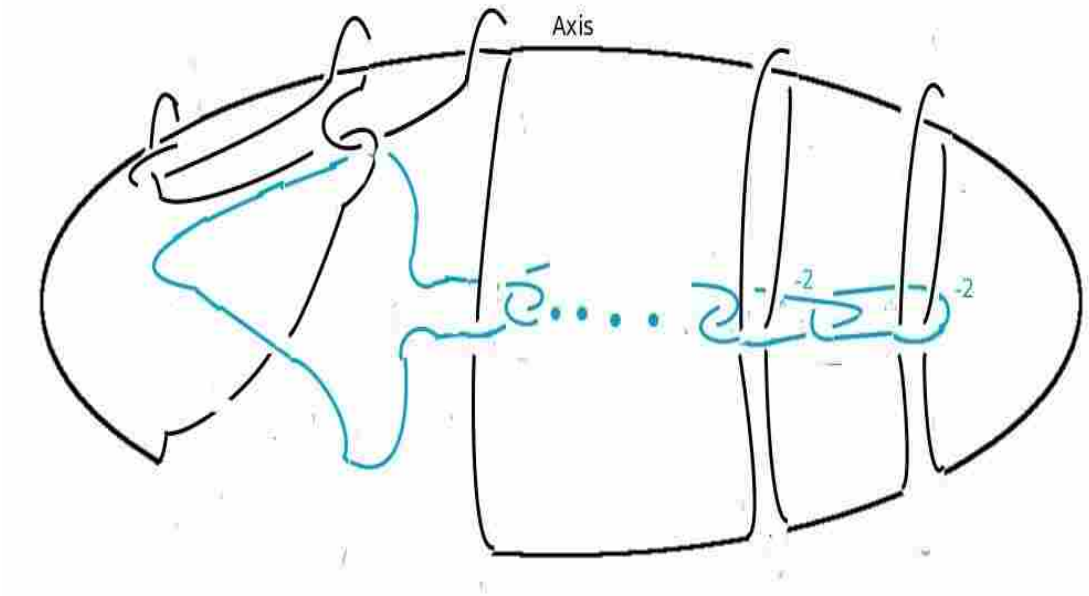

Figure 8.40: Regular Twist- CCL-j: Lift Out Rectangle

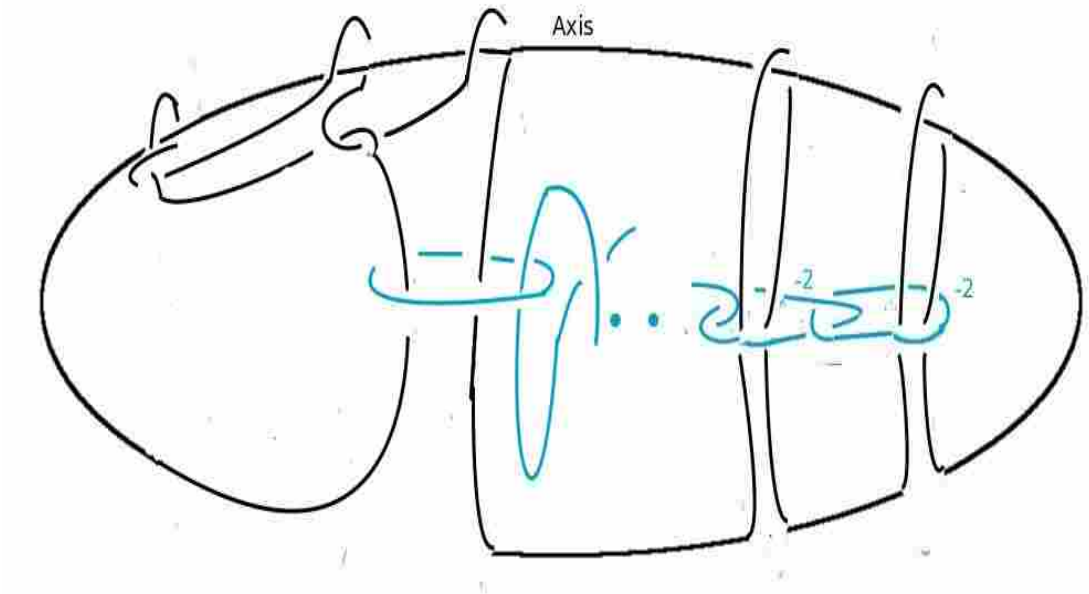

Figure 8.41: Regular Twist- CCL-k: Straighten Last Two Blue Circles

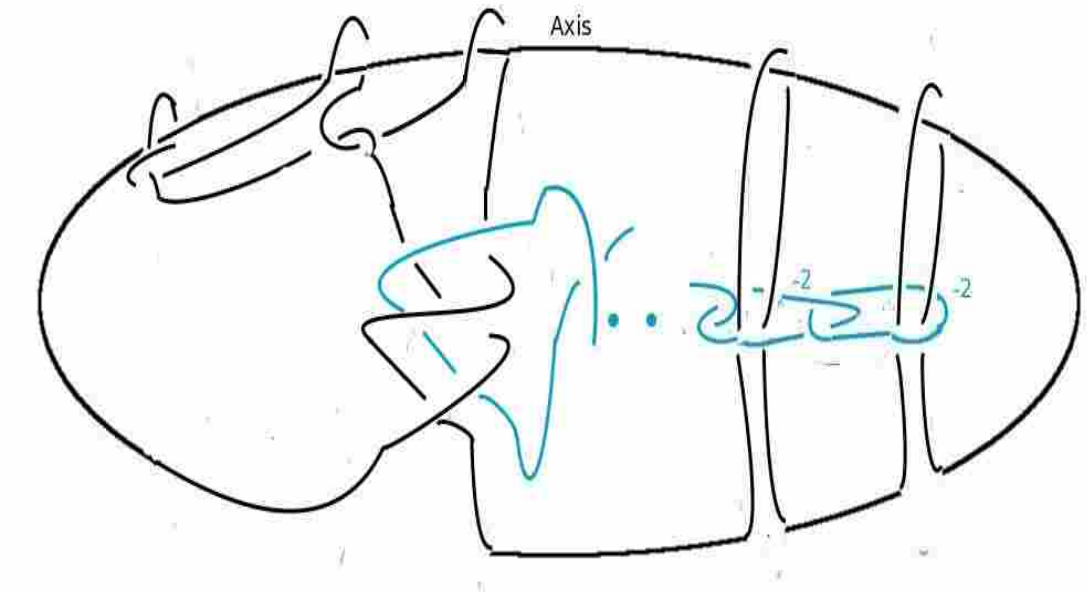

Figure 8.42: Regular Twist- CCL-m: +1 Twist on -1 Component

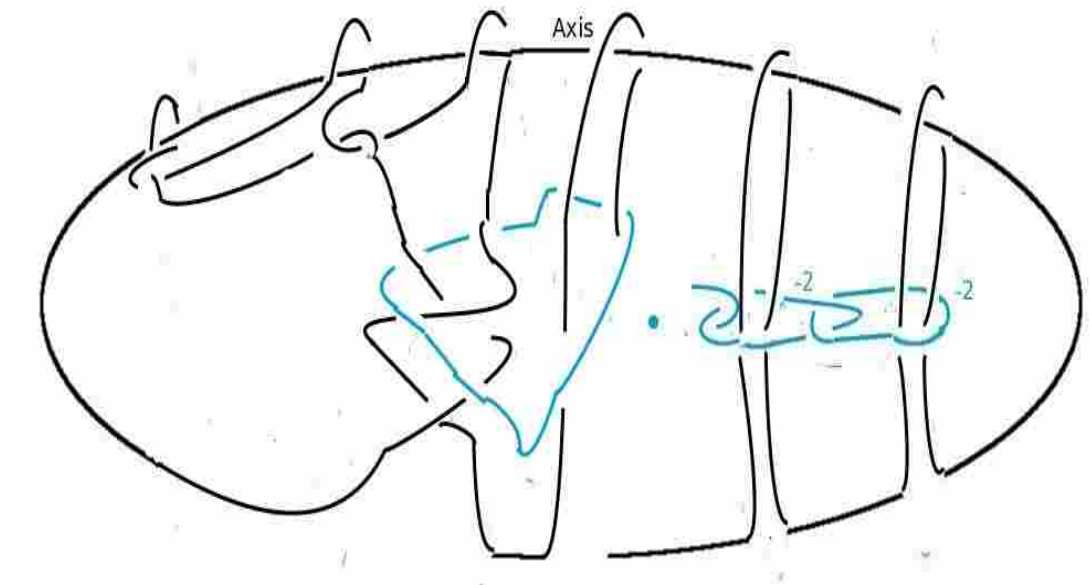

Figure 8.43: Regular Twist- CCL-n: Untwist Left Blue Circle

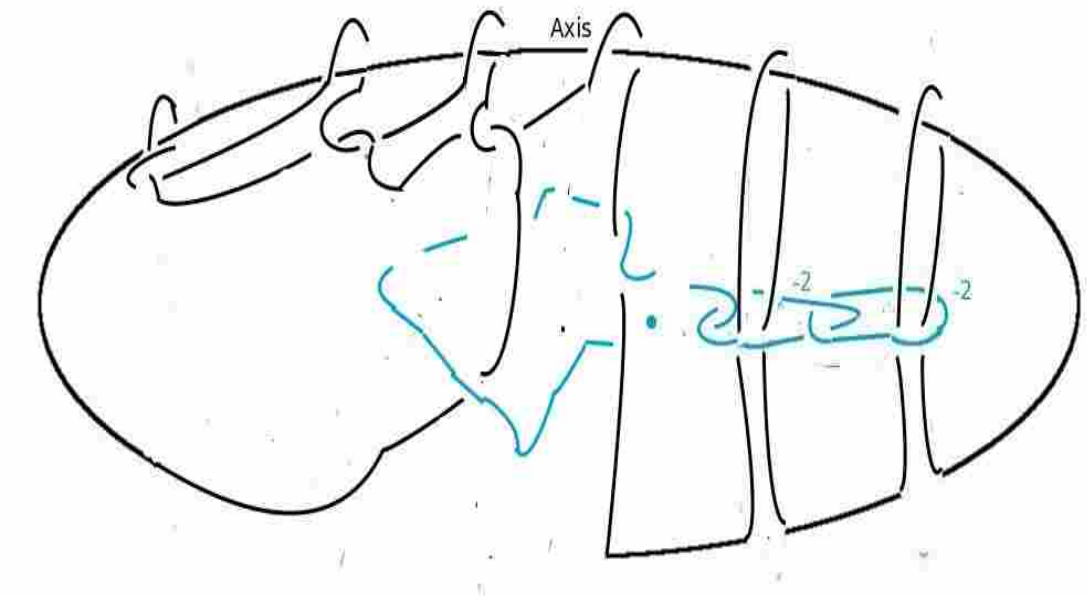

Figure 8.44: Regular Twist- CCL-o: Lift Out Rectangle

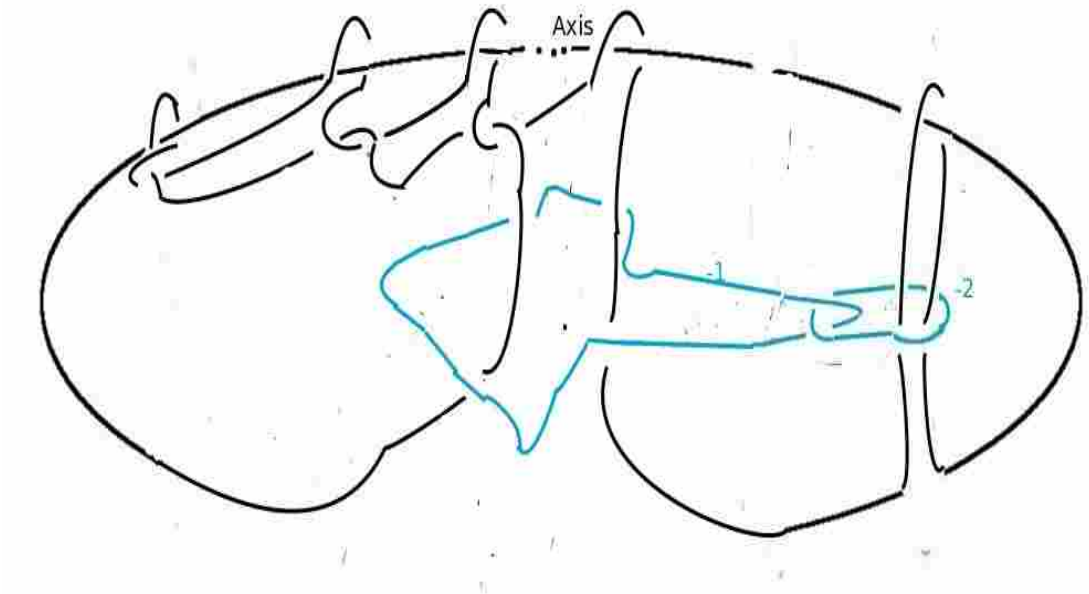

Figure 8.45: Regular Twist- CCL-p: Move Dots to Top Axis

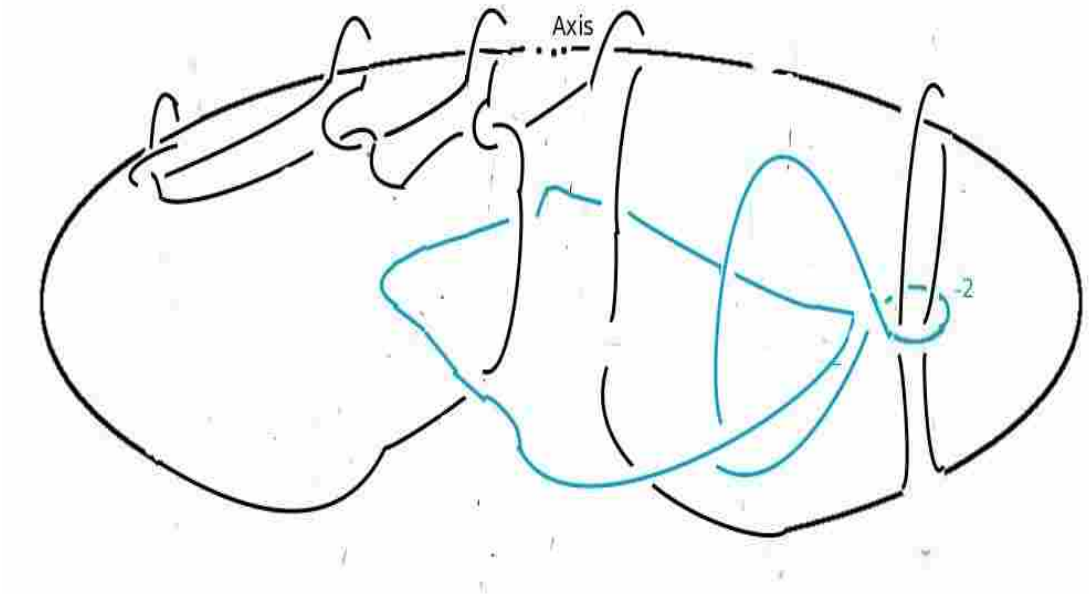

Figure 8.46: Regular Twist- CCL-q: Straighten Left Two Blue Circles

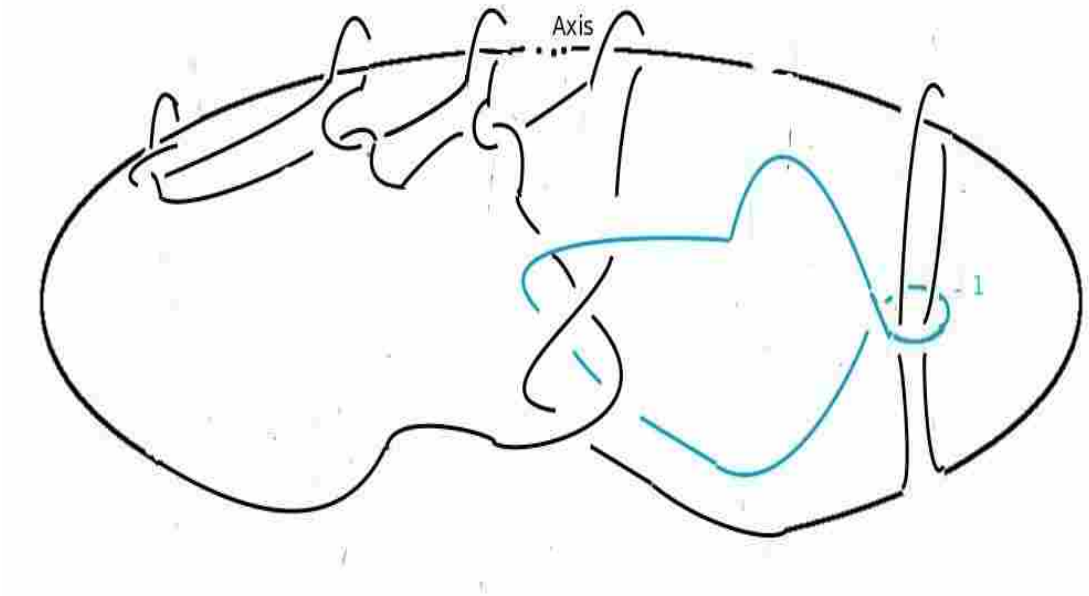

Figure 8.47: Regular Twist- CCL-r: +1 Twist on -1 Component

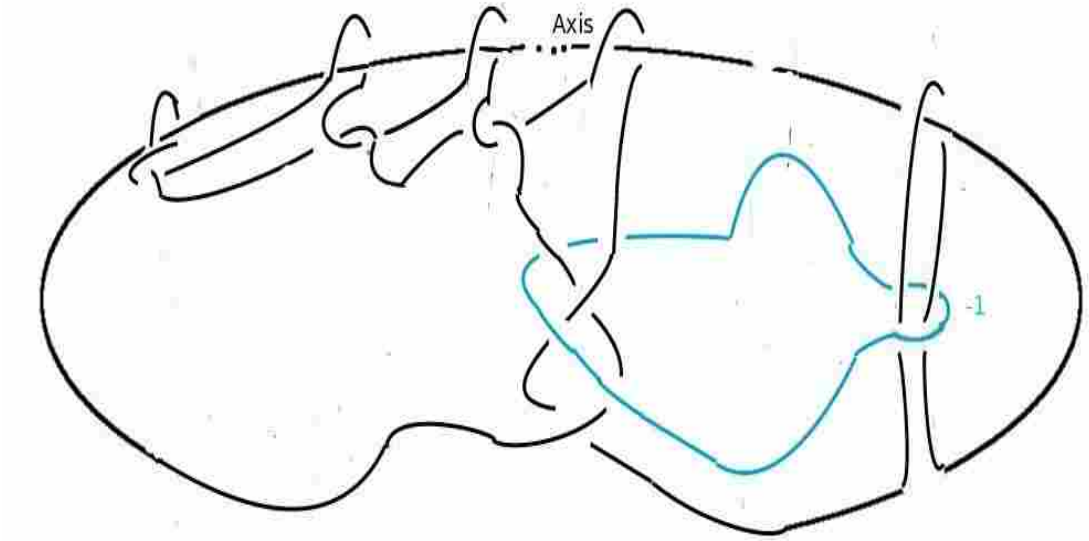

Figure 8.48: Regular Twist- CCL-s: Untwist Blue Circle

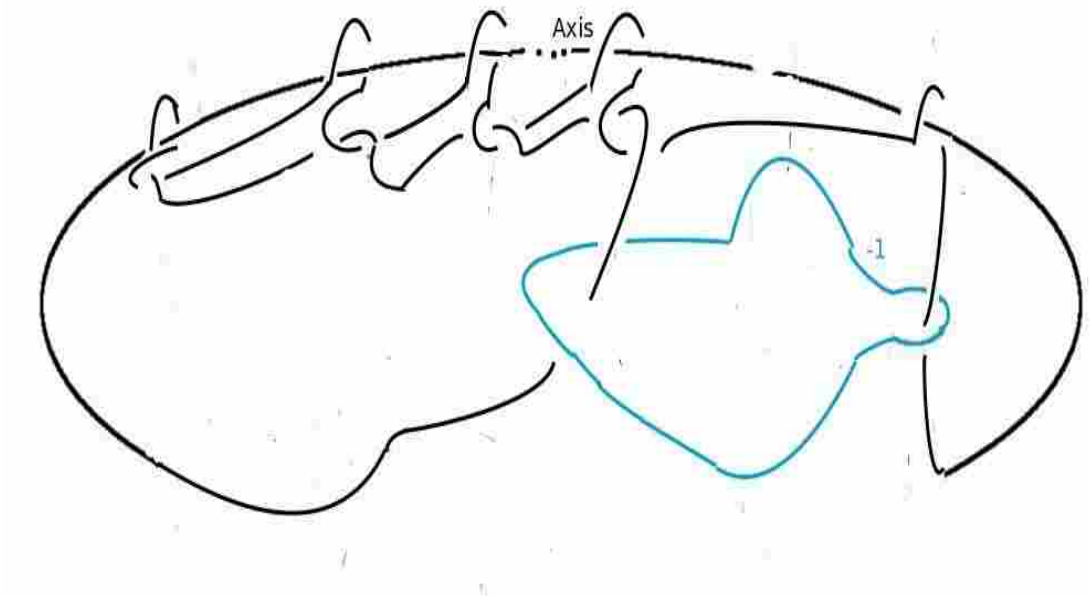

Figure 8.49: Regular Twist- CCL-t: Lift Out Rectangle

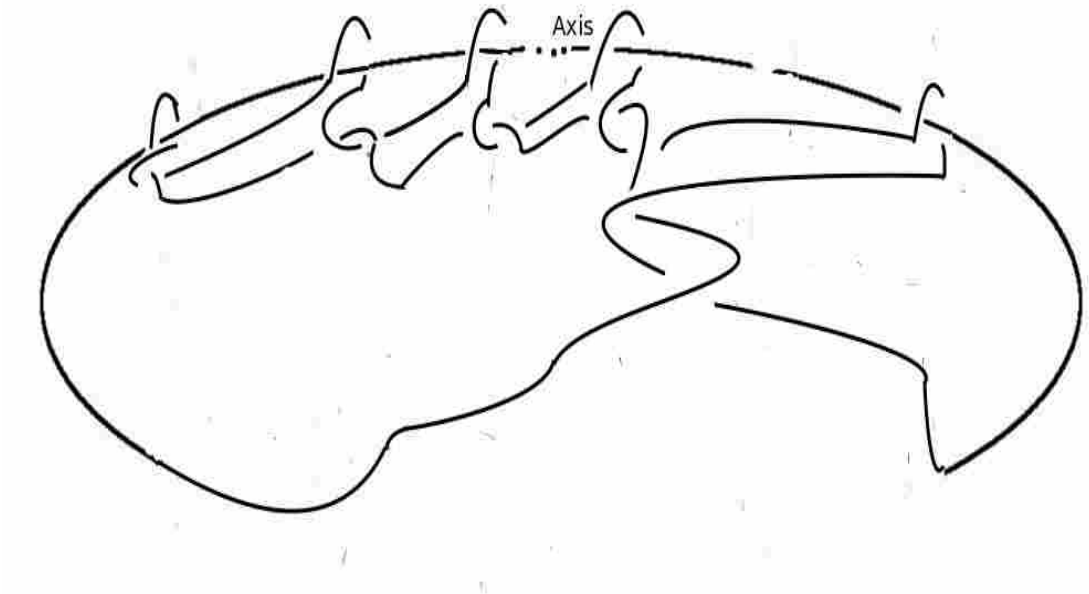

Figure 8.50: Regular Twist- CCL-u: +1 Twist on Last -1 Component

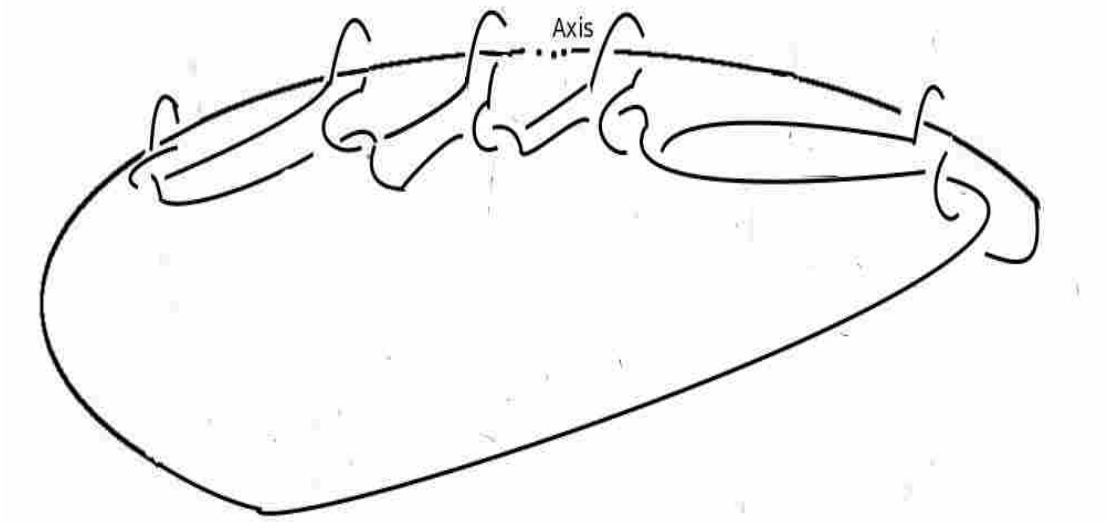

Figure 8.51: Regular Twist- CCL-v: Straighten Last Loop

We see the generalized figure-8 knot, when circle edge cycles have a +1 twist factor. This shows that the generalized Fibonacci manifold with n radials is an n-fold cyclic branched cover of $\mathbb{S}^3$, branched over the generalized figure-8 knot, with the knot crossings increasing with the number m of concentric circles in the upper hemisphere.

8.7 Antipodal Construction

As a final example, we would like to present a different construction of manifolds similar to the Sieradski manifolds without using the twist construction. This construction shows that infinite families of manifolds can be created with little effort. We start with the general case of n pieces to the pie (only one concentric circle). The original development was to map faces to their exact opposite or antipodal face. So for five slices one would map face 1 top to face 3 below. By going directly through the 3-ball, an outside vertex goes to the inside, thus moving two pie slices ahead, doing a counter-clockwise twist and projecting directly down to the lower pie slice. In doing the generalization to n slices, rather than projecting exactly to the antipode slice, it worked best to keep the same structure of 2 slices forward, twisting and projecting down. We start with the familiar n-slice 3-cell as in figure 8.52

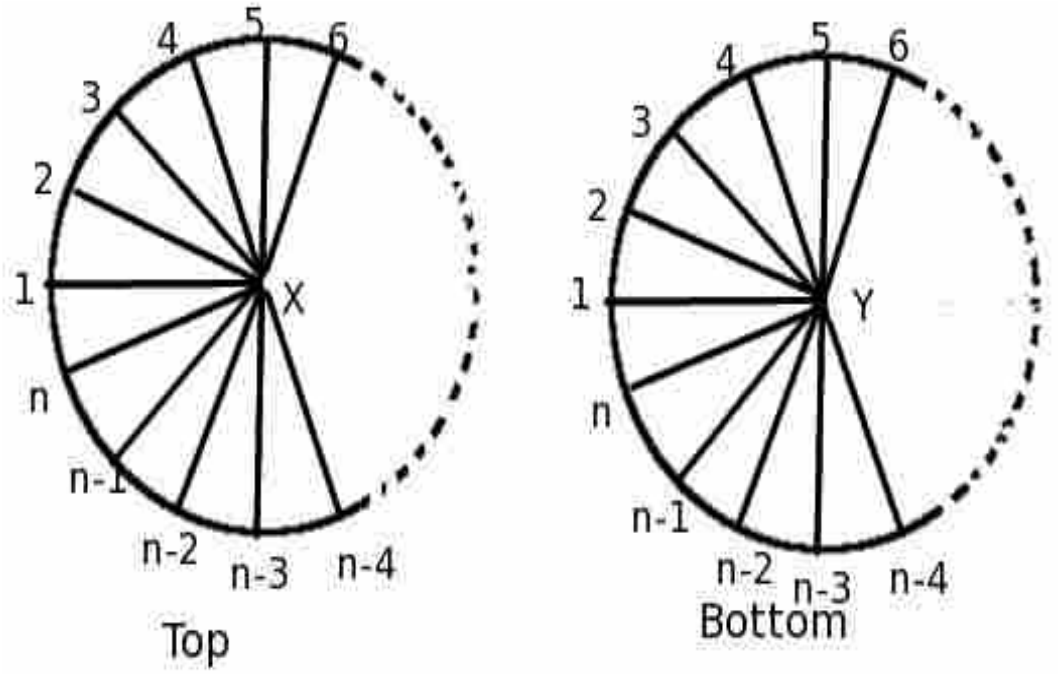

Figure 8.52: Antipodal Map

Following the described construction the maps become:

$$\begin{pmatrix} 1 & 2 & X \\ Y & 3 & 4 \end{pmatrix}$$

$$\begin{pmatrix} 2 & 3 & X \\ Y & 4 & 5 \end{pmatrix}$$

$$\begin{pmatrix} 3 & 4 & X \\ Y & 5 & 6 \end{pmatrix}$$

.....

.....

.....

$$\begin{pmatrix} n-3 & n-2 & X \\ Y & n-1 & n \end{pmatrix}$$

$$\begin{pmatrix} n-2 & n-1 & X \\ Y & n & 1 \end{pmatrix}$$

$$\begin{pmatrix} n-1 & n & X \\ Y & 1 & 2 \end{pmatrix}$$

$$\begin{pmatrix} n & 1 & X \\ Y & 2 & 3 \end{pmatrix}$$

First, we look at the vertices after doing the identifications. Following the maps, we see that all vertices are identified together. Looking at the edges we obtain the results below. We continue to avoid long subscripts by using X(1) in place of X_1

$$1\ 2 \overset{X(1)}{\longrightarrow} Y\ 3 \overset{X^{-1}(n)}{\longrightarrow} n\ X \overset{(n-1)}{\longrightarrow} 1\ 2 \qquad mappings : X(1)X^{-1}(n)X(n-1)$$

$$2\ 3 \overset{X(2)}{\longrightarrow} Y\ 4 \overset{X^{-1}(1)}{\longrightarrow} 1\ X \overset{X(n)}{\longrightarrow} 2\ 3 \qquad mappings : X(2)X^{-1}(1)X(n)$$

$$3\ 4 \overset{X(3)}{\longrightarrow} Y\ 5 \overset{X^{-1}(2)}{\longrightarrow} 2\ X \overset{X(1)}{\longrightarrow} 3\ 4 \qquad mappings : X(3)X^{-1}(2)X(1)$$

$\ldots$

$\ldots$

$\ldots$

$$n-2\ n-1 \overset{X(n-2)}{\longrightarrow} Y\ n \overset{X^{-1}(n-3)}{\longrightarrow} n-3\ X \overset{X(n-4)}{\longrightarrow} n-2\ n-1$$

$$mappings : X(n-2)X^{-1}(n-3)X(n-4)$$

$$n-1\ n \overset{X(n-1)}{\longrightarrow} Y\ 1 \overset{^{-1}(n-2)}{\longrightarrow} n-2\ X \overset{X(n-3)}{\longrightarrow} n-1\ n$$

$$mappings : X(n-1)X^{-1}(n-2)X(n-3)$$

$$n\ 1 \overset{X(n)}{\longrightarrow} Y\ 2 \overset{X^{-1}(n-1)}{\longrightarrow} n-1\ X \overset{(n-2)}{\longrightarrow} n\ 1$$

$$mappings : X(n)X^{-1}(n-1)X(n-2)$$

Looking at the fundamental group and first homology, we see that these two sets of groups (Sieradski and antipodal) have the same values. To show this we map $1 \to n; 2 \to n-1; 3 \to n-2$ etc. down to $n \to 1$. The relator $X(1)X^{-1}(2)X(3)$ becomes $X(n)X^{-1}(n-1)X(n-2)$. These new relators for the fundamental group are the same as the Sieradski manifolds relators.

Chapter 9. Questions and Problems

After doing this work, it is worth considering what kind of questions and problems might direct future research.

1. Can we find simple bitwist expressions for all sequences of cyclic branched covers of knots?

2. How common is the periodicity for the cyclic branched covers of knots?

3. Is there a 3-manifold that is not a twist manifold? We know that all are bitwist manifolds.

4. Is the previous question related to left veering and right veering contact structures on manifolds?

5. How does one calculate distance algorithmically in the curve complex? Can such a calculation help in determining properties of a twist or bitwist manifold?

6. Are all regular twist manifolds irreducible with nontrivial fundamental group?

7. Is there an easy way to show that the fundamental groups of the clockwise twist and the counterclockwise twist are isomorphic?

Bibliography

[1] J.W. Cannon. Geometric group theory. *Handbook of Geometric Topology*, 111:261–305, 2002.

[2] Nathan M. Dunfield and William Thurston. Finite covers of random 3-manifolds. *Invent. Math.*, 166:547–521, 2006.

[3] J.W. Cannon W.J. Floyd and W.R. Parry. Sieradski manifolds. *Preprint.*

[4] J.W. Cannon W.J. Floyd and W.R. Parry. Introduction to twisted face-pairings. *Math. Res. Lett.*, 7:477–491, 2000.

[5] J.W. Cannon W.J. Floyd and W.R. Parry. Twisted face-pairing 3-manifolds. *trans. Amer. Math. Soc.*, 354:2369–2397, 2002.

[6] J.W. Cannon W.J. Floyd and W.R. Parry. Heegard diagrams and surgery descriptions for twisted face-pairings for 3-manifolds. *Algebr. Geom. Topol.*, 3:235–285, 2003.

[7] J.W. Cannon W.J. Floyd and W.R. Parry. Bitwist 3-manifolds. *Algebr. Geom. Topol.*, 9:187–220, 2009.

[8] R. E. Gompf and A. I. Stipsicz. *4-Manifolds and Kirby Calculus, Graduate Studies in Math., Vol. 20.* Amer. Math. Soc., Providence, 1996.

[9] J.Milnor. *On the 3-Dimensional Brieskorn Manifolds M(p,q,r), Knots, Groups, and 3-Manifolds (Papers dedicated to the memory of R. H. Fox)*, volume 84. Ann. of Math. Studies, Princeton Univ. Press, 1975.

[10] James R. Munkres. *Topology, Second Edition.* Prentice Hall, Upper Saddle River, NJ, 2000, 1975.

[11] Grisha Perelman. The entropy formula for the ricci flow and its geometric applications. *arXiv:math.DG/0211159.*

[12] Grisha Perelman. Finite extinction time for the solutions to the ricci flow on certain three-manifolds. *arXiv:math.DG/0307245.*

[13] V. V. Prasolov and A. B. Sossinsky. *Knots, Links, Braids, and 3-Manifolds.* Amer. Math. Soc., Providence, 1997.

[14] Jennifer Schultens. The stabilization problem for heegaard splittings of siefert fibered spaces. *Topology and Its Applications.*, 73-2:133–139, 1996.

[15] Peter Scott. The geometries of 3-manifolds. *Bull. London Math. Soc.*, 15:401–487, 1983.

[16] W.P. Thurston. *Three Dimensional Geometry and Topology, Vol. 1.* Princeton University Press, Princeton, 1997.